12-2018

Finite Element Modeling and Experimental Characterization of Knot Configuration Effect on the Mechanical Performance of Surgical Suture

Arz Y. Qwam Alden
Western Michigan University, arzrzayyig@gmail.com

FINITE ELEMENT MODELING AND EXPERIMENTAL CHARACTERIZATION OF KNOT CONFIGURATION EFFECT ON THE MECHANICAL PERFORMANCE OF SURGICAL SUTURE

by

Arz Y. Qwam Alden

A dissertation submitted to the Graduate College
in partial fulfillment of the requirements
for the degree of Doctor of Philosophy
Mechanical and Aerospace Engineering
Western Michigan University
December 2018

Doctoral Committee:

Dr. Peter A. Gustafson, Ph.D., Chair.
Dr. Daniel Kujawski, Ph.D., D. Sc.
Dr. James W. Kamman, Ph.D.
Dr. Andrew Geeslin, M.D.

ACKNOWLEDGMENTS

First and foremost, I thank God for giving me the power, the patience, the health and the opportunity to accomplish my work and earn my Ph.D. Degree.

I would like to express my deepest gratitude to my advisor, Dr. Peter Gustafson for his encouragement, understanding, profound interest, valuable guidance, all the useful discussions, and brainstorming sessions. This project would not have been successful without him. He has always been a mentor and a teacher. Under his sound guidance and teaching, I have gained so much knowledge and experience from his deep insights thought process, views, and expertise that allowed me to enhance my research skills and prepared me for my professional career. And in times of success, he never forgot to celebrate. In the words of my second favorite Newton (Sir Isaac), “If I see further it is by standing on the shoulders of giants.”

I would like to thank and acknowledge the members of my graduate committee, Dr. Daniel Kujawski, Dr. James W. Kamman, and Dr. Andrew Geeslin for their support, valuable guidance, and motivation through the research project. I wish also to appreciate Dr. Andrew for providing us with the multifilament suture samples required for experimental tests.

Very special thanks to Dr. Marianne Di Pierro, for her valuable advice and feedback that highly improved my work and dissertation quality.

I would like to recognize the Department of Mechanical and Aerospace Engineering, for their help and support of this study. Also, I wish to thank Mr. John Cernius and Mr. Peter Thannhauser for their help during the experimental work. I thank my friends who have allowed me to pursue my passion for research and have given me encouragement and support.

I would like to extend my warm thanks to my wonderful family for their prayers, guidance and continued support throughout my academic career. Especially my parents are the major reason for my success in my studies and in my life. You have always been a source of love and inspiration to me. My thanks also go to my brothers and sisters for them love and support and proving that distance apart is nothing when you live with each other in your heart every day. Also, I want to show my infinite gratitude to my wife and our children for their ongoing love and continued support during my research endeavors and my whole life, and for the personal sacrifices they have made. I certainly wouldn't have made it without you, you've been with me from the beginning. Thank you so much.

I am grateful for this opportunity to share the knowledge I gained as a biomechanical engineer with this dissertation and hope it will eventually be of benefit for our patients. Last but not least, I would like to thank the Higher Committee for Education Development in Iraq (HCED) for their support, financially and for being my mentor. I am indebted to my country for helping me to finish my Ph.D. degree. Finally, I would like to dedicate this work to my beloved parents, and to my loving wife, children, sisters, and brothers.

Arz Y. Qwam Alden

FINITE ELEMENT MODELING AND EXPERIMENTAL CHARACTERIZATION OF KNOT CONFIGURATION EFFECT ON THE MECHANICAL PERFORMANCE OF SURGICAL SUTURE

Arz Y. Qwam Alden, Ph.D.

Western Michigan University, 2018

Tendon injuries in orthopedic surgery and sports medicine are escalating; hence there is great interest in improving tendon repair. The integrity of tendon repair depends in part on a combination of suture material, suture size and knot configuration. Recent studies have indicated the failure of surgical knots as a failure mode during surgical repair. Further, there is still no consensus on the ideal (best/safest) surgical knot techniques. Also, this failure mode is related to stress concentrations, which cannot be easily established with traditional tensile testing. Most researchers have focused on the measurement and comparison of the gross structural response of non-knotted and knotted suture, without direct investigation of the governing mechanics. Therefore, the purpose of this study is to develop a finite element approach to analyze the mechanical behavior of surgical sutures. Also, this analysis is necessary to differentiate the responses of several knot configurations and be validated against experiments.

To achieve this purpose, experiments and finite element models are performed to analyze the mechanical behavior of two types of sutures: monofilament and multifilament. Fixtures are experimentally designed to test (non-knotted/ knotted) sutures under tensile load until failure. The

knotted sutures are included single, two and three throws-knots. Non-knotted suture and a single throw-knot are modeled and analyzed. Finite element model and experimental results are presented using as-manufactured multifilament surgical suture: core and jacket. The experimental results indicate suture mechanical behavior is influenced by increasing number of throws; this effect is highly dependent on the suture constituents. The presence of a knot reduces failure load; thus rupture occurs consistently at the knot region. The finite element models predict maximum stress regions; the regions are correlated with experimental failures. This study also investigates the shear lag phenomenon of partially failed multifilament suture by analyzing the stress distribution under static and cyclic loading. Furthermore, a valid design for testing the knotless anchors is reported.

TABLE OF CONTENTS

ACKNOWLEDGMENTS ii

LIST OF TABLES x

LIST OF FIGURES xi

CHAPTER

I. INTRODUCTION 1

1.1 Background 2

1.1.1 Tendon 2

1.1.2 Surgical suture techniques 3

1.1.3 Composite materials and shear-lag 6

1.1.4 Finite element method (FEM) 7

1.2 Significance of the research 8

1.3 Objective and structure of the dissertation 11

1.4 Publications related to this dissertation 13

II. LITERATURE REVIEW 16

2.1 Background 16

2.2 Suture and suture techniques studies 16

2.3 Knot studies 18

2.4 Anchor studies 19

2.5 FE studies 20

Table of Contents—Continued

CHAPTER

2.6 Shortcomings of existing literature 22

III. MONOFILAMENT SUTURE 24

3.1 Introduction 24

3.2 Methods 25

3.2.1 Mechanical testing 25

3.2.1.1 Non-knotted suture 26

3.2.1.1.1 Image methodology 28

3.2.1.1.2 Procedure validation 29

3.2.1.2 Knotted suture 29

3.2.2 FEA models 32

3.2.2.1 Non-knotted suture 32

3.2.2.2 Knotted suture 32

3.3 Results 34

3.3.1 Experimental results 34

3.3.1.1 Non-knotted suture 34

3.3.1.1.1 Material characterization (diameter and density) 34

3.3.1.2 Mechanical properties 35

3.3.1.2.1 Poisson's ratio 35

Table of Contents—Continued

CHAPTER

3.3.1.2.2 Load and displacement 36

3.3.1.2.3 Stress and strain 37

3.3.1.2 Knotted suture 38

3.3.2 FE results 43

3.3.2.1 Non-knotted suture 43

3.3.2.2 Knotted suture 46

3.3.2.2.1 Effect of coefficient of friction on the knot model results 47

3.3.2.2.2 Effect of integration points and Poisson's ratio on the knot model results ... 48

3.3.2.2.3 Effect of mesh size on the knot model results 49

3.3.2.2.4 Knot model results. 50

3.4 Discussion 54

3.5 Conclusions 56

IV. MULTIFILAMENT SUTURE 58

4.1 Introduction 58

4.2 Methods 59

4.2.1 Mechanical testing 59

4.2.1.1 Non-knotted suture and knotted suture 59

4.2.2 FEA models 60

Table of Contents—Continued

CHAPTER

4.2.2.1 Non-knotted suture 60

4.2.2.2 Knotted suture 62

4.3 Results 62

4.3.1 Experimental results 63

4.3.1.1 Non-knotted suture 63

4.3.1.1.1 Material characterization (diameter and density) 63

4.3.1.1.2 Mechanical properties 66

4.3.1.1.2.1 Poisson's ratio 66

4.3.1.1.2.2 Load and displacement 66

4.3.1.1.2.3 Stress and strain 71

4.3.1.1.2.4 Suture behavior under different speed rates 72

4.3.1.2 Knotted suture 73

4.3.2 FE results 78

4.3.2.1 Non-knotted suture 78

4.3.2.2.1 Effect of coefficient of friction on the suture model results 78

4.3.2.2.2 Effect of Poisson's ratio on the suture model results 79

4.3.2.2.3 Effect of mesh size on the suture model results 79

4.3.2.2.4 Suture model results 80

Table of Contents—Continued

CHAPTER

4.3.2.2 Knotted suture 81

4.4 Discussion 86

4.5 Conclusions 88

V. SHAER-LAG PHENOMENON 90

5.1 Introduction 90

5.2 Methods 91

5.2.1 Mechanical testing 91

5.2.2 FEA models 91

5.3 Results 94

5.3.1 Experimental results 94

5.3.2 FE results 94

5.3.2.1 Effect of mesh size on the suture model results 94

5.3.2.2 Effect of coefficient of friction on the sutures models results 95

5.3.2.3 Validation of experimental and FE results 96

5.3.2.5 Static loading results 97

5.3.2.5 Cyclic loading results 101

5.4 Discussion 105

5.5 Conclusions 107

Table of Contents—Continued

CHAPTER

VI. FUTURE RESEARCH 109

6.1 Knotless glenoid suture anchors 109

6.1.1 Background 109

6.1.2 Anchors 111

6.1.3 Fixture components 111

6.1.3 Validation of experimental setup 113

6.1.4 Calibration of load transducer 117

6.1.5 Proposed biomechanical testing 117

6.2 Modeling of tendon and suture 119

6.3 Recommendations 122

REFERENCES 126

APPENDICES 148

A. Dial gauge setup 148

B. Calibration 150

C. Cyclic loading 156

LIST OF TABLES

1: Average load of failure and standard deviation of knotted monofilament sutures for five samples 42

2: Selected literature for comparison of FiberWire diameter 65

3: FiberWire, core and jacket densities 65

4: Selected literature for comparison of maximum stress and elastic modulus 72

5: Average load of failure and standard deviation of knotted FiberWire sutures for five samples 76

LIST OF FIGURES

1: Diagram shows the hierarchy of tendon [13] 3

2: Typical stress-strain for tendon [12] 3

3: General relationship between different suturing techniques and strength, gapping resistance, complexity, handling and gliding resistance [11] 6

4: The graphical representation of the research 12

5: (A) Full apparatus of the suture prior to tensile test (experimental setup), (B) Schematic diagram 28

6: Stress-strain curve of the music wire steel 29

7: Testing device for monofilament suture load-extension (scale in (cm)) 31

8: Examples of the throws, monofilament suture, (Approximate scale (mm)) 31

9: The knot mesh 34

10: Poisson's ratio of the monofilament suture 36

11: Load-Displacement curves of monofilament sutures 37

12: Stress-Strain curve of monofilament sutures 38

13: Load-Displacement curve of single throw knot of monofilament suture 40

14: Load-Displacement curve of two throws knot of monofilament suture 40

15: Load-Displacement curve of three throws knot of monofilament suture 41

16: An example of failure region of monofilament suture 41

17: Relationship between the mean load and number of throws, monofilament suture 42

18: Relationship between the mean stiffness and number of throws, monofilament suture 42

19: Effect of Poisson's ratio on the load-displacement behavior of non-knotted suture 44

20: Effect of integration points on the load-displacement behavior of non-knotted suture 45

List of Figures—Continued

21: Effect of mesh density on the load-displacement behavior of non-knotted suture 45

22: FE versus experimental results of the non-knotted monofilament suture 46

23: Effect of frictional coefficient on the load-displacement results of the knot model 48

24: Effect of full integration and reduce integration on the load-displacement results of the knot model 49

25: Effect of Poisson's ratio on the load-displacement results of the knot model 49

26: Effect of mesh density on the load-displacement results of the knot model 50

27: FE models of single, two, and three throws knot 52

28: Experimental versus FE model results of single throw model 52

29: Von Misses stresses of single throw model. Stresses in (MPa) 53

30: Deformation of single throw model. Deformation in (MPa) 54

31: Internal energy and kinetic energy in logarithmic scale of single throw model 54

32: Testing device for multifilament suture load-extension (scale in (cm)) 60

33: Examples of the throws, multifilament suture, (Approximate scale (mm)) 60

34: Axial cut of the FE mesh of the suture (core and jacket) 61

35: Nikon Measurescope 20 of measuring the suture diameter 64

36: An example of measuring method of the suture diameter 65

37: Poisson's ratio of the FiberWire suture 66

38: Load-Displacement curves of core and jacket of FiberWire suture 68

39: Load-Displacement curves of FiberWire sutures 69

40: Locations failure of the FiberWire suture 69

41: Mean load for breakage versus the number of failures 70

List of Figures—Continued

42: Selected literature for comparison of peak load to failure and loading type of FiberWire suture 70

43: Tensile test results of the FiberWire, core and jacket 71

44: Stress-Strain curve of FiberWire sutures 72

45: Load versus displacement at pull rates (0.1, 5, 12.5, and 33 mm/sec) 73

46: Load-Displacement curve of single throw knot of FiberWire suture 75

47: Load-Displacement curve of two throws-knot of FiberWire suture 75

48: Load-Displacement curve of three throws-knot of FiberWire suture 76

49: An example of failure region of FiberWire suture 76

50: Relationship between the load and number of throws, FiberWire suture 77

51: Relationship between the stiffness and number of throws, FiberWire suture 77

52: Effect of frictional coefficient on the failure load results of the suture model 78

53: Effect of Poisson's ratio on the maximum load results of the suture model 79

54: Effect of mesh size on the maximum stress results of the suture model 80

55: FE versus experimental results of the non-knotted FiberWier suture 81

56: FE models of one, two, and three throws knot 83

57: Experimental versus FE model results of single throw model 83

58: Internal energy and kinetic energy in logarithmic scale of single throw model 84

59: Von Misses stresses of single throw model. Stresses in (MPa) 85

60: Schematic diagram of the physical model of a core and jacket suture with notation, (a) longitudinal cross section of the jacket with intact core, (b) longitudinal cross section of the jacket with broken core, and (c) transverse cross section of the suture (core and jacket) 93

List of Figures—Continued

61: (A) Model mesh and boundary conditions, broken core, (B) Axial cut of the model mesh of the suture (core and jacket) 93

62: Effect of mesh size on the maximum stresses results of (intact/broken) core sutures models 95

63: Effect of frictional coefficient on the maximum stresses results of (intact/broken) core sutures models 96

64: Internal energy and kinetic energy in logarithmic scale, intact core 97

65: Internal energy and kinetic energy in logarithmic scale, broken core 97

66: Suture model, intact core 99

67: Suture model, broken core 99

68: Shear stresses of the suture model, broken core 100

69: Normal stresses along the suture model 100

70: Shear stresses along the suture model 101

71: Displacement along the suture length, broken and intact core 101

72: Locations of nodes on the core edge 103

73: The loading/unloading cyclic tensile stress-strain curve of broken core 104

74: The hysteresis corresponding to different applied cycles 104

75: Displacement vs time, broken core 105

76: Effect of coefficient of frictions on the stresses along the core interface 105

77: Schematic drawing of the fixture 113

78: Setup method of fixture, bone, screw and rod, and dial indicators 115

79: Values of deflection for dial indicator and MTS machine 115

80: The time lapse of the screw during tensile portion of test 115

List of Figures—Continued

81: Load-Displacement results of MTS machine versus dial 3 and (dial 2 - dial 1) 116

82: The planned experimental set-up is shown, demonstrating the method for stabilization of the femur 119

83: Model dimensions [31] 120

84: Boundary conditions [31] 121

85: Mesh of parts, left: suture and right: tendon 121

86: FE results 122

87: Knot configuration 124

88: Primary result of FE model 124

CHAPTER I

INTRODUCTION

Medical costs of damaged tendon treatment are increasing due to the recovery time, increasing sports participation, and increasing human population and their ages [1–4]. Basic considerations for repairing tendon may include the following: the selection of appropriate suture material, the suture diameter, the knot configuration, the length of the cut ends [5], and the surgeons' skills [6], [7]. A defect in any of these factors can contribute to the failure of repair.

Clinically, surgical suture is used to hold body tissue together after having been severed by an injury, incision or surgery. Suturing and knot tying is the most common surgical repair of tendon and other soft tissue injuries [8]. The modes of failure for surgical repair can be classified into tissue failure, knot failure, suture failure, and slippage of the knot [9],[10]. The strength of tendon repair depends on the coefficient of friction between the suture material and the tendon (i.e., the holding capacity of the suture within the tendon); the strength of the knot; the strength of the suture material itself (i.e., monofilament or multifilament); and the tendon properties [11]. The suture diameter, suturing technique, and knot configuration determines the suture performance in wound closure in terms of the strength and security of the knot and handling characteristics [11].

Patient outcomes regarding suturing quality can be affected by the human factors such as tendon quality and surgeons' ability about repair quality. Surgeons can exert control only over knot failure, breakage and/or slippage, depending on the choice of suture material, suture size, and knot configuration. Measurement and comparison of the strength of knotted suture are problematic

because there is no universal test method (neither in vivo nor ex vivo) [7]. At the same time, there is no universal agreement in the literature on the ideal surgical knot techniques. However, measures of performance such as the stress distribution of the knot cannot be established using traditional tensile testing.

1.1 Background

1.1.1 Tendon

In anatomical terminology, a tendon is dense connective tissue that connects muscle to the bone [12]. The essential function of a tendon is to transmit the mechanical force produced by the muscle to the bone. Tendon failures are prevalent and problematic, particularly among young people and athletes and frequently occurs during exercise activities, as well as during the execution of simple everyday activities [4]. Tendons usually fail by tearing away from the bone and/or rupturing within the tendon structure themselves [1], [12].

Tendons are classified into three hierarchical regions: primary, secondary and tertiary bundles, Figure 1 [13]. The collagen-rich tissues are considered an important component of tendon function, especially in strength transmission and stability to a joint [14]–[16]. Collagen behavior is anisotropic as it has unequal mechanical properties in different directions when it is loaded. When tendon is subjected to a uniaxial tensile test along the fiber direction from an unloaded state, the stiffness starts low and then increases; this effect occurs due to reducing the crimp angle of the collagen fibers at rest. The stress-strain curve of a tendon is non-linear and can be classified into four main regions as portrayed in Figure 2 [12].

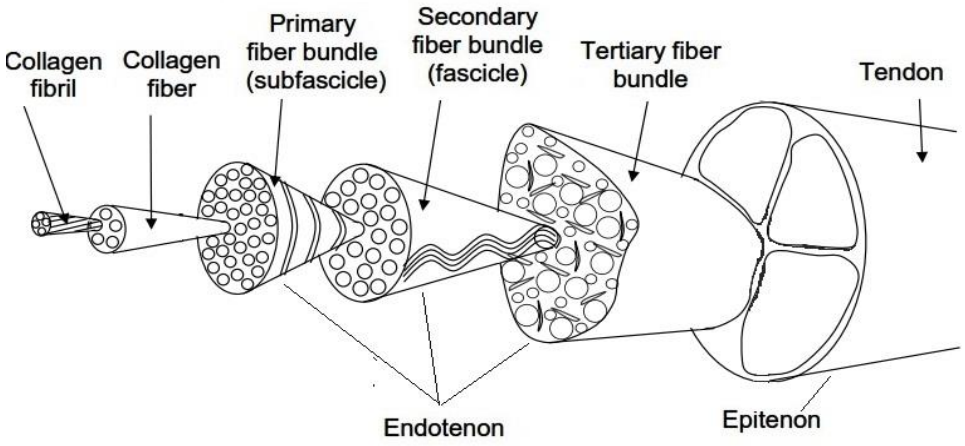

Figure 1: Diagram shows the hierarchy of tendon [13]

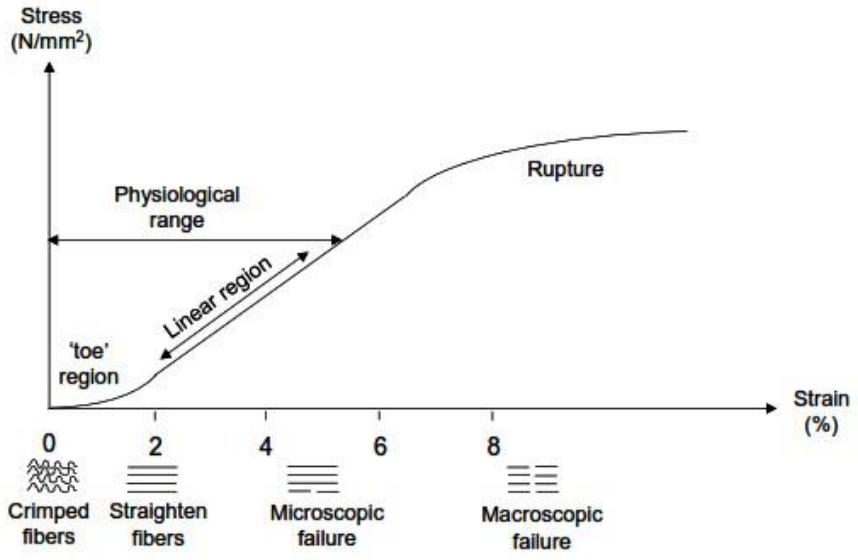

Figure 2: Typical stress-strain for tendon [12]

1.1.2 Surgical suture techniques

Surgical suture is a medical device used clinically to hold the tissue together after they have been severed by injury, incision or surgery. It can be used in nearly every part of the body, internally and externally. Sutures have been developed throughout history, and they are classified

by: (1) Spontaneous degradation (absorbable/non-absorbable), (2) Composition (natural/synthetic), and (3) Structure (monofilament/multifilament). The typical performance of suture material is based on their distinct physical properties, handling characteristics, and biological properties. Therefore, suture materials are a prime consideration for surgeons, especially as they select appropriate suturing techniques for wound closure.

Suturing has been the most common form of repairing tendon injury [17], although other methods of repair are available [17], [18]. Immediately after a tendon repair, the suture material and suture technique are the sole contributors to the repair strength [19]. Suture failure may happen by either knot untying, slippage, or knot breaking [8], [20], [21]. The knot slippage is one of the contributors to the failed tissue approximation [21]. Approximation in medical definition is, in surgery, bringing tissue edges into desired apposition for suturing [22]. To achieve proper healing, the tissue edges should be approximated with a minimal trauma to eliminate the gap and attain the best approximation. The space between the wound ends is called a gap [18]. The existence of the gap causes a decrease in the strength of the wounded tendon and the risk of infection [8]. Besides, the sutures must be loose enough to avoid discomfort and pain during recovery, ischemia, and tissue necrosis during tissue healing [8], [19]. Knot slippage can be prevented by using more throws than throws that are necessary for knot security [23]. A throw indicates to a particular step or layer used to make a knot, and a knot is made out of two or more throws in succession [23]. But these additional throws are time-consuming and add more suture material to the injury [6], [24]. Thereby, those additional throws decrease the resistance of tendon to infection [6], [24]. The amount of knot slippage is affected by a diversity of parameters, e.g. coefficient of friction of the suture material, suture diameter, knot configuration, length of the cut ears, and moisture [24]. The surgeon must tie a safe knot, with every suture utilizing the least number of throws [6].

In addition to using knots in surgical stitching patterns, they are also used in many applications such as climbing, fishing, sailing, and tying shoes [18], [25], [26]. The knot configuration can be arranged by the spatial relationship between the loop and the knot ears, where ears are the suture ends [6]. There are many factors contributing to the overall integrity of a knot, such as suture material, suture diameter, and knot configuration: including number of throws in each knot [6], [27]. Seemingly small changes in knot configuration can produce knots with significantly different apparent mechanical properties for the surgical construct. Under tension, the strength of the knot is significantly affected by knot configuration, complex contact, and large elongation [28], [29]. Several test methods have been used to measure the tensile strength of a knotted suture. The most commonly used methods are (e.g. “ear”, “loop”, “cut-loop”, and “cut-loop and ear”) are detailed by [29], [30].

Figure 3 illustrates the general relationship between different suturing techniques and strength, gapping resistance, complexity, handling and gliding resistance [31]. In fact, the possible disadvantages of knots are a theoretical risk of tissue irritation, potential postoperative joint clicking from large knots and surgeons knot-tying skill [32]. A surgeon must be well practiced in tying knots on models before doing so on patients to obtain reliable, reproducible knots every time [33].

Suture Anchors useful fixation devices for fixing tendon to bone. Suture anchors may be made of metal or biodegradable material that have two sutures each attached to them. The suture anchors are inserted in bone and the sutures are then used to sew the tendons to bone arthroscopically. There are many suture anchors on the market, each with slightly different characteristics and indications. Anchors can be knotted or knotless [34]. The knotted anchor has two sutures, allowing for more points of tissue fixation with a single anchor. These sutures also

provide a greater degree of control over tissue tension [34]. The knotless suture anchor has a short loop of suture secured to the tail end of the anchor [35]. One of the advantages of using knotless anchors is the possibility of reducing surgical time [34].

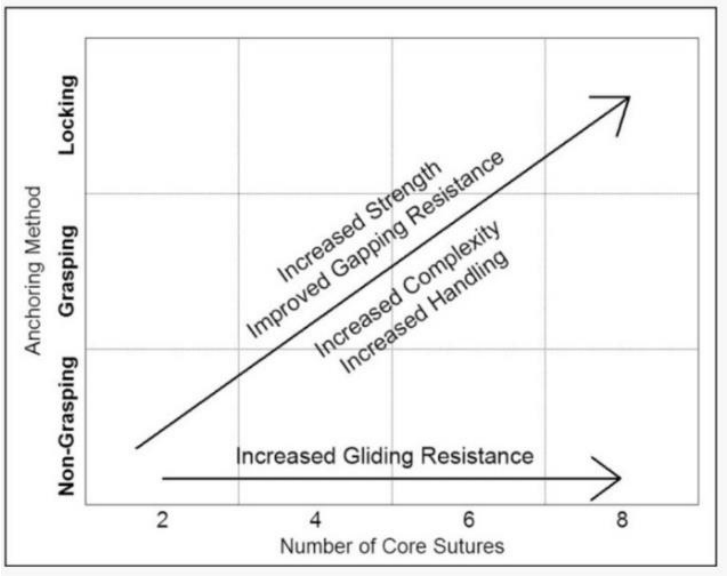

Figure 3: General relationship between different suturing techniques and strength, gapping resistance, complexity, handling and gliding resistance [11]

1.1.3 Composite materials and shear-lag

Composite materials are the material system that consists of two or more phases on a macroscopic scale. One of the most important constituents is called fibers which are used for reinforcement of the matrix material. The properties of a composite material depend on the properties of the constituents, geometry, and the orientation of the reinforcement.

In a recent review, composite materials have received considerable attention in the field of materials research because of lighter weight, the high specific modulus, good wear resistance, high specific strength, and high fatigue [36],[37]. Predicting failure of composite structures remains challenging due to the complex internal structure of fiber reinforced composites and complex

interactions between fiber and matrix as well as the difficult experimental validation [38], [39]. The applications of composite materials are many such as aerospace, biomedical, and industry [40].

FiberWire suture is a long fiber composite structure comprised of a multifilament core surrounded by a braided jacket. Shear lag is a well-known concept in composite materials and used to analyze stress transfer problems in regions of changing normal stress such as at fracture points or geometric discontinuities. Shear lag is partially dependent on the relative stiffness of the connection versus the direction of the application of the load. Computer modeling is one of the methods used to solve the shear-lag model because of the complexity of the matrix constitutive behavior [41]. There are four common methods that describe load sharing by determining how to stress redistributed when fiber breaks. The methods are: 1. very local load sharing, 2. local load sharing, 3. global load sharing, and 4. equal load sharing [38].

1.1.4 Finite element method (FEM)

FEM is a numerical method used to perform finite element analysis (FEA) of any given physical phenomenon [42]. FEM is now widely used to solve typical problem areas of interest include structural analysis, fluid flow, heat transfer, and multi-physics problems. The analyses in engineering are performed to assess designs and to obtain insight into and ideally to predict natural phenomena [43]. The main objective of FEM is to divide the domain of the problem into a collection of subdomains and represent the subdomains by an assembly of simpler finite sized elements [42]. It may be challenging for physicians to traverse the wide array of suture materials and techniques without appropriate support. So, several numerical approaches are used in an orthopedic biomechanics analysis. One of these approaches is FEA. FEA can be used in

biomechanics to identify the governing mechanics of surgical technique of suture repairs based upon suture properties and knot configuration. FEA promise to provide an understanding of stresses and strains within the suture knot and a further insight into their complex distribution. FE model of a knot can show the effects on internal forces when adding or subtracting a throw.

1.2 Significance of the research

According to the National Institute of Health, soft tissue injuries remain a persistent clinical challenge. Annually, an estimated 30 million cases of human tendon and ligament injuries take place worldwide [1], [2], [4]. In the U.S. alone, the medical services expenditure is estimated at US$30 billion per year [1], [2], [4]. Surgical intervention of tendon injuries is considered a widespread repair technique to restore normal tendon length and tension, thereby achieving optimal function [2]–[4], [6]. However, this repair process may not be without complications such as failure to restore the functional properties of repaired tendon. Failure of functional recovery is often associated with prolonged disabilities and/or chronic pain that require long and expensive treatments and a painful rehabilitation period [1], [3], [4]. Nevertheless, there is still a lack of universal agreement on the ideal suturing technique of tendon repair [44][45]. Tensile testing of the repaired tendon has been used to assess the efficacy of surgical knot tying techniques [46]. The configuration of a knot alters the biomechanics of the suture, the tendon, and their interface. The effect of knot configuration on the repair strength has not been well quantified. Therefore, improving the knot technique may have a significant impact on enhancing the functional regeneration of repaired tendon [3].

Suturing and tying knots are challenging and highly dexterous tasks in surgery [47]. Sutures and knots are in common use for surgical repair of tendon and other soft tissue injuries for

millennia, dating back to sutures used in ancient Egypt from 3000 to 1600 BC [17], [48], [49]. Failure of surgical knots is one of the failure modes during surgical repair [10], [46]. This failure mode is related to stress concentrations which cannot be easily established with physical testing. Multiple biomechanical studies and reports have attempted to identify the best surgical technique, for multifilament and/or monofilament sutures [6], [24], [58], [50]–[57]. Those studies identified the techniques based on suture properties, technical modifications, and repair configurations. The measurement and comparison of the gross structural response of non-knotted and knotted suture were reported in several prior studies [6], [11], [54]–[61], [17], [24], [46], [47], [50]–[53], however, they evaluate or compare without direct investigation of the governing mechanics. Several prior biomechanical studies assess the mechanical properties of FiberWire suture [6], [11], [54]–[63], [17], [64], [24], [46], [47], [50]–[53]. Most of these studies evaluate material properties of specific suture knots [6], [65], or comparison of one type of suture versus another [24], [53], [60]–[63]. Little has been reported about the constituents of the suture, the core and jacket separately, nor their impact on the knot strength and failure mechanisms. However, there are still concerns about the tying of Fiberwire suture and required knots for obtaining a secure repair [66].

Further, FiberWire (core-jacket) suture subject to tensile stress can undergo extensive core cracking normal to the jacket, while the jacket remains intact. Suture fails for various reasons, e.g., mechanical trauma in use can result in a discontinuity in the suture material [27]. The "shear-lag" phenomenon is frequently used to describe the interplay between axial and shear stress around fracture points or geometric discontinuities and provides ongoing load transfer after the initial compromise of a structure. Many researchers have recognized that understanding the mechanical behavior of composites needs to understand the internal stress distribution [33, 34]. Despite, the approach remains limited by the ability to represent the mechanism of load transfer between suture

constituents [17]. However, it is not easy to determine precisely the internal stress distribution of FiberWire suture due to the complexity of interactions between its constituent. Yet, traditional tensile testing alone cannot fully describe the mechanics of the driving shear-lag phenomenon.

Finite element (FE) model of a knot can show the effects on internal forces when adding or subtracting a throw. However, it is a significant challenge due to the complex contact, friction, and large displacements of the model. Moreover, FE model provides a useful tool to describe the shear-lag phenomenon of suture failure by examining the distribution of normal and shear stresses distribution along a broken and intact core reinforcing jacket, of a FiberWire suture. Further, there exists a paucity of literature on the use of FE models describing the biomechanics of surgical knots and the effect of knot configuration on the failure mechanism of surgical sutures and of tendon [11]. To date, nothing has been reported in the modeling of non-knotted and/or knotted FiberWire suture.

The outcomes of this dissertation describe a model that can represent the initial failure process leading to knot breakage and mechanics of load transfer in the surgical sutures. The difference between non-knotted and knotted suture specimens may provide useful information on which to base a choice for knot stability and strength. In the future, the results may provide a framework for optimally choosing the suture and knot types for tendon repairs. Further, the outcomes of this study may assist the orthopedic surgeon to improve the reconstruction quality of wounded tendons. In addition, this research help enhances engineers' and surgeons' knowledge of factors influencing knot performance.

1.3 Objective and structure of the dissertation

This dissertation investigates the impact of throws number on the mechanics of sutures and their effects on the suture strength. The long-term goal of this research is to apply knot modeling techniques to establish the biomechanics of the suture to bicep tendon interface. FEM and experiments are performed for these investigations. Figure 4 shows the graphical representation of the research approach.

The chapters of this dissertation are organized as follows. After an introduction in Chapter 1, the main concepts of the tendon, sutures, suturing, knot, shear lag, and composite materials have been explained. Further, the significance of this work has been demonstrated. Chapter 2, an overview of the existing literature that examined the effect of the suture material, suture techniques, size, and knot configuration, and tendon repair. Moreover, the shortcomings of the existing literature are clarified. In chapters 3 and 4, a 3D FEAs and lab experiments are used to discern the tensile performance of (non-knotted/knotted) monofilament and FiberWire sutures. The experimental study provides the necessary data to validate the FE models. In these chapters, model results are only for the non-knotted and the single throw-knot cases. The experimental results are extended to the two-throws and three-throws knots to examine the impact of knot configuration and other factors governing the mechanics of sutures and their effects on the sutures strength. The load transfer mechanism behavior in FiberWire suture plays an important role in determining its mechanical properties. Therefore, chapter 5 includes FE model to assess the distribution of normal and shear stresses along (intact/broken) core of FiberWire suture. In assessing process, static and cyclic loading are implemented. Second, the clinical implications of the shear-lag phenomenon are described.

A specific fixture is required to evaluate and compare variations in the biomechanical properties of various commercially obtainable knotless suture anchors for glenoid labral repair. Thus, chapter 6 includes three parts: (1) Assessing the fixture that is designed to test the knotless suture anchors experimentally to ensure that the fixture is able to carry a high load and that there is negligible relative movement between the entire system (fixture, bone) during the pullout test. (2) propose a preliminary 3D FE model to calculate the stress distribution on the tendon due to the application of a tensile load on the suture. The model consists of two components tendon and suture. (3) finally, recommendations for future work.

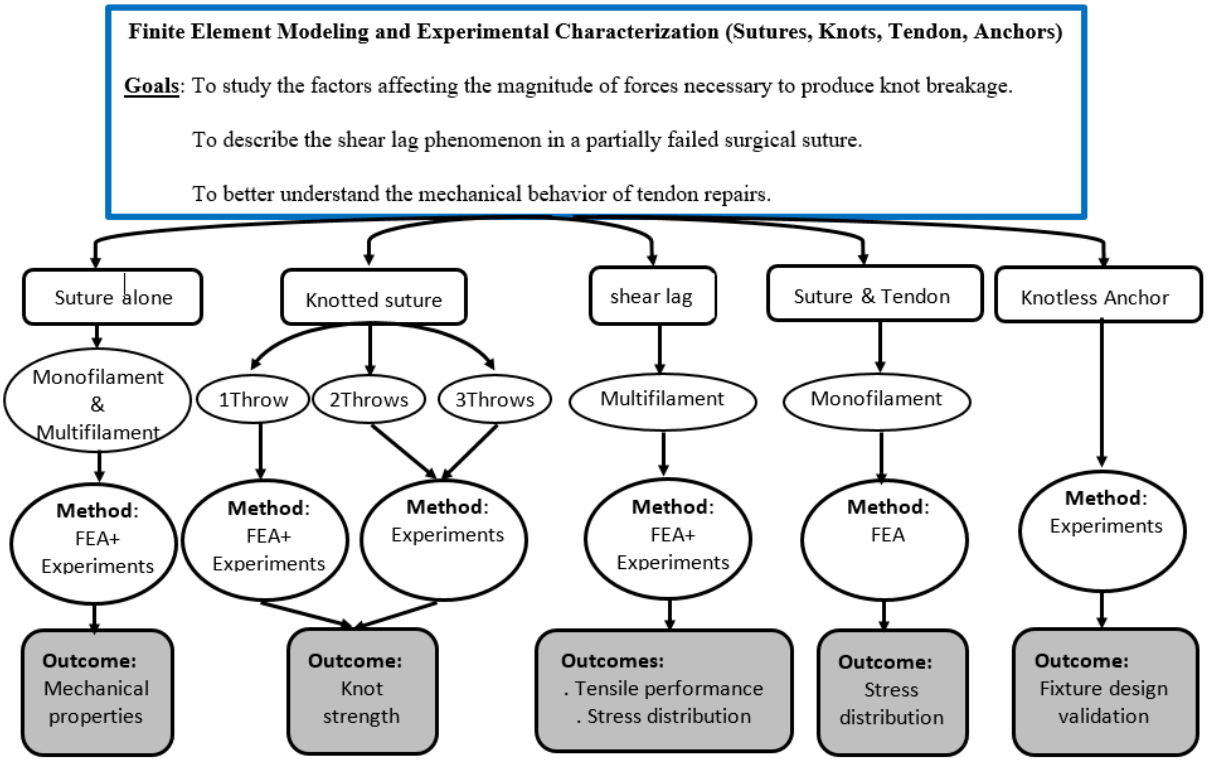

Figure 4: The graphical representation of the research

1.4 Publications related to this dissertation

Journals:

Arz Y. Qwam Alden; Andrew G. Geeslin; Jeffrey C. King; Peter A. Gustafson. A Finite Element Model of a Surgical Knot. In Journal of Biomechanical Engineering (2018) ASME. TO BE SUBMITTED SOON 2018.

Arz Y. Qwam Alden; Andrew G. Geeslin; Peter A. Gustafson. Validation of a model of the effect of knot topology on the mechanical performance of surgical suture. In Journal of Biomechanical Engineering (2018) ASME. TO BE SUBMITTED SOON 2018.

Arz Y. Qwam Alden; Peter A. Gustafson Finite Element Simulation and Experimental Investigation of Shear Lag Load Transfer in A Partially Failed Directional Composites Surgical Suture Under Axial Loading. In Journal of Composite Materials (2018). TO BE SUBMITTED SOON 2018.

Technical Papers:

1. Validation of a model of the effect of knot topology on the mechanical performance of surgical suture, ASME's International Mechanical Engineering Congress and Exposition (IMECE), David L. Lawrence Convention Center, Pittsburgh, PA, USA, November 9-15, 2018. (Accepted)

2. A Finite Element Model of a Surgical Knot, ASME International Mechanical Engineering Congress and Exposition (IMECE), Volume 3: Biomedical and Biotechnology Engineering, Tampa Convention Center, Tampa, Florida, November 3-9, 2017. Paper No. IMECE2017-72201, pp. V003T04A030; 9 pages doi:10.1115/IMECE2017-72201, ISBN: 978-0-7918-5836-3.

Conferences (Presentations):

1. An experimental and numerical investigation of shear lag load transfer in a partially failed composite surgical suture, 8th World Congress of Biomechanics (WCB2018), July 8 – 12, 2018, Dublin, Ireland.

2. Mechanics of progressive failure of No. 2 FiberWire suture, 36th Annual Kalamazoo Community Medical and Health Sciences Research Day, Kalamazoo, Michigan, May 2, 2018.

3. Shear lag in a partially failed in FiberWire surgical suture, American Society of Biomechanics (ASB) East Coast Meeting, Reading, PA, USA, April 20th – 21st, 2018

4. Finite Element simulation and experimental characterization of surgical knot performance, Summer Biomechanics, Bioengineering, and Biotransport Conference (SB3C), Tucson, AZ, June 21 – 24, 2017.

5. Experimental characterization and numerical simulations of surgical knots, The 35th Annual Kalamazoo Community Medical and Health Sciences Research Day, Kalamazoo, Michigan, May 2, 2017.

Conferences (Posters):

1. Effect of knot configuration on the mechanical performance of a multifilament surgical suture, 8th World Congress of Biomechanics (WCB2018), July 8 – 12, 2018, Dublin, Ireland.

2. Validated Finite Element model of a monofilament surgical knot, 8th World Congress of Biomechanics (WCB2018), July 8 – 12, 2018, Dublin, Ireland.

3. Impact of knot configuration on suture performance: experiments and numerical models, 36th Annual Kalamazoo Community Medical and Health Sciences Research Day, Kalamazoo, Michigan, May 2, 2018.

Awards

1. 36 Annual Kalamazoo Community Medical and Health Science Research Day. It is the award for "Top Awarded Poster". These awards are presented by Western Michigan University (WMU) Homer Stryker M.D. School of Medicine / USA.

2. Graduate Student Make a Difference Award 2018 in the category of "Academic Support". It is the award for demonstrating outstanding collaboration with Western Michigan University (WMU) peer graduate students in instructions, tutoring, partner learning. These awards are presented by the Graduate Student Association (GSA) at WMU / USA.

CHAPTER II

LITERATURE REVIEW

2.1 Background

Tendon injury may occur from sports, physical activity, and simple daily activities [3]. Therefore, tendon repair is very important to restore the tendon to full activity. Optimal repair of the tendons is achieved when the knot is secure and is tied with the appropriate suture material [67]. The knot that requires the smallest number of throws to achieve high strength and security is the ideal knot [6], [50], [67]. During the past decade, many efforts have been made to understand the mechanisms of tendon repair by utilizing different suture materials and surgical knot tying techniques [68], [69]. These efforts have been associated with many experimental [69]–[73] and clinical biomechanical [74]–[77] studies. However, suture materials and surgical knot tying techniques remain limited by the ability of the suture to transfer load to the repaired tissue [17], [69].

2.2 Suture and suture techniques studies

Despite millennia of experience with injury closure, there was no final agreement in literature on the ideal suture material [78][45], suture technique, and knot configuration for tendon repairs [44][45]. Ketchum [79] concluded that immediately after repair the tendon had no contribution to the repair strength because there is a gap between tendons ends. At this time, the sole contributors to the repair strength were the suture itself and suture technique. After several weeks of repair, the suture material and technique became secondary to tendon healing because the repair site is gradually strengthened with the tendon regeneration. The

study exhibited that the stainless-steel suture was difficult to handle and form a bulky knot in spite of it is the strongest material that can be used. Chauhan et al [52] also achieved the same results when investigated four different techniques with two alternative suture repairs: stainless steel and FiberWire. The results showed that increasing the number of throws were more useful to repair the large tendons than small tendons. Because, increasing number of throws resulted in an increase in bulk, tissue handling, suture passes, and technical difficulty.

Rudge et al [66] examined six types of suture materials and five different techniques. The study revealed that the suture diameter had a high influence on the tensile strength, the repair movement, and the friction coefficient. Similar results were also obtained by Taras at al [80] when investigating the effect of suture diameter variation on tensile strength in three types of tendon repairs. Four diameters of braided polyester suture were used with each type of repair. Also, similar findings were reached by Viinikainen et al [81] when used porcine tendons to compare the influence of five suture techniques under tensile testing. The outcomes indicated that the suture diameter and the suture technique impact on the strain at the failure point.

Kudur et al [82] discovered that the selection of suture material depends on several factors such as injury location, injury tension (static and dynamic), the existence of injury infection or fever, and suture material cost. Further, the study compared between monofilament and multifilament sutures in terms of advantages and disadvantages. Advantages of monofilament suture include ease of passage through tissue, ease of removal, and decreased tendency of infection. The disadvantages of monofilament suture are poor handling characteristics and decreased knot security. Multifilament sutures are more prone to

infection and exhibit high tissue reactivity. Multifilament sutures also involve the following advantages: ease of handling, low memory, and increased knot security.

Kubota et al [83] used human cadaver flexor tendons to assess the mechanical properties of six suture techniques using polypropylene monofilament suture material. For all suture techniques, values of tensile strength and the required force to initiate the gap formation were affected directly by the number of throws. Moreover, the findings indicated that the suture technique had a significant influence on the tensile strength of repair for all suture throws numbers.

2.3 Knot studies

Recently, researchers had a detail of attention to the knot configuration due to its effect on the knot security. The security of the knot relies on specific parameters; which are as follow: suture type, suture diameter, knot configuration, length of the cut ends, and moisture [84]. Small changes in knot configuration can yield large changes in mechanical properties.

Hockenberger et al [6] described the knot performance of monofilament and braided polyamide sutures by employing two different types of knots and numbers of throws. The findings demonstrated that after getting a secure knot, an additional throw has no significant impact on the required force to break the suture. Suture diameter also affected the knot performance. Similar results were obtained by Silver et al [50] when investigated the knot security in relation to surgical tying techniques, suture materials, suture diameter, and number of throws. The study showed that the clinicians should use a minimum of 4 throws and should never use 2 throws. After 5 throws, tying an additional throw was redundant and did not contribute to knot security. Also, the study found that the suture diameter had less effect than

suture material, tying technique, and number of throws on the knot security. While Van et al [51] concluded that adding extra throws to the knot add less influence to the total amount of foreign body and tissue reaction in the wound than the use of thick-gauge suture material.

Heward at el [7] conducted a series of experiments to determine the tensile performance of non-knotted and knotted monofilament sutures. The results showed that the failure of sutures occurred at the knot rather than along the suture because of the high-stress concentration at the knot region. The outcomes also demonstrated that the presence of a knot resulted in lower tenacity and ultimate strain values for all sutures.

Based on experimental and theoretical investigations, slender elastic rods under tension were used by Jawed et al [18] to examine the influence of knot topology on the mechanics of knots. This study was the first study included experiments and theoretical models together. The analytical solution described how the physical and topological parameters of the knot set the required tensile force for equilibrium. Experimental and theoretical results indicated a good agreement for overhand knots over several number of throws.

2.4 Anchor studies

Goble and Somers developed the first suture anchor in 1985, obtaining a patent in 1986 [85]. Since their introduction, suture anchors have become one of the most utilized methods for securing soft tissues to the bone. Kubiak et al [85] performed a pullout test on the threaded anchors inserted into polyurethane foam at varying insertion angles. The purpose of the testing was to examine the impact of insertion angle on the number of cycles, the ultimate pullout strength, and the stiffness of suture anchors. The results pointed out that the insertion angle in

relation to the direction of suture pull had a notable impact on the failure load and construct stiffness. The obtuse insertion angle withstands a greater load to failure and provides a stiffer construct than the acute insertion angle. Ranawat et al [86] tested the failure modes, ultimate load to failure, and stiffness of knotless and knotted anchors using FiberWire N0.2 suture. Under the same test conditions, the outcomes exhibited that failure often occurs at the suture–tissue interface and as well as in the anchor–bone interface for both knotless and knotted anchors.

In a vivo study, the histologic response and a biomechanical analysis of two small glenoid anchors were studied by Pfeiffer et al [87]. The study employed six adult dogs for histologic analysis and eight humans cadaveric for biomechanical testing. The findings of the biomechanical testing and histology suggested that both suture and the anchor may be at risk for clinical failure. The movement of the suture and anchor more than 2 mm was described as the clinical failure.

2.5 FE studies

Since the 1970s, several studies have focused on improving the biomechanical and tendon researches using FEA [31]. García-González et al [88] used a 1D FE model to assess the stress concentration of Flexor digitorum longus tendon. 2D and 3D FE models were constructed to represent the supraspinatus tendon by Wakabayashi et al [89] and Sano et al [90] respectively. In all investigations above, the behavior of tendon was described as an isotropic linear elastic. Studies by Herchenhan et al [91] and Reese et al [92] had also presented the tendon as a composite to explain the high Poisson's ratios that occur in tendons.

A 3D FE model was employed by Rawson et al [31] to observe the stress distribution in the tendon tissue when a load was applied to a sutured tendon repair. The behavior of microstructure tendon tissue was assumed as a continuous fiber reinforced composite. Tendon tissue was represented using both isotropic and orthotropic linear elastic descriptions. While the suture was described as a homogenous linear elastic material. FEA and laboratory results were validated for a sutured tendon repair model subjected to tension. The study observed that the stress was low at the cut ends of the tendon due to lack of tensile stress. The presence of the suture resulted in a high stress around the suture in contact with the tendon.

To analyze the internal stress distribution of composite materials, researchers employed several analysis methods such as the shear-lag theory and the FE method [93]. Shear-lag models were used successfully to calculate the stress concentrations and/or ineffective length in fiber composites. Many early analytical shear lag models were developed to predict the stress redistribution around broken fibers: first, for 1D [94], then extended for 2D [95]–[97]. However, recent efforts have been made to propose and develop a 3D shear lag model for simulating the mechanical behavior of fiber reinforced composites [98]–[103] in spite of the fact that it is computationally intensive.

The shear stress concentration in an axially symmetrical model of a single filament glass-resin composite under tension had been calculated by Carrara and McGarry [104], utilizing the FE method. Various fiber end geometries and aspect ratio of the fiber were used. The results show that the distribution of stresses near the end were depended strongly on the geometry of the fiber end. Also, the shear stress concentration had exhibited a minimum at the longitudinal axis equal to twice the fiber diameter. The FE results of stress patterns in the matrix were compared with the previous experimental and analytical data.

2.6 Shortcomings of existing literature

It is observed from the literature review that several investigators have used the suture materials and tying techniques to improved tendon repair strength. Until today, there is no superiority of one construct (material or configuration) over another. Further, several biomechanical studies and reports in the literature throughout the years have attempted to identify the biomechanical properties of FiberWire [53], [59]–[63], [105]–[107] and the importance of suture material on the strength of tendon repair [31]. The existing research studies have compared or assessed the knotted suture based on the evaluation of the gross mechanical performance of knots using FiberWire versus other sutures. However, none of the previous research studies have investigated the details effect of knot configuration and tying technique on the mechanical performance of FiberWire suture. Also, how it influences the tendon failure mechanisms and load carrying capability. on the other hand, only a few computational models exist that describe the effect of knot configuration on the failure mechanism. Moreover, it seems clear that there are concerns about tying of Fiberwire and its impact on the knot in terms of strength and security [66].

FiberWire suture is a common pattern for surgical repair of tendon and other soft tissue injuries [17], [48]. Due to the complexity of interactions between the core and jacket, none of these studies have provided an important comparison of the mechanics of failure under any type of loading. Further, none of the previous studies have reported the behavior of the core and jacket of No2 FiberWire separately.

Tying secure knots is essential in surgery and is challenging for the surgeon [108]. A lot of practice is needed to achieve reliable and reproducible knots every time [109]. Therefore, knot modeling plays an important role in the development of surgical repair. It has

been known that FE modeling is a beneficial tool can be used to analyze the strength and behavior of knot by assessing the stress concentration areas.

In fact, they were a study have been achieved by Rawson et al [31], all be it for a different purpose, which was to observe the arising stress and deformation in the tendon tissue, not the suture. Rawson created a 3D FE model tendon and suture to predict failure location of suture repairs model subjected to tension. The numerical results were correlated with laboratory results, thus deeming their attempt a success. But at the same time, the effect of knot configuration and tying technique on the tendon repair were not considered in Rawson work. Therefore, the development of a FE model can describe the effect of knot configuration on the tendon repair remains an area of intense research and may be helpful to improve the tendon repair.

CHAPTER III

MONOFILAMENT SUTURE

3.1 Introduction

Monofilament nylon is one of the suture materials that has been historically used in vitro for biomechanical testing of tenorrhaphy patterns [110]–[112]. In medical terminology, tenorrhaphy is a surgical suture to hold a divided tendon together. Nylon is a polymer that is the most common and popular medium used to extract the monofilament fishing line. Monofilament sutures are made of a single strand of material. This structure has several advantages, such as low-cost manufacturing, various strength levels, abrasion resistance, and less resistance to passing through tissue than multifilament suture. Also, monofilament suture has a minimal tissue reaction and anti-bacterial properties upon degradation [110], [111], [113]. Because monofilament suture construction is stiff, intense care must be taken in handling and tying those types of sutures. Hence, crushing or crimping this suture may happen and that can weaken the suture and lead to undesirable premature failure [114].

Biomechanical bench top experiments have attempted to identify the relation between the strength of the repair and the type of suture, the tying technique, and the configuration of the suture loops. Thus, small changes in knot configuration may produce different apparent mechanical properties for the surgical construct. The effect of knot configuration on the strength has not been well quantified. In addition, there exists a lack of numerical simulations that describes the effect of knot configuration on the failure mechanism of surgical sutures [31].

Due to the complexity of modeling multifilament suture structure, a sequential approach is conducted. Monofilament structure is chosen in this study to simplify the model. Moreover, monofilament sutures are not expensive, available, and known mechanical properties. Subsequently, this chapter includes experimental and FE studies of (non-knotted / knotted) monofilament sutures. The objectives of this chapter are: (1) testing the (knotted/ non-knotted) sutures to specify the breakage load, failure mode, mechanical behavior, (2) proving the validity of the designed fixture to inspect the suture, (3) validating a simplified biomechanical FE model of homogenous non-knotted suture versus experiments, (4) developing and validating a 3D FE model of a single throw knot to investigate the effect of knot configuration on the mechanics of the suture, (5) Non-knotted sutures and knotted sutures of single, two, and three throws-knots are tested to failure in a laboratory setting. In this investigation, gross loads are compared when the knot reached a localized material yield stress in the model or when the failure occurred in laboratory tests that have the same suture configuration.

3.2 Methods

3.2.1 Mechanical testing

To obtain material properties and validation data for the FE model, an experimental study was performed on a monofilament suture to determine the gross load and strain response of the suture in uniaxial tensile load parallel to the fiber direction. The specifications of the monofilament suture (nylon) were (Model: M1460, LB test: 60 Ib = 266.8 N, Brand: south-bend) [115]. Subsequently, three different throws-knots were investigated in this study.

3.2.1.1 Non-knotted suture

The experimental setup of the suture and the fixture was shown in Figure 5. The setup-controlled suture stretching and suture digital images acquisition. The experimental fixture consisted of two pulleys made from aluminum with a diameter of 63 mm; each pulley had a "V" shaped groove and compression plates to grip the suture as depicted in Figure 5(A). The groove in each pulley secured the suture and prevented lateral migration during testing. The compression plates were slotted, and the depth of the slot varied from the suture diameter to zero at the two ends. This slot provided support for the suture material and made the load transfer more gradual than if the slot was not presented. These slots minimized the stress concentration and prevented breakage of the suture material in the clamping area. Compression across the thread was applied using two screws. The plates and pulleys were connected to a MTS Bionix servo hydraulic load frame (Model 370.02 Axial+Torsional, Eden Prairie, Minnesota, USA) in the Advanced Composite Laboratory / Western Michigan University. An electromechanical device (Interface load cell, S-Type, model SM-100Ib) was used to record experimental tests data precisely. The load cell was linked between the top pulley and the top section of the MTS machine as depicted in Figure 5(A). The specimen was aligned along the axis of the load frame. Figure 5(B) shows the schematic drawing of the fixture.

The experimental protocol was adapted from a prior biomechanical study [60]. The terminal end of the suture was compressed between the plates. The suture was wrapped over the pulley to align with the gauge section. Two dots of 2 mm diameter identified the gauge section (Figure 5) to allow the image-based strain calculation. In addition, dots were placed

close to the plate edges to allow visual detection of slippage during the test. Slippage was not observed.

A 10 N tensile preload was applied to each specimen to establish a reference position. The reference position provided a well-defined starting point for data recording. Also, the reference position prevented potential errors produced from slack in the construct (not tight) in the loops and stretching of the suture materials and ensured consistency in actual length. Displacement was applied at the pulley center at 0.5 mm/sec up to failure and an initial length of the sample of 150 mm. At present, there was not any standard or official procedure giving gauge length or other testing conditions for suture tensile strength measurements. The 150-mm gauge length was mentioned in technical application reports [116], [117], which described tensile testing of surgical sutures using straight-pull test. Hong, et.al [118] used a similar procedure when testing the mechanical behavior of monofilament sutures. Displacement and axial force were recorded at 102.4 Hz. Images were captured with a high-resolution camera (Canon- micro lens 100 mm and Canon-VIXIA HF R42) and achieved approximately 2275 pixels longitudinally between the dot centers and 50 laterally across the thread. Longitudinal and lateral strains of the suture were primarily computed from imaging: tracking both dot centers and the changing in the average diameter along the suture length respectively. Image-based strain was found to be in approximate agreement with a strain measure based on pulley center-to-center displacements of MTS-machine.

The accuracy of the entire setup was determined by marking the two dots from a specific distance at the middle of the suture. These dots were used to detect the strain in the axis of stretching as described below and as depicted in Figure 5.

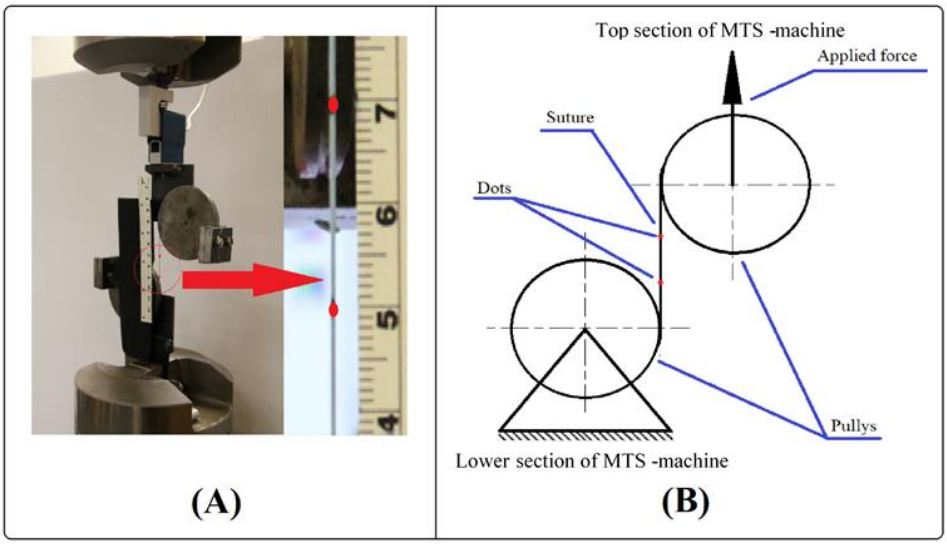

Figure 5: (A) Full apparatus of the suture prior to tensile test (experimental setup), (B) Schematic diagram

3.2.1.1.1 Image methodology

The camera was positioned such that the whole suture could be viewed in the imaging window. To overcome possible errors, the center of the camera's lens was approximately aligned with the suture center. As the camera was stationary during the test, the changes in suture strains were calculated according to the relative movement of the dots. The relative movement of the dots was considered with reference to an undeformed suture image. The suture images were captured using the timer command of the camera. The images were captured every 0.1 sec. This process resulted in a series of images at different strokes during stretching the suture uniaxially.

The methodology of image thresholding was adopted. A limited number of pixels within a defined neighborhood was analyzed to avoid the non-uniformity of light distribution and/or variation in the surface material grains. The imperfect threshold, especially around the

edge of the dots, may have contributed to some errors in the results. Therefore, the size of the dots had to be kept small to eliminate the chances of error in locating the dots' centroids.

3.2.1.1.2 Procedure validation

To validate the previous procedure of obtaining suture tensile strength, the procedure was again applied on a music wire steel of gauge #10 (diameter 0.610 mm). The theoretical value of tensile strength and elastic modulus are 2350-2600 MPa and 207-210 GPa respectively [119], [120]. A reasonable coincidence between the theoretical and the experimental tensile strength values was gained as shown in Figure 6.

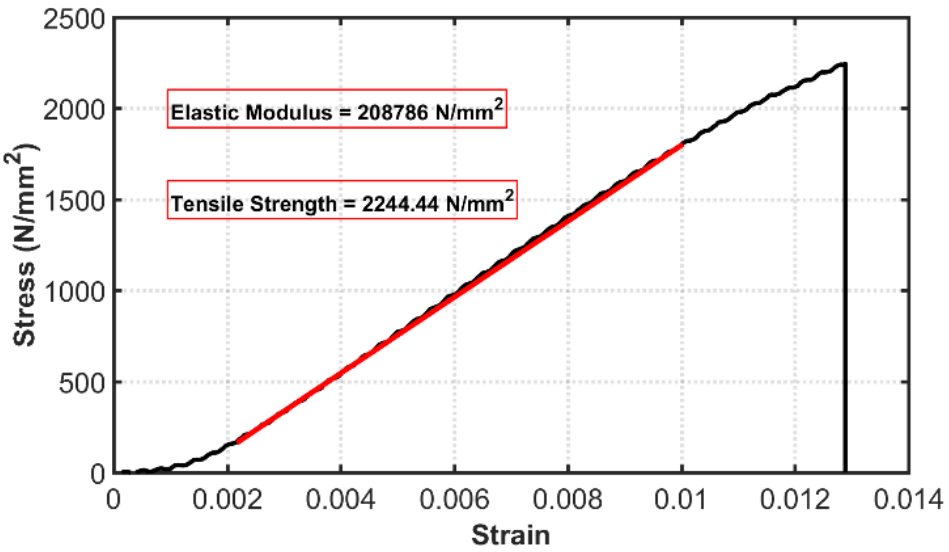

Figure 6: Stress-strain curve of the music wire steel

3.2.1.2 Knotted suture

This experimental setup was different than that of the non-knotted suture. The difference was that the two grips were made of steel and each grip consisted of a fixed plate and a movable plate to grip the suture. The plates were connected to a MTS-machine. To establish a reference position, the sutures samples were placed at a distance 38 mm from the

two grips. A load cell (Interface model SM-100) was used to record load. Load extension curves of knotted sutures were obtained using a constant-rate-of-extension, which was 0.5 mm/sec up to failure and an initial length of the sample of 40 mm, as shown in Figure 7. At present, there was not any standard or official procedure giving gauge length or other testing conditions for knotted suture tensile strength measurements. All samples were tested at the same gauge length to compare knot properties of different number of throws.

The experimental protocol consisted of using the ear method [30], [121]. Three different types of throws (one, two, and three throws) were implemented in this investigation as shown in Figure 8. To minimize knot variation, the study had one person tied all the knots [122]. Five samples of each throw type and suture type were tested. Each sample was looped over a standardized stainless-steel rod of a diameter 10 mm that provided a consistent starting circumference for each throw during laboratory tests. The completed suture loops were removed from the standardized rod and loaded onto MTS-machine. The free ends of the sutures were secured with the clamp plates, then the two plates were tightened [123], [124]. Two dots were placed close to the plate edges to allow visual detection of slippage during the test shown. Slippage was not observed. The following variables were recorded for each suture sample (n=5): (1) the load at failure, (2) the displacement at failure, (3) the stiffness as the ratio of load to displacement on the linear portion of the load- displacement curve, and (4) the location of material failure.

A 10 N tensile preload was applied to each specimen to establish a well-defined starting point for data recording and to avoid potential errors produced from initial slack in the suture loop. This is similar to the technique described by [59], [122], [125]–[127]. The axial displacement and the load were recorded at a rate of 102.4 Hz during the test.

Displacement measurements were taken from grip-to-grip values. A load–time curve was recorded per each sample by tracking sample response across the applied displacement increments. For each load–displacement curve, the peak load, the stiffness, and the elongation were determined. The mean peak load and mean stiffness data were calculated across all samples for each throw type. Maximum load was calculated as the ultimate failure strength of the suture. For each test, a Canon EOS 60D camera and EFS 18–135mm lens was used to record video of knot failure.

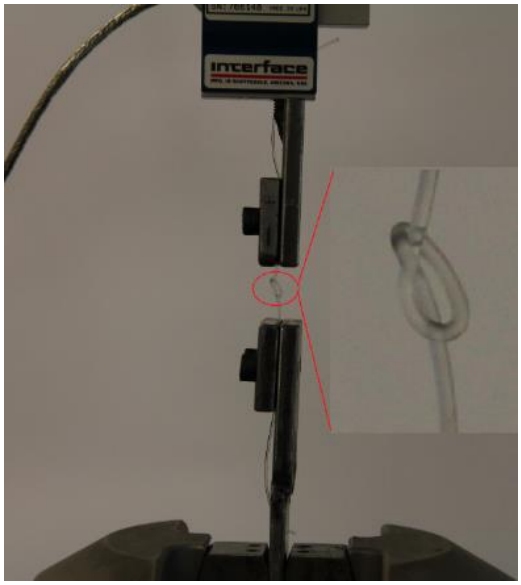

Figure 7: Testing device for monofilament suture load-extension (scale in (cm))

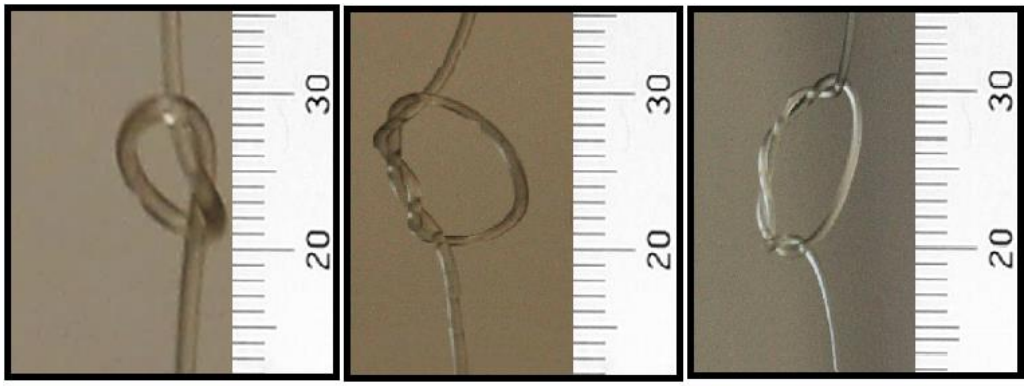

Figure 8: Examples of the throws, monofilament suture, (Approximate scale (mm))

3.2.2 FEA models

3.2.2.1 Non-knotted suture

The material properties of the monofilament suture were determined through experimentation. ABAQUS (Version 6.16, Dassault Systemes Simulia Corp.) was used to create a three-dimensional FE model of the monofilament suture. The model was composed of reduced integration hexahedral elements (C3D8R). The suture was assumed homogenous and isotropic elastic.

Displacement control was applied at end of the suture; the other end was fixed. Mass scaling was used to increase the stable time increment; thus, the knot was modeled assuming a quasi-static load in an explicit dynamic model. The ratio of kinetic energy to internal energy was monitored to ensure the mass scaling and a quasi-static assumption was appropriate.

3.2.2.2 Knotted suture

Considerations should be taken to maintain stable knots and to produce a basic model adequate for this undertaking. It was necessary to tie knots in an effort to simulate suturing in FE. To do this, a sturdy and integral dynamic model was required to provide a firm solution for the detection of the collision among the materials; this collision can result in deformed self-converging shapes that no longer have integrity. There were several interdependent difficulties that would be addressed by this work and were reveal instabilities that might lead to systematic divergence. The knotted models were generated using points in 2D plane. Those points were lately extended to 3D space. There were several problems in this method to obtain a geometry that was smooth and mimicked the experimental knots. Knot slipping or a

degenerate oscillatory behavior caused the divergence. The high curvature of the rope, opposing internal forces, and multiple collisions generated a potentially unsteady state around the area of knot tightening. Generally, numerical errors were aggregated quickly.

There was a wide range of potential applications that interface with the mechanics of knots, which had not evolved to a highly-sophisticated level. To go beyond a purely geometrical configuration of knots, the theory of elasticity was normally used to inform the problem. The instance of tight knots leads to the problem of 3D elasticity with geometrical nonlinearities (finite rotations), finite strains, and self-contact along an obscure surface. FE analysis of this issue raised compelling challenges as well, which had not yet been handled, such as nonlinearities due to contact.

Abaqus was used to create and solve the monofilament suture consisting of a single throw knot. The model was composed of reduced integration hexahedral elements (C3D8R). The suture was assumed homogenous and isotropic elastic. Knots involved complex contact conditions, self-contact, and large deformations; therefore, an explicit dynamic solver was used to overcome these severe nonlinearities, Figure 9.

Displacement control was applied at 0.5 mm/sec at end of the knot; the other end was fixed. Mass scaling was used to increase the stable time increment; thus, the knot was modeled assuming a quasi-static load in an explicit dynamic model. The ratio of kinetic energy to internal energy was monitored to ensure the mass scaling and a quasi-static assumption were reasonable.

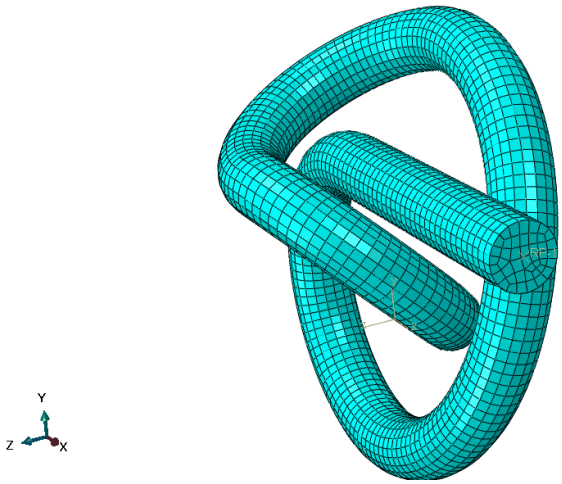

Figure 9: The knot mesh

3.3 Results

After finding the material characterization and the mechanical properties of the monofilament suture, two types of comparisons were made to differentiate the impact of a knot topology on the mechanical behavior of the suture. First, a comparison was made between the experimental results of the three knots (single, two and three) throws. Second, a comparison was made between the experimental and the FE results of a single throw knot.

3.3.1 Experimental results

3.3.1.1 Non-knotted suture

3.3.1.1.1 Material characterization (diameter and density)

The monofilament suture diameter was measured and recorded based on two procedures:

1. Using a digital caliper: the suture diameter was measured at five different locations along the suture length prior to testing and found to have a mean diameter of 0.86 mm.

2. Using the screenshot images: the suture diameter was measured by acquiring the screenshot images of the first image of deformed suture based on the proportional values. Public domain image-processing software named GIMP was utilized to analyze the images. Assuming the cross-sectional area of the suture as circular, the average diameter of the suture was calculated along the suture length and was found to be 0.8586mm. For all sutures, the suture diameter was measured and compared to the properties of a manufactured suture and was found to be correlated.

The mass of "long length" of the monofilament suture was measured using a highly sensitive weight device. Approximate density was calculated from the mass and the computed volume of the suture. For the volume calculation, the cross section was assumed circular and the diameter was assumed to be constant (0.86mm). The density of the suture was calculated and was found to be 1.216*10-3 g/mm3.

3.3.1.2 Mechanical properties

3.3.1.2.1 Poisson's ratio

A sequence of images showing the translation of ink spots marked on the monofilament sutures was analyzed to give longitudinal strain (ε1) and lateral strain (ε2). These several levels of strains were employed to measure Poisson's ratio (υ) as follows: $\upsilon = -(\varepsilon 2/\varepsilon 1)$. Poisson's ratio of monofilament suture was calculated and was found to be approximately 0.4. Figure 10 illustrates the Poisson's ratio values of monofilament suture at various levels of strain.

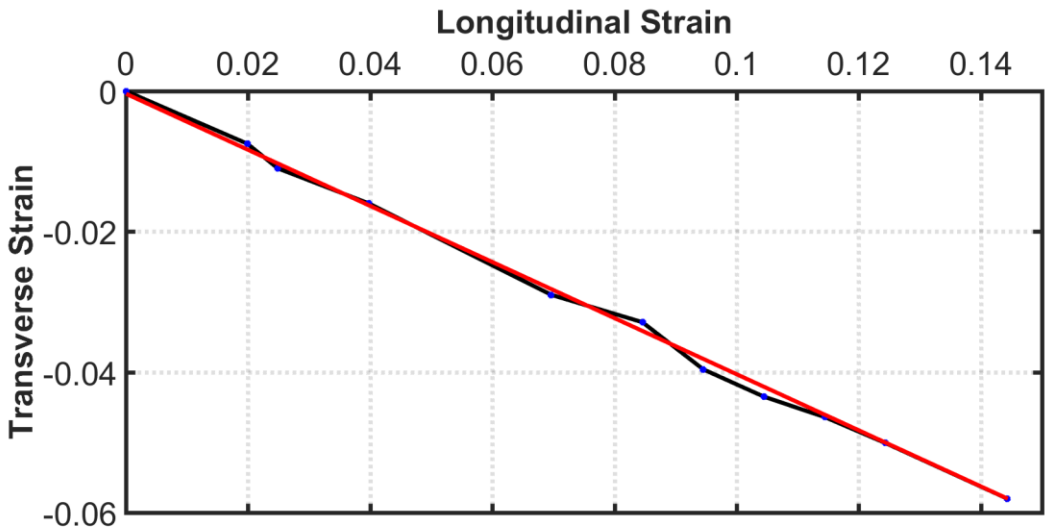

Figure 10: Poisson's ratio of the monofilament suture

3.3.1.2.2 Load and displacement

Figure 11 shows the load-displacement behavior of five monofilament sutures tests in one scale. The average peak load of the five tests to failure was calculated and was found to be 251.5 ± 8.688 N. For all sutures, the peak load to failure was consistent with the properties of a manufactured suture (266.8 N) [115].

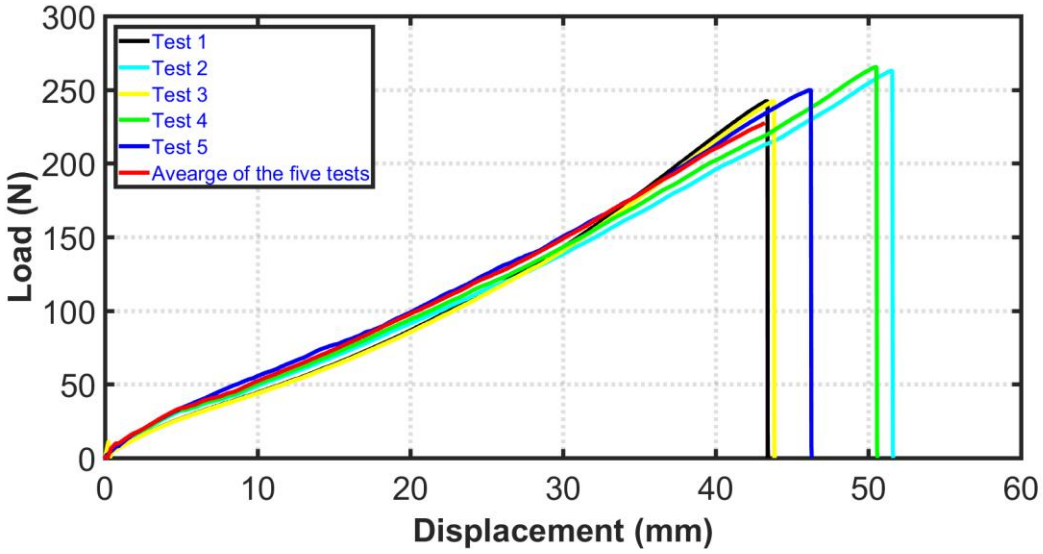

Figure 11: Load-Displacement curves of monofilament sutures

3.3.1.2.3 Stress and strain

Five specimens of monofilament sutures were tested and corresponding images recorded. The homogenized stress-strain curves of the suture (image based and based on displacements) are shown in Figure 12. The primary strain calculations were based on two procedures: pulley displacement and imaging. In image procedure, load and displacement were measured between two dots that were elected by collecting the data from the images that were captured by the camera. As stress = force/area, and strain = change in length/ original length, the average of the stress strain curves of the suture for both of collected data and the MTS machine data were drawn, as shown in Figure 12. Both of the two computed strain outcomes were found to be in agreement. For all sutures, the modulus of elasticity and the maximum stress at failure were calculated and compared to the properties of a manufactured suture and were found to be associated. Modulus of elasticity does not depend on the material

dimensions (cross sectional area and length) and the force exerted on the material. It depends only on the nature of the material.

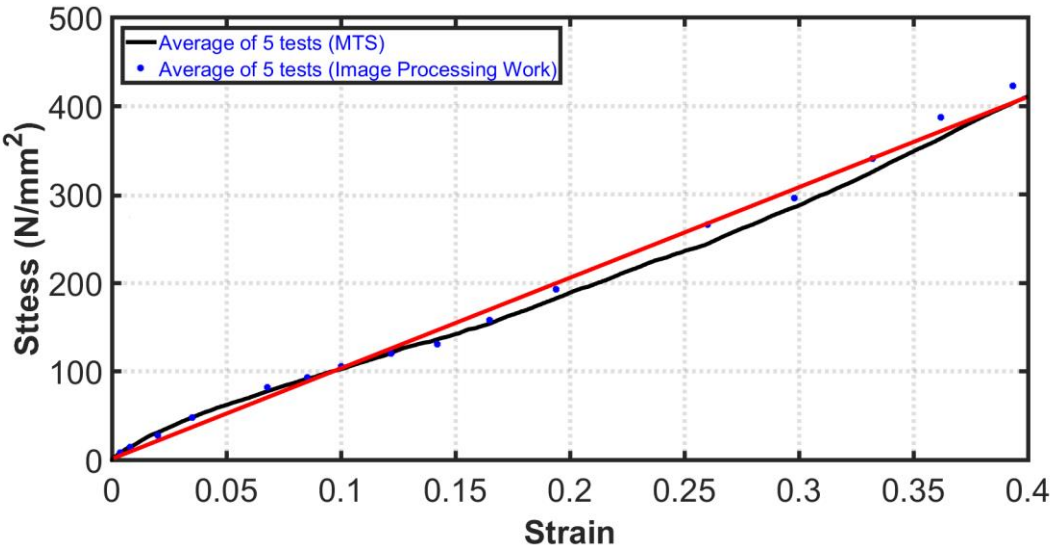

Figure 12: Stress-Strain curve of monofilament sutures

3.3.1.2 Knotted suture

Subsequently, monofilament suture was used to create: single, two and three throws-knots. Figure 13-Figure 15 show the load-displacement curves of failure region of five tests of monofilament sutures for each knot type. Moreover, the figures show that, for all sutures tests, the monofilament sutures had a single load drop. At all the monofilament sutures tests, the failure was occurred adjacent to the knot rather than along the suture. Figure 16 show an example of the picture of failure region. This indicates the influence of the knot and its high stress concentration and friction contact. This result was consistent with published results [7].

Further, the results showed that the required force to break a tied suture was lower than the force required to break an untied suture by 40-50%. That was due to the stresses from bending, twisting, and frictional contact as depicted in Figure 17. This result was consistent

with other studies that have reported that the knot was the weakest part of any suture or ligature when subjected to tension [6, 117, 118]. Also, the mean load at breaking of each throw type was calculated and compared with non-knotted suture as shown in Figure 17. The failure load and elongation were found to increase with number of throws. For five repetitions of monofilament sutures for each knot test, the average load to failure and standard deviation were calculated as depicted in Table 1. These results were compared with other published data and were found to be correlated [58], [130]–[134].

The stiffness was averaged for each group of throws. The process to estimate the stiffness was to take a straight line from the failure load point to the inflection point of the load-displacement curves. Figure 18 depicts the stiffness of monofilament suture at different number of throws. At the knot region, the distribution of strain in the material was non-uniform. This distribution could relate to the breakage point and its impact on the tensile strength of a knotted suture. Further, the overall stiffness of monofilament suture decreased when the number of throws increased as shown in Figure 18. Adding knots to the suture added different deformation mechanisms: bending, contact, and twisting. Each one of these mechanisms had a direct contribution to the maximum load to failure. However, the quantification of these mechanisms was not evaluated due to timing issues and exploring other parameters. In general, adding a knot increased the contact area and the bending deformation. It was worth noting that the models were created without any pre-stresses due to the addition of knots, in essence, the models were created using an idealized initial geometry for the number of throws based on a constant radius for the throws and no stresses were introduced due to this throw creating process. Also, the increase in number of throws included an increase in the suture length. Suture length increase caused an increase in the suture extension.

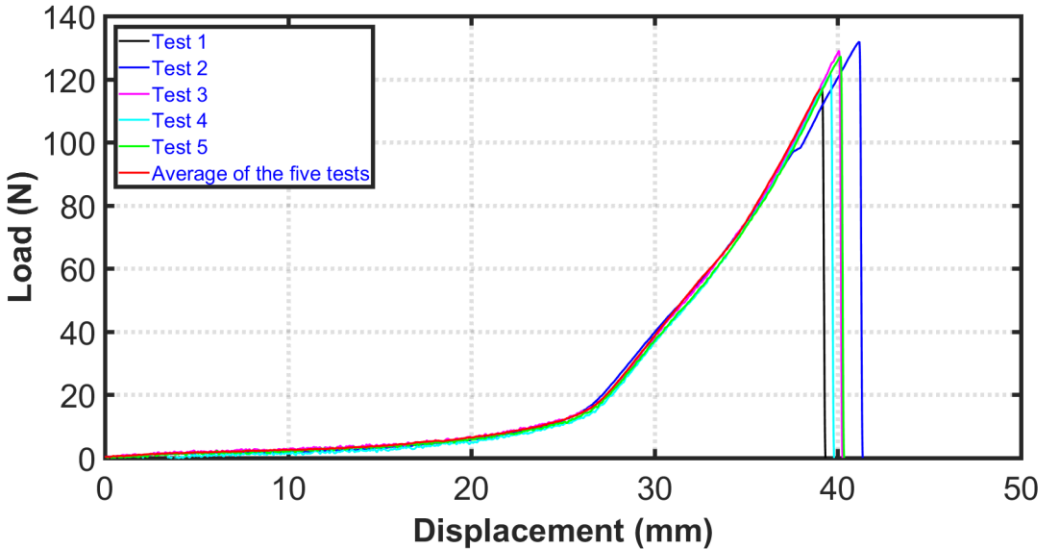

Figure 13: Load-Displacement curve of single throw knot of monofilament suture

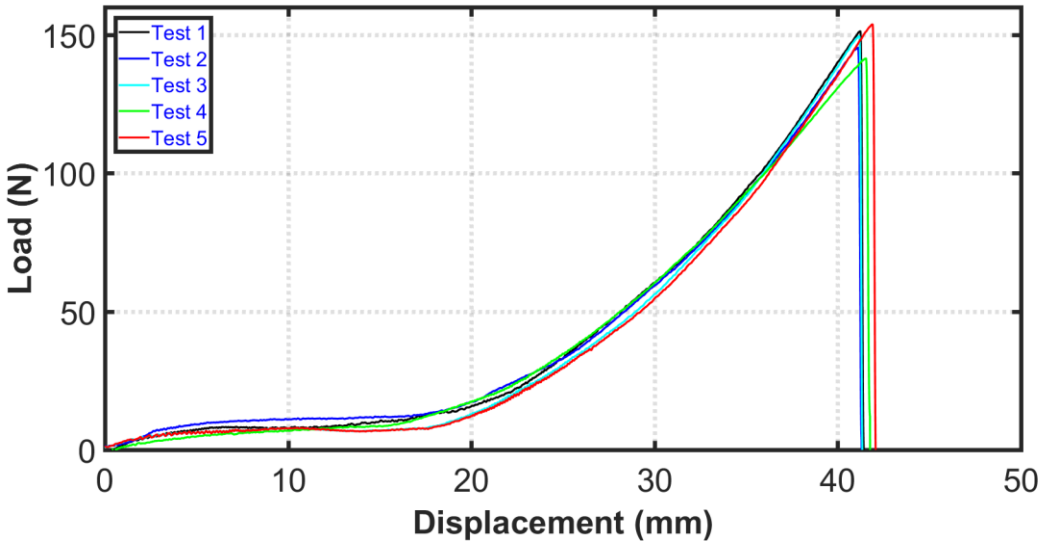

Figure 14: Load-Displacement curve of two throws knot of monofilament suture

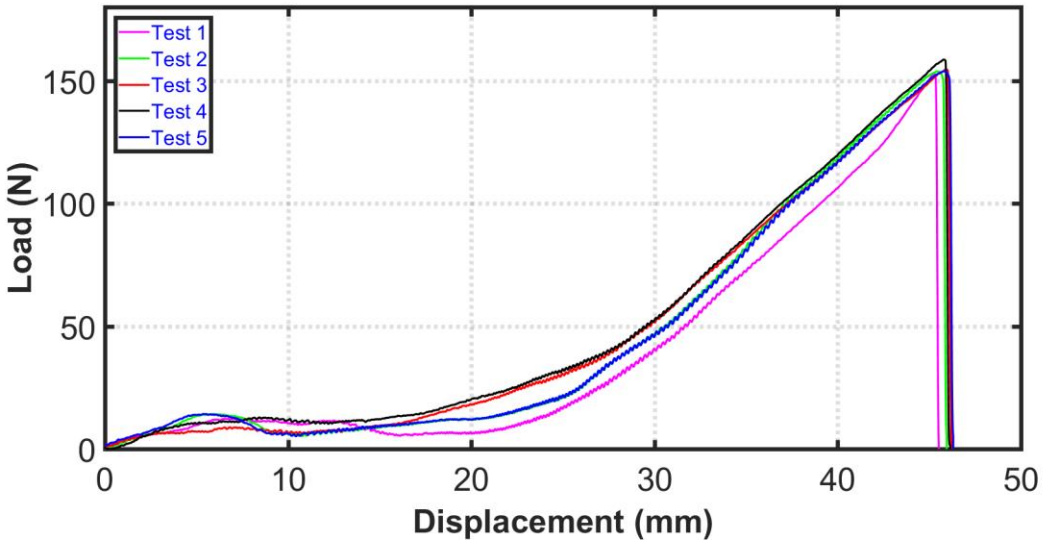

Figure 15: Load-Displacement curve of three throws knot of monofilament suture

Figure 16: An example of failure region of monofilament suture

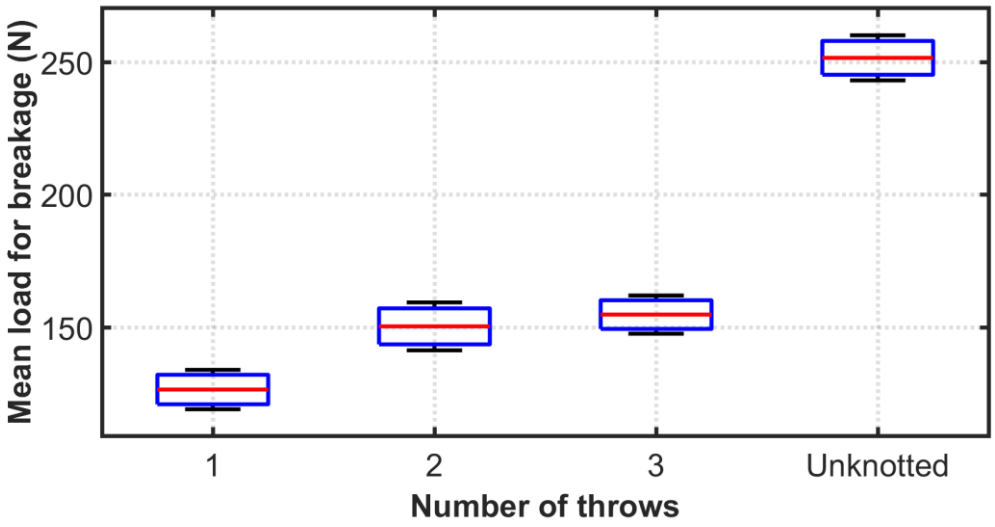

Figure 17: Relationship between the mean load and number of throws, monofilament suture

Table 1:Average load of failure and standard deviation of knotted monofilament sutures for five samples

Number of Throws		
One	Two	Three
126.43±7.42 N	150.24±9.03 N	154.69±7.20 N

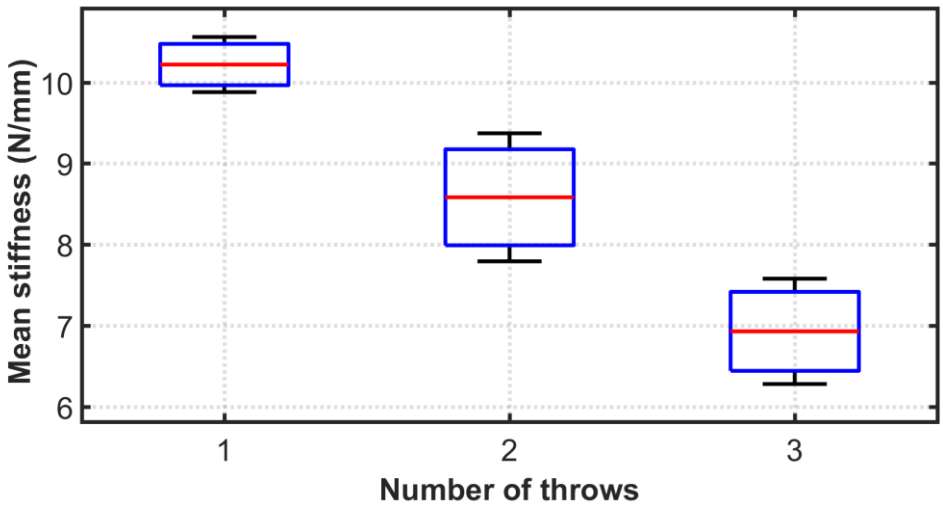

Figure 18: Relationship between the mean stiffness and number of throws, monofilament suture

3.3.2 FE results

3.3.2.1 Non-knotted suture

A 3D FE model of the non-knotted suture was implemented and evaluated considering several parameters. Three parameters were studied as follows:

1. Effect of Poisson's ratio: three Poisson's ratios were considered (0.35, 0.4 and 0.45).

2. Effect of mesh size: three seed sizes were considered (0.1, 0.15 and 0.2).

3. Effect of integration points: full integration versus reduces integration.

The length and diameter of the suture model were 30 mm and 0.86 mm, respectively. Effect of Poisson's ratio on the load-displacement behavior of the model was studied as shown in Figure 19. The results were calculated by using reduce integration points and maximum seeds size. Figure 19 illustrates that the Poisson's ratio had no effect on the results. Integration points represented a very important parameter; the outcome showed that full integration points provided stiffness greater than that of reduced integration points, as shown in Figure 20. Poisson's ratio (0.4) and seeds size (0.1) have been used to solve the non-knotted suture model. A FE model was approximate and it erred by being stiffer. Over stiffness happens by using more Gauss points to integrate element stiffness matrices because additional points capture higher order terms in stiffness matrix [k]. More integration points improved the accuracy of calculations while fewer integration points provided quick computations. Moreover, Figure 21 shows the effect of mesh density on the load-displacement curves. The results were calculated using reduce integration points and Poisson's ratio (0.4). Element edge size was chosen 0.2 mm as a starting point to undersigning it was a coarse mesh. Then, a mesh

sensitivity study was performed using 0.15 and 0.1 mm respectively. The results show that the finer mesh was closer to experimental results.

The average experimental results were compared with the FE model results as indicated in Figure 22. The figure also demonstrated that the FE results were stiffer than the experimental results. For a structural FE, the stiffness matrix contained the geometric and material behavior information that indicated the resistance of the element to deformation when subjected to loading. Such deformation might include axial, bending, shear, and torsional effects. There were several parameters tend to add stiffness to the model (stiffer than the real system): over constrained, redundant supports.

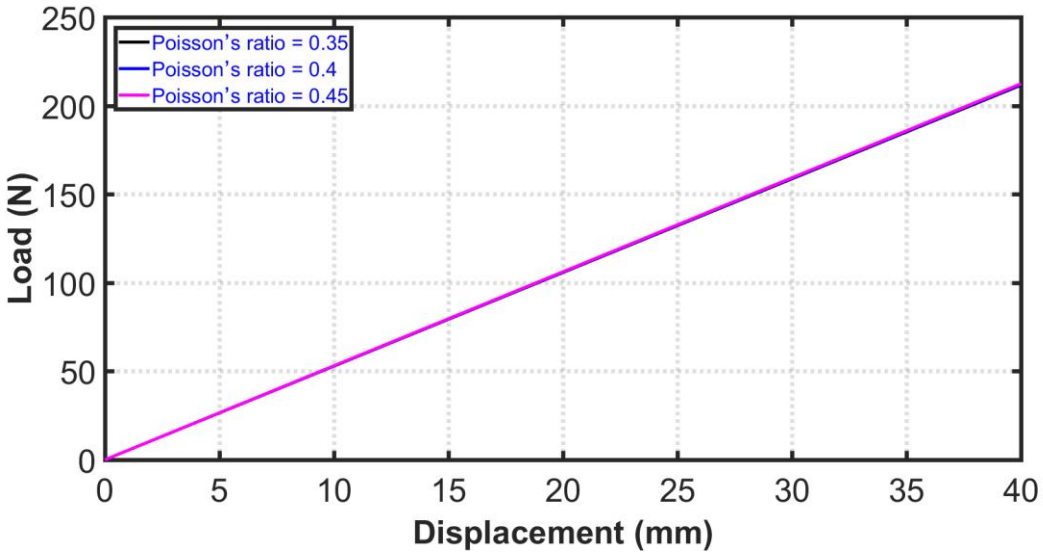

Figure 19: Effect of Poisson's ratio on the load-displacement behavior of non-knotted suture

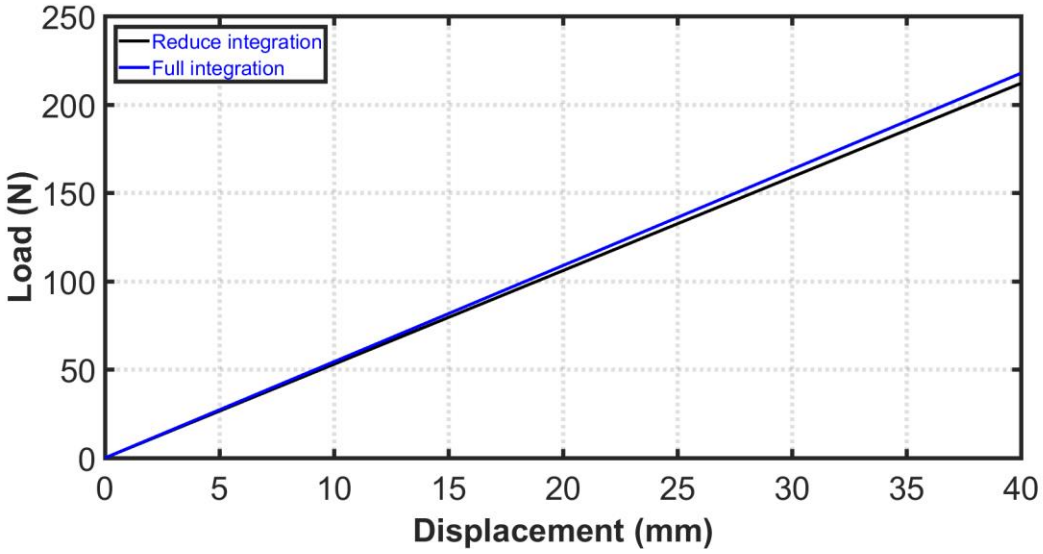

Figure 20: Effect of integration points on the load-displacement behavior of non-knotted suture

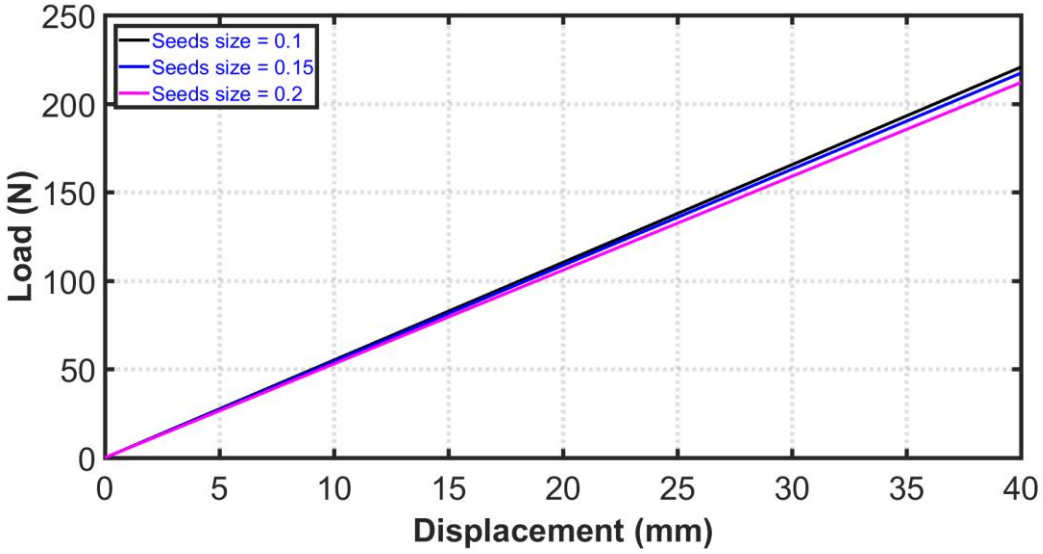

Figure 21: Effect of mesh density on the load-displacement behavior of non-knotted suture

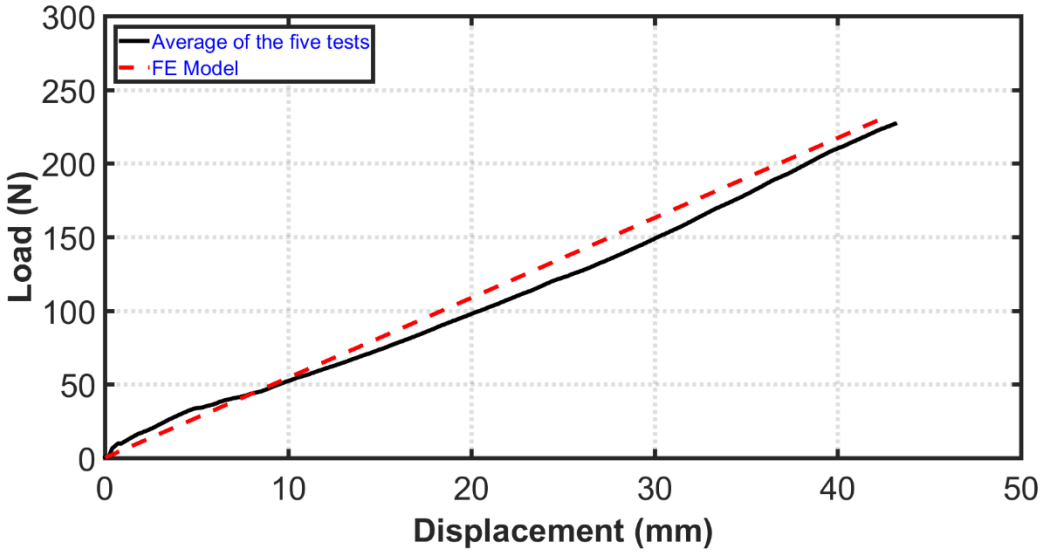

Figure 22: FE versus experimental results of the non-knotted monofilament suture

3.3.2.2 Knotted suture

The material properties of monofilament suture were determined through experimentation. Once the knot had been tightened by pulling the suture ends, its loosening was simulated by fixing one of the ends while applying a tensile force to the other end. The configuration could be characterized by the angle formed by both free tails and by the approximate radius of the loop. Hence, to improve the results of knot model, the effect of friction coefficient, integration points, Poisson's ratio, and mesh size on the model results were investigated.

To increase the time step and reduce the run time, there were three parameters that could be adjusted: element size, Young's modulus, and suture material density. While the mesh could be adjusted to increase the element sizes, this was often impractical in stances when geometries were complex with small features and automatic mesh. Young's modulus represents a material stiffness property, and artificially lowering it will adversely affect

accuracy. Artificially increasing density could also adversely affect accuracy (think force = mass times acceleration). However, the idea of mass scaling was an automated procedure whereby the code increased the time step by scaling up the density in the specific elements that were controlling the time step, as long as it did not significantly increase the overall mass of a part. Mass scaling enabled an analysis to be performed economically without artificially increasing the density. Mass scaling was a try and a proof method which was often used in Abaqus/Explicit for reducing run times in quasi-static analyses. Hence, the velocity was low and the kinetic energy was very small relative to the internal energy. It was possible to implement mass scaling effectively in the model using either fixed or variable mass scaling, but it should be done carefully. Validation required checking both the relative increase in mass, as well as the location of the added mass. Only very small amounts of mass should be added in locations where critical results were being evaluated [135].

3.3.2.2.1 Effect of coefficient of friction on the knot model results

Friction was a complex phenomenon and it was typically characterized by a coefficient of friction, which was the ratio of the frictional resistance force to the normal force that presses the surfaces together. The coefficient of static friction and plasticity of a given material had a direct bearing on the security and strength of the knots. Thus, the assumed friction coefficient might be an influential parameter on the FE results. The effect of the friction assumption was quantified over the range of 0.0 to 0.4 as shown in Figure 23. The outcomes refer to the fact that the amount of force necessary to cause a knot to slip was proportional to the frictional force, which was dependent on the coefficient of friction. The maximum load to tie a knot changed approximately by (40N) within the minimum and maximum limits of coefficient of friction. Further, this result confirmed the view that the coefficient of friction was a function

of various variables, including suture structure, suture material, and applied load. Therefore, the coefficient of friction should be investigated further.

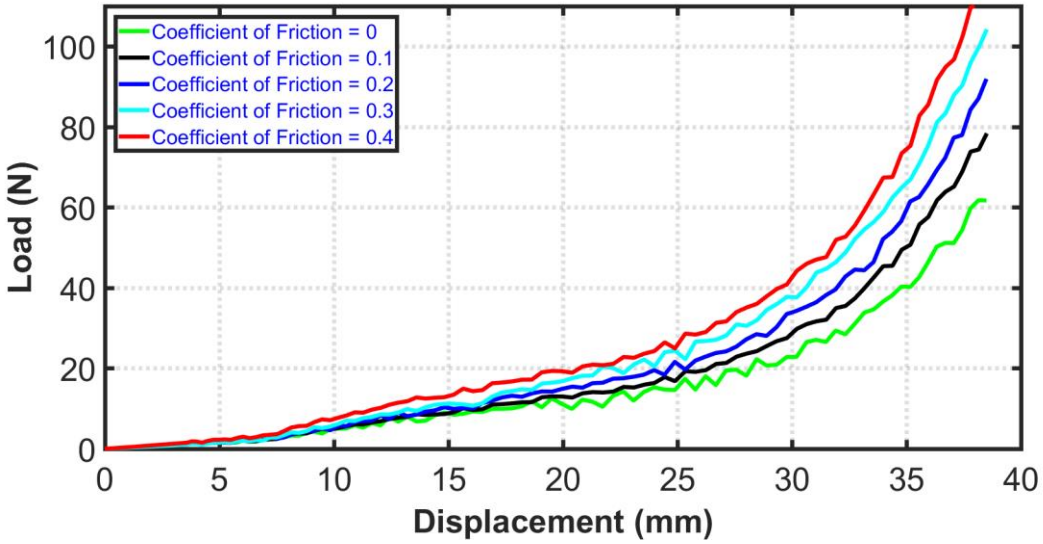

Figure 23: Effect of frictional coefficient on the load-displacement results of the knot model

3.3.2.2.2 Effect of integration points and Poisson's ratio on the knot model results

Figure 24 shows the effect of integration points on the results of the knot model. The outcomes also show that the full integration points provided stiffness that was higher than that of reduced integration points. The full integration points result was closer to the experimental data. The results were calculated at the Poisson's ratio (0.4). Also, the reduce integration points had a good agreement with experimental data and reduced time of FE solution. The Poisson's ratio had an insignificant impact on the results as shown in Figure 25. The changes in the Poisson's ratios caused relatively small changes in the cross-section area.

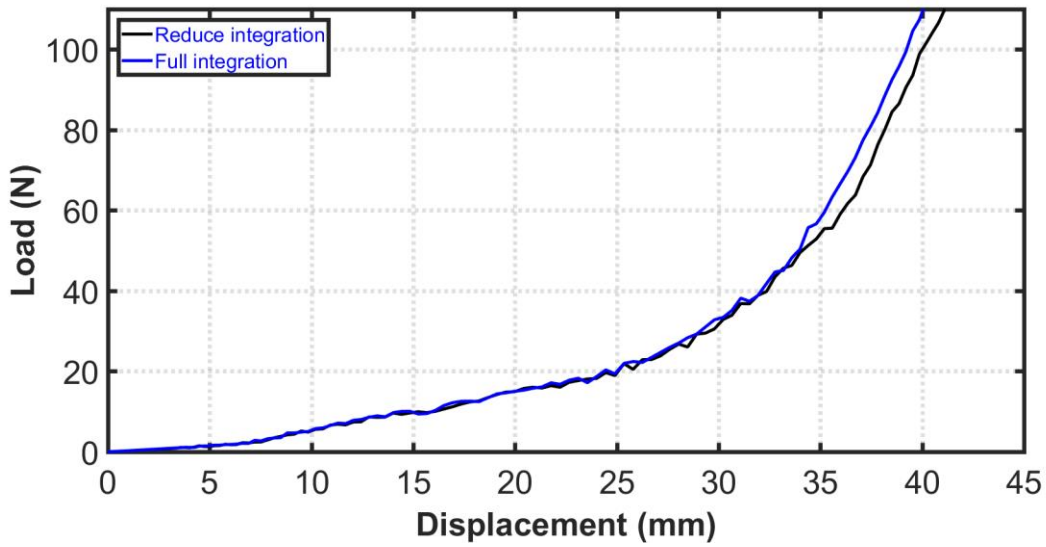

Figure 24: Effect of full integration and reduce integration on the load-displacement results of the knot model

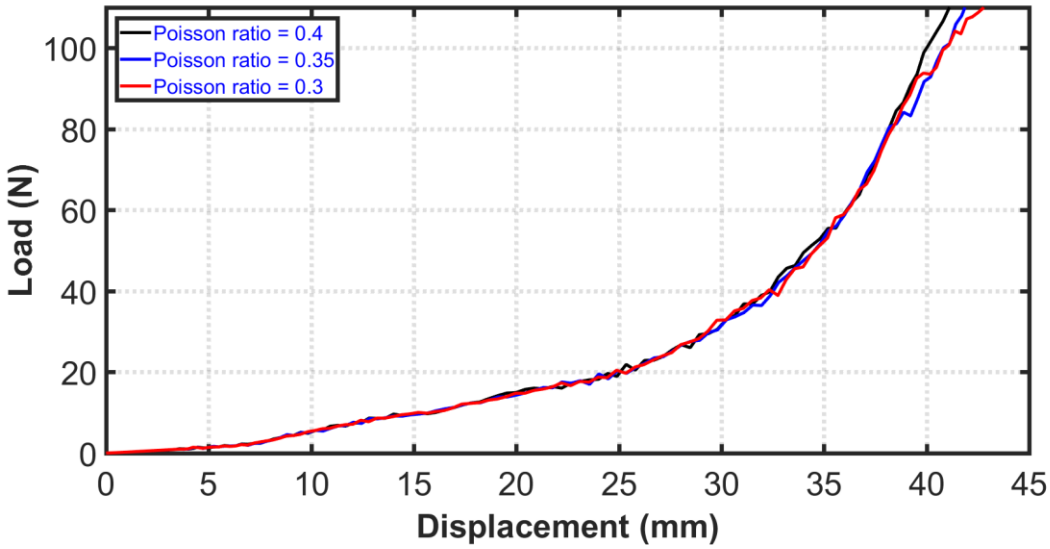

Figure 25: Effect of Poisson's ratio on the load-displacement results of the knot model

3.3.2.2.3 Effect of mesh size on the knot model results

Figure 26 depicts the effect of mesh density on the load-displacement curves and demonstrate that the proceeding figures where the results of a converged mesh. Four seeds sizes were implemented in this investigation (0.2, 0.15, 0.1, and 0.05). Although, the mesh

convergence study showed that the course mesh had more “noise” (variations in load) than the fine mesh. However, the loads predicted by the finest meshe (Seeds size: 0.05) were in closer agreement with experimental results.

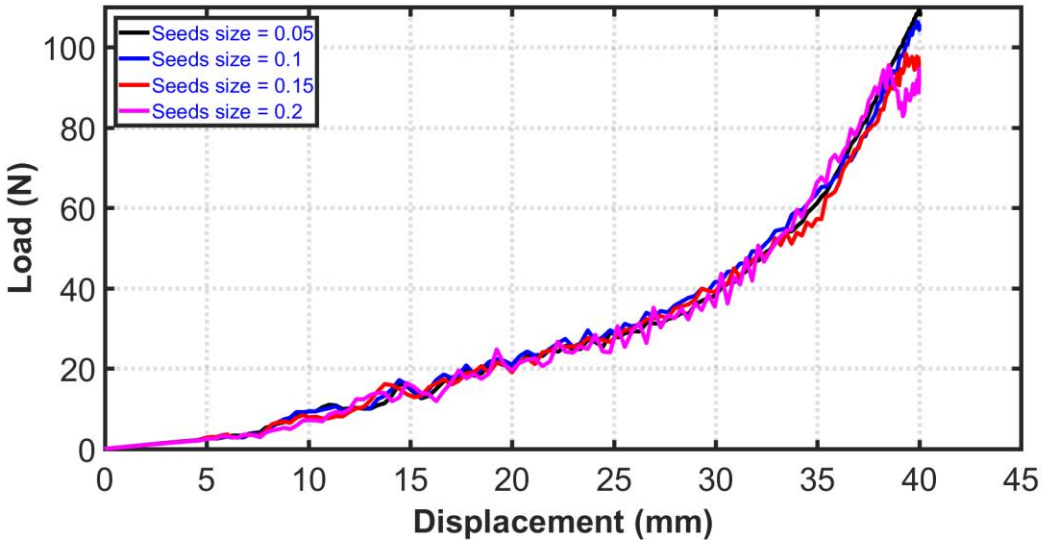

Figure 26: Effect of mesh density on the load-displacement results of the knot model

3.3.2.2.4 Knot model results

Three models of throw-knots were created: one, two, and three throws as depicted in Figure 27. The FE results of single throw monofilament suture were compared with the experimental results. The consistency of single throw monofilament suture FE results with experimental results is shown in Figure 28. It was worth noting that the FE results were stiffer than the experimental results. This could be attributed to a number of parameters associated with the FE model. In addition, the FE model results predicted strength of a tied monofilament suture was lower than an untied suture, this fact is evident as depicted in Figure 11 and Figure 28 respectively.

Figure 29 shows the scenario of tying a single throw knot of monofilament suture. Loads were small until the knot tightened, and the subsequently the load increased with additional applied displacement. The predicted stresses and strains were in locations that are qualitatively consistent with expectation. The FE results shown in Figure 29 supports the fact that the maximum stresses existed at (and/or) around the knot. Deformation of the knot model is shown in Figure 30.

Figure 31 clarifies the internal energy and kinetic energy in a logarithmic scale. The figure illustrates that the total kinetic energy of the model was found to be small relative to the strain energy over the whole loading cycle, excluding the initialization where strain was very small. The kinetic energy was small and less than 1% of the internal energy in critical phases. Therefore, it was deemed reasonable to treat the results as quasi-static. With a simulation in a quasi-static analysis, the inertial forces were already established and were negligible because the velocity of the material in the model was very small. The results overwhelmingly supported the corollary to both of these conditions was that the kinetic energy might not exceed a small fraction, typically 5% to 10%, of the internal energy throughout most of the process [135], [136].

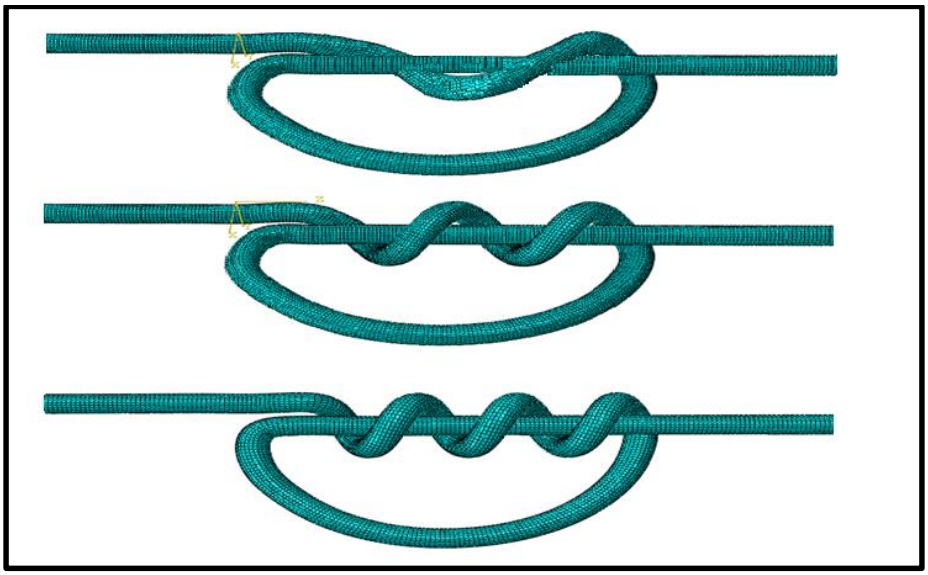

Figure 27: FE models of single, two, and three throws knot

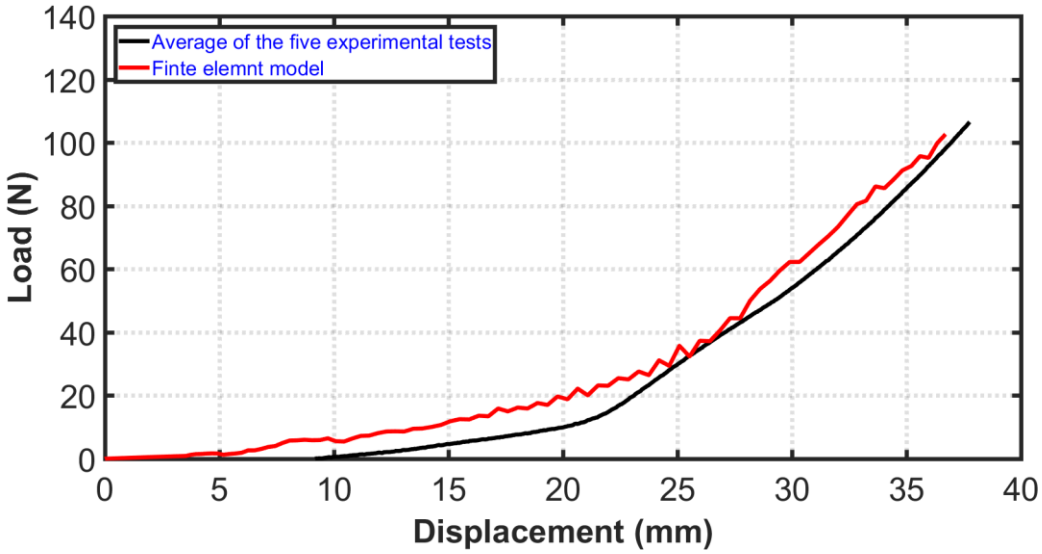

Figure 28: Experimental versus FE model results of single throw model

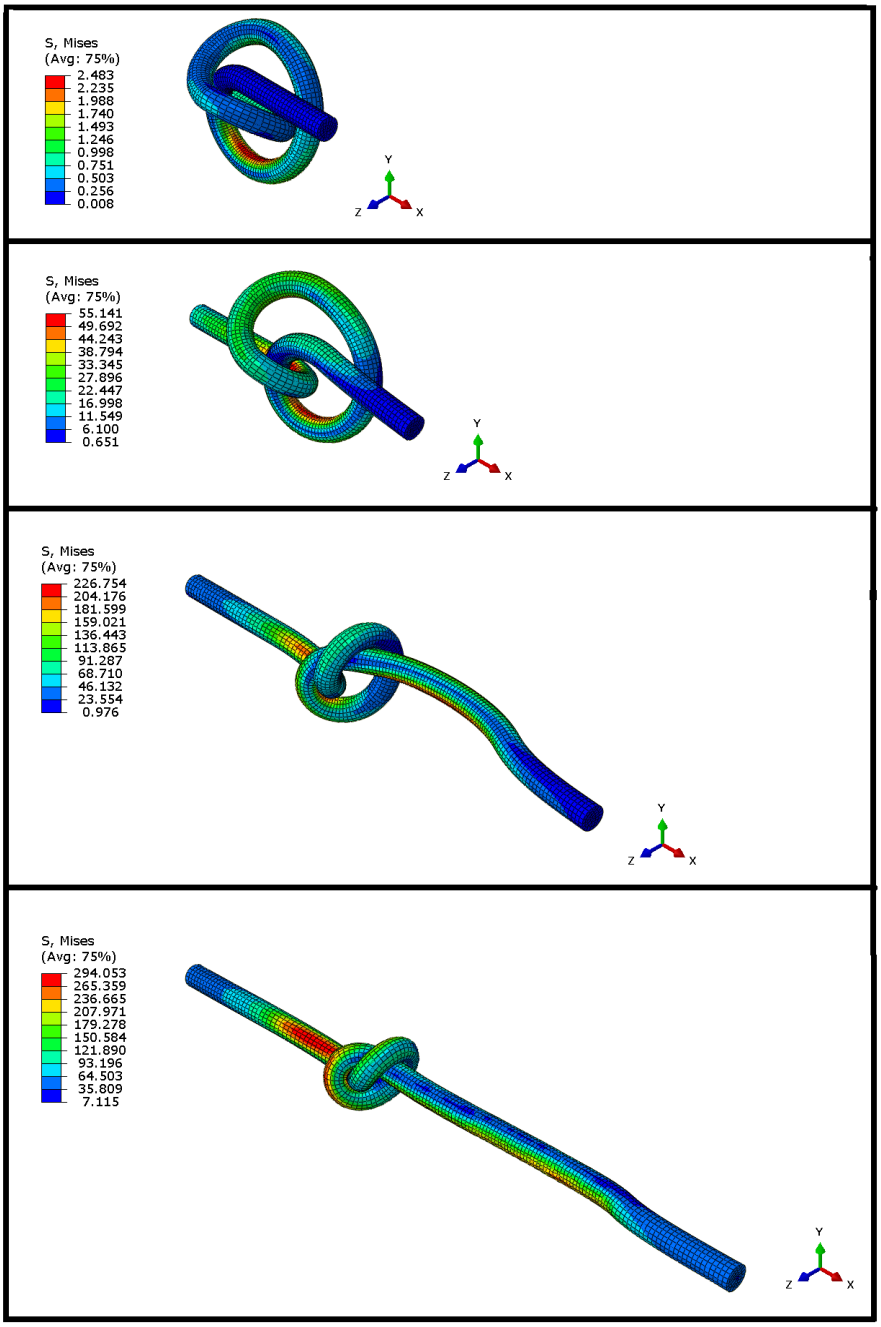

Figure 29: Von Misses stresses of single throw model. Stresses in (MPa)

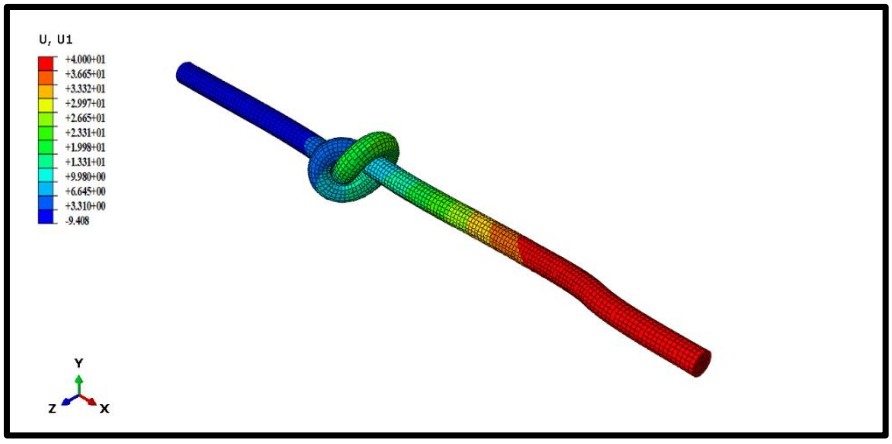

Figure 30: Deformation of single throw model. Deformation in (MPa)

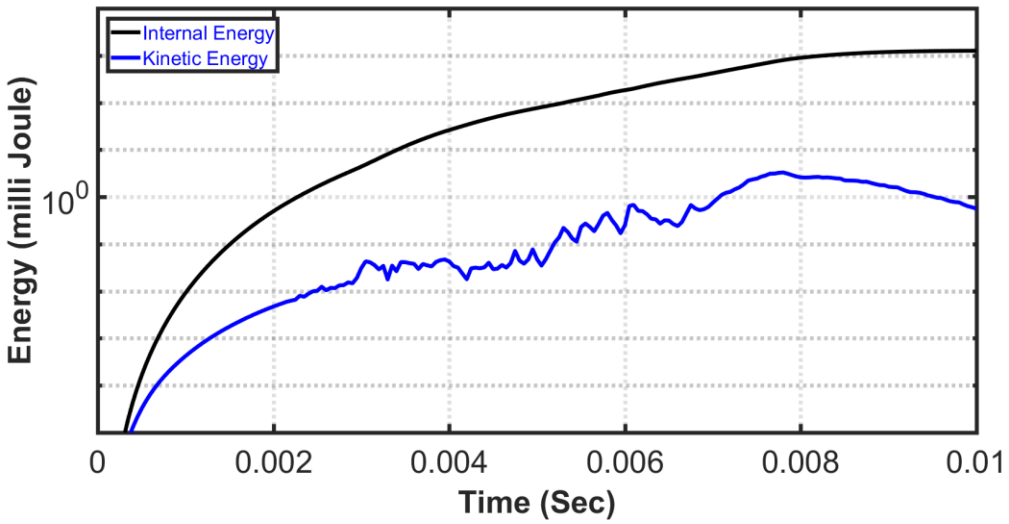

Figure 31: Internal energy and kinetic energy in logarithmic scale of single throw model

3.4 Discussion

The pulley fixtures ensured that the suture failure occurred between the two pulleys for all tested suture samples. The diameter and average peak load of the tests to failure were compared to the properties of a manufactured suture and were found to be well correlated. Furthermore, there was no significant slippage observed in any of the samples. The force necessary to cause a knot to slip was approximately proportional to the assumed coefficient

of friction. However, the differences in force in this phase were small relative to the forces required to lock the knot.

The difference between load-extension curves of knotted and non-knotted sutures provided useful information to identify the knot strength. The single throw knot resulted in ~50% strength reduction relative to untied suture and was consistent with published results [6], [128]. This was due to the stresses from bending, twisting, and the stress concentrations from knot frictional contact. Other studies had reported that the knot is the weakest part of any suture or string when subjected to tension [6], [7], [128], [129]. The FE models result of the single throw knot were qualitatively correct and were based on the experimental outcomes. Also, the model result was stiffer than the experiments by approximately 10%. Further, the failure load increased experimentally with increasing number of throws. The limitations of the current study were the following:

(1) The contribution and quantification of the stress concentrations at the knot region due to bending, twisting, and contact were not separable in the FE model so their relative contributions are not completely known. Further, they will be impacted by the assumption of initial geometry.
(2) FE model results were reported only for the single throw knot.
(3) Only the overhand knot with a different number of throws was examined using FE and experiments.
(4) Pre-stressed FE models were not studied. It was worth noting that the process of forming the knot and loading angle could have an influence on the final load to failure of the suture. Also, only one shape and loading angle were used in this study.

(5) Two and three throws-knot models were not completed and validated yet; that was because of the following limitations. While the remaining timeframe of this work was short, extended time was required to have many attempts to obtain robust results. Also, Abaqus license on-campus had some limitations; e.g., limited number of elements, a limited computer technical specifications and frequent license freezing. This work could be a part of the future work.

3.5 Conclusions

In the present work, the mechanical behavior of (non-knotted / knotted) monofilament sutures was analyzed. The experimental results helped to prove the reliability of the designed fixture to inspect the (non-knotted / knotted) suture. The knot topology and suture material had an important influence on failure load and elongation of the suture. The presence of a knot lowered failure load, increased the elongation, and rupture occurred consistently at the knot region. The single throw knots reduced failure strengths relative to non-knotted suture by approximately 50% for monofilament sutures.

This study presents a validated FE model of a single throw surgical knot. FE models provided qualitatively descriptive and quantitatively accurate results when compared to experiments. Furthermore, the FE models quantified the stress concentrations at the knot due to bending, twisting, and friction which could not be easily identified experimentally. The FE model was also consistent with published strength reductions. The FE modeling technique showed promise for evaluating the effect of surgical knot topology (i.e., surgical technique) as well as the effect of suture materials on soft tissue repairs. Knot modeling might help engineers and surgeons to understand and better optimize surgical procedures. While this

study provided a useful baseline for clinicians, additional validation was recommended prior to using this modeling technique in surgical decision making.

CHAPTER IV

MULTIFILAMENT SUTURE

4.1 Introduction

The tensile strength of a knotted suture material is a commonly used selection criterion, but, there is still a lack of evidence in the published literature on the ideal test method. However, there exists a paucity of literature on the use of FE models describing the biomechanics of surgical knots [31]. Furthermore, to our knowledge, no FE models using (non-knotted/knotted) multifilament surgical suture have been reported. This chapter builds on that work by adding a focus on knot configuration while expanding the scope of the modeled behavior of the suture and knot.

In this chapter, multifilament structure, # 2 FiberWire surgical suture, has been chosen. The goals of this chapter are: (1) to determine the diameter of the core, jacket, and the suture, (2) to find the maximum load to failure and the mechanical properties of FiberWire suture, (3) to implement 3D FE model and bench experimentation of the multifilament sutures to find the maximum load to failure, the strain, the stiffness, and the location of material failure for different knot configuration, (4) to discuss the potential clinical impact of the number of throws on failure risk in a surgical knot. Non-knotted/knotted sutures have been tested to failure in a laboratory setting. Three different number of throws have been investigated in the laboratory tests. In this investigation, non-knotted suture and a single throw knot have been modeled and analyzed to investigate the mechanical behavior and to validate the model against experiments. Several comparisons have been made to validate the FE model. Gross

loads have been compared when the knot reached a localized material yield stress in the model or when the failure occurs in laboratory tests that have the same suture topology.

4.2 Methods

4.2.1 Mechanical testing

An experimental, comparative study was performed on common orthopaedic suture. Multifilament non-absorbable sutures was performed to observe the governing mechanics, to obtain material properties and validation data for FE model. The multifilament non-absorbable suture material is numbers 2 FiberWire. Braided non-absorbable FiberWire (Arthrex, Naples, FL) is a surgical suture in common use. FiberWire suture was constructed of a multi-strand, long chain ultra-high molecular weight polyethylene (UHMWPE) core with a braided jacket of polyester. FiberWire's materials were less stiff but have a higher coefficient of friction. FiberWire's combination generally provided a high strength, soft suture with abrasion resistance that virtually eliminates suture breakage during knot tying [110], [137], [138]. Due to the complexity of FiberWire suture, a sequential approach was conducted. First, FiberWire suture was examined to validate a simplified FE model of a multifilament "surgical" suture. Second, the core had been separated from the jacket to test each individually to determine the mechanical properties more precisely. Third, different number of throws were investigated: one, two, and three throws-knots.

4.2.1.1 Non-knotted suture and knotted suture

Experimental test of non-knotted suture was explained in section 3.2.1.1. Experimental test of knotted suture was explained in section 3.2.1.2. Figure 32 and Figure 33 show the

experimental setup and an example of the throws that were implemented in this investigation, respectively.

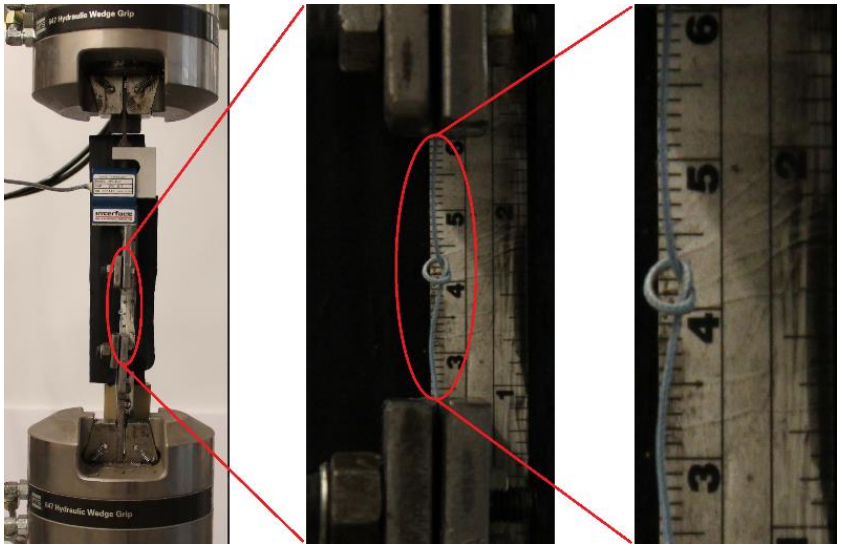

Figure 32: Testing device for multifilament suture load-extension (scale in (cm))

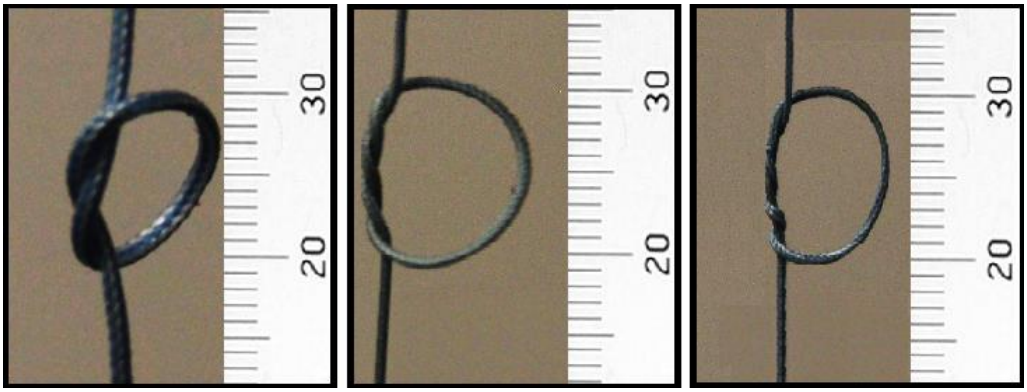

Figure 33: Examples of the throws, multifilament suture, (Approximate scale (mm))

4.2.2 FEA models

4.2.2.1 Non-knotted suture

The material properties of the multifilament FiberWire surgical suture as well as its core and jacket constitute separately were determined through experimentation. MATLAB

was used to create a 3D FE model of the non-knotted suture, which consist of core and jacket. The jacket was meshed using reduced integration hexahedral elements (C3D8R). While the core was meshed using two types of elements: 1. reduced integration hexahedral elements (C3D8R) and 2. wedge elements (C3D6), as depicted in Figure 34. The FE model of the core and the jacket were assumed homogenous and isotropic elastic material. Because the model involves contact interactions; an explicit dynamic solver was used to overcome this severe nonlinearities (Abaqus Version CAE V6.16).

Displacement control was applied at end of the suture; the other end was fixed. Mass scaling was used to increase the stable time increment; thus, the knot was modeled assuming a quasi-static load in an explicit dynamic model. The ratio of kinetic to internal energy was monitored to ensure the mass scaling and a quasi-static assumption were reasonable. Moreover, a mesh convergence study was conducted to establish an appropriate mesh density. The influence of assumed coefficient of friction was found to be small on the resulting load-displacement curves.

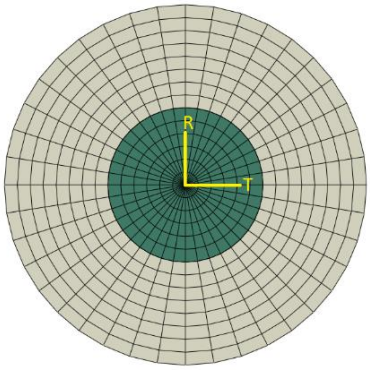

Figure 34: Axial cut of the FE mesh of the suture (core and jacket)

4.2.2.2 Knotted suture

A 3d FE model of the knotted suture, which consist of core and jacket, was created. The suture components were meshed using reduced integration hexahedral elements (C3D8R). The FE model of the core and the jacket were assumed homogenous and isotropic elastic material. Suture material properties were held constant while knot topology varied. Abaqus was used to solve the knotted suture consisting of a single throw knot. Knots involved complex contact conditions "self-contact and surface to surface contact" and large deformations; therefore, an explicit dynamic solver was used to overcome these severe nonlinearities.

Displacement control was applied at 0.5 mm/sec at the end of the knot; the other end was constrained in all directions. A fixed mass scaling was used, factor =5. Mass scaling was used to increase the stable time increment; thus, the knot was modeled assuming a quasi-static load in an explicit dynamic model. The ratio of kinetic to internal energy was monitored to ensure the mass scaling and a quasi-static assumption were reasonable. Moreover, a mesh convergence study was conducted to establish an appropriate mesh density. The influence of assumed coefficient of friction was found to be significant on the resulting load-displacement curves, see section 3.2.2.2.

4.3 Results

After finding the material characterization and the mechanical properties of the FiberWire suture, two types of comparisons were made to differentiate the impact of a knot configuration on the mechanical behavior of the suture. First, a comparison was made between

the experimental results of the three knots (single, two and three) throws. Second, a comparison was made between the experimental and the FE results of a single throw knot.

4.3.1 Experimental results

4.3.1.1 Non-knotted suture

4.3.1.1.1 Material characterization (diameter and density)

The FiberWire suture diameter was measured and recorded based on two procedures to confirm the results:

1. Using Nikon Measuring Microscope 20: Figure 35 and Figure 36 show the Nikon setup and an example of the picture of the measuring method that were implemented in this investigation, respectively. the cross-sections area of the suture, jacket, and core were assumed circular. Twelve points along the suture were evaluated to determine the average diameter and standard deviation. Furthermore, the suture diameter was compared to published literature and was found to be consistent, as depicted in Table 2.

2. Using the screenshot images: the suture diameter was measured by acquiring the screenshot images of the first image of undeformed suture based on the proportional values. Public domain image-processing software named GIMP was utilized to analyze the images. Assuming the cross-sectional area of the suture as circular, the average diameter of the suture was calculated along the suture length, as depicted in Table 2.

The mass of “long length” of the FiberWire suture was measured using a highly sensitive weight device. Approximate density was calculated from the mass and the computed volume of the FiberWire. For the volume calculation, the cross section was assumed circular

and the diameter was assumed to be constant. The density of the suture, core and jacket were calculated, as depicted in Table 3. Average diameter and density of two methods were implemented in the FE models.

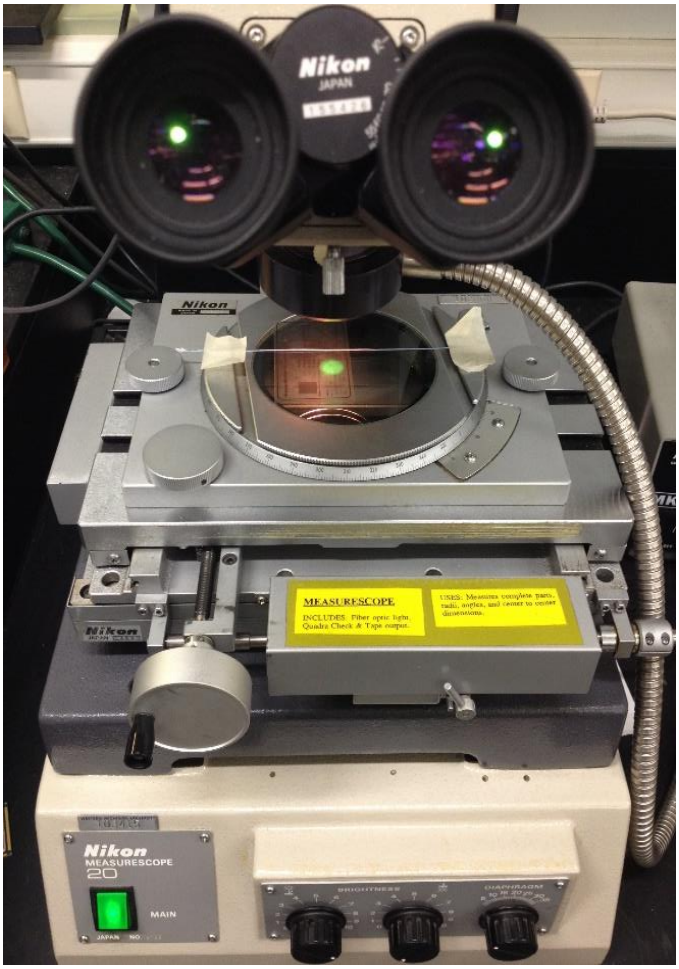

Figure 35: Nikon Measurescope 20 of measuring the suture diameter

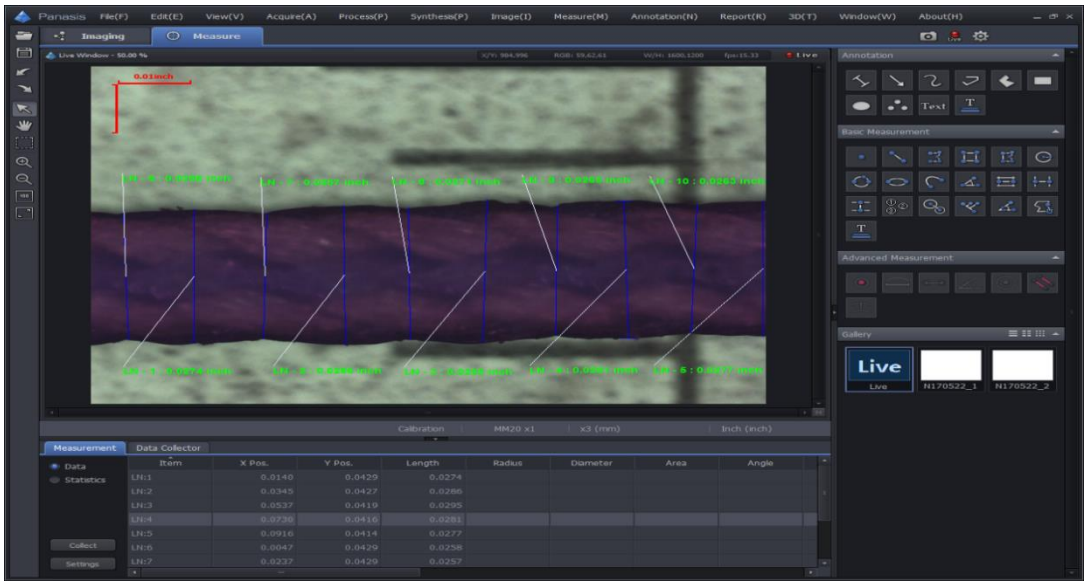

Figure 36: An example of measuring method of the suture diameter

Table 2: Selected literature for comparison of FiberWire diameter

Diameter	Study type			
(mm)	Present study (1)	Present study (2)	Najibi 2010, [60]	Wright 2006, [61]
Suture	0.693±0.0012	0.703±0.002	0.69	0.705
Core	0.279±0.0009	0.28±0.0016	-	-

Table 3: FiberWire, core and jacket densities

Density	Study type	
(g/mm^3)	Present study (1)	Present study (2)
Suture	$7.357*10^{-4}$	$7.146*10^{-4}$
Core	$3.869*10^{-5}$	-
Jacket	$6.97*10^{-4}$	-

4.3.1.1.2 Mechanical properties

4.3.1.1.2.1 Poisson's ratio

For more details, see 3.3.1.1.2.1. Figure 37 illustrates the Poisson's ratio values of FiberWire suture at various levels of strain and found to be approximately 0.38.

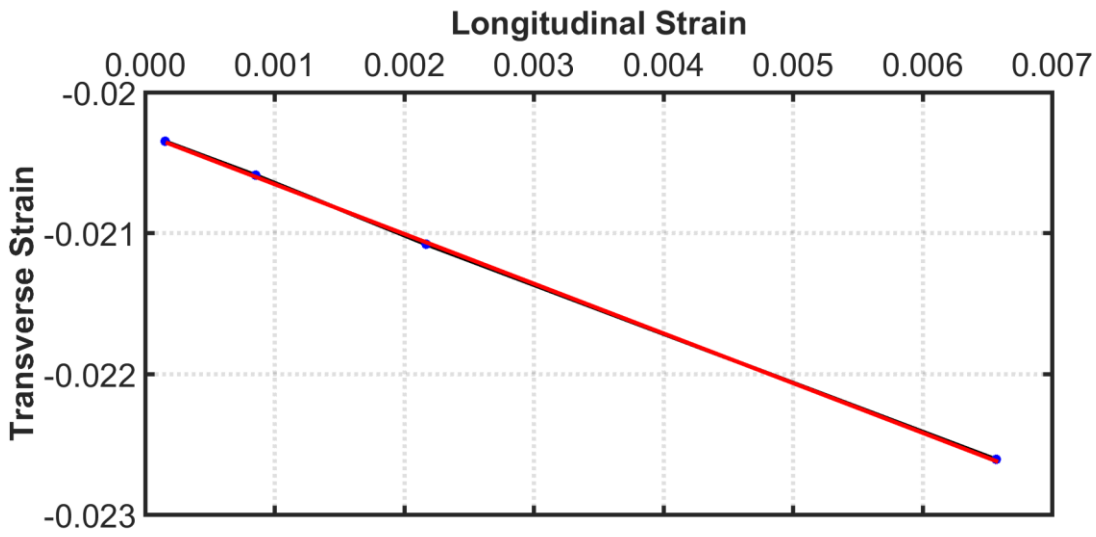

Figure 37: Poisson's ratio of the FiberWire suture

4.3.1.1.2.2 Load and displacement

The core was separated from the jacket to test each one individually to determine the mechanical properties more precisely. Figure 38 shows the load-displacement behavior of the core and jacket in one scale respectively. The results illustrated that the jacket had higher load and extension to failure when compared to the core. The maximum load of the core and jacket were approximately 65 N and 210 N respectively. The maximum strain was 2.6% for the core and 9% for the jacket.

Four specimens of whole FiberWire sutures were tested and images recorded. Figure 39 shows the load-displacement behavior of tests. The behavior of all the tests were similar.

The shape of load-displacement curves showed a nonlinear response at low extension due to friction between suture and pulleys; thereafter, the curves shows a near linear response due to suture composition, and then increase load to failure. In each test, there were at least two regions where load drops occurred in sequence: the core and the jacket, this behavior akin to a child's "finger trap" toy. Each drop was corresponded with a failure region in the core. The magnitude of the load drop was approximately proportional with the load carried by the core of the suture. When the core failed, there was a disruption in its carrying load capacity, thus the remaining load was that carried only by the jacket. These stages were followed by the last stage, in which the jacket failed. The value of the failure load corresponded with the load carried by the jacket.

Figure 40 clarifies the relationship between the picture (locations of failure in core and jacket) and one of the four sutures tests. The picture presented four red circles; three locations of failure in the core and one location of failure in the jacket. The curve of one of the four tests showed that there were four drops. In fact, the jacket failed only one time (the other two breaks in the jacket were after the test to examine pieces of the core). The three core failures corresponded with the first drops in load. The last drop was corresponded with the single jacket failure. Figure 41 shows that the average load for breakage decreased as the number of failures increased. The actual mechanism for the decrease in the subsequent load drops is still unclear, however, one could attribute this mode of failure to the fact that the core is composed of multiple strands of polyethylene which may fail sequentially as the continued loading occurs until reaching the final failure of the core. For example, at the first drop the averaged load was 95 N, while for the second drop it was approximately 80 N, and finally, for the last drop, it was 65 N (all averaged of 4 tests). Looking also at the amount of displacement to the

failure of each drop it could be noted that it was decreasing as well, from 7 mm, to 5 mm, and finally to 3 mm (all averaged of 4 tests). This suggests that the braiding angle at the failure point has a small displacement contribution to the overall deformation. However, the strain continues to accumulate in the core and jacket during the continued loading giving rise to the next failure, until the final failure of the jacket is reached.

For all sutures, the peak load to failure was calculated. Then, the average peak load to failure was calculated and compared to published literature and were found to be consistent, as shown in Figure 42. To demonstrate the interaction between the core and the jacket during the tensile test, the load versus displacement of average of the four tests of the suture, core, jacket, and core and jacket were drawn in one scale, as shown in Figure 43. At the beginning, the individual constituents sum to be similar to the suture as a whole. And, there was deviation between the results ± 30 as shown in Figure 43. Moreover, Figure 43 shows that the suture failed at higher load than the jacket due to the load sharing between the jacket and the core.

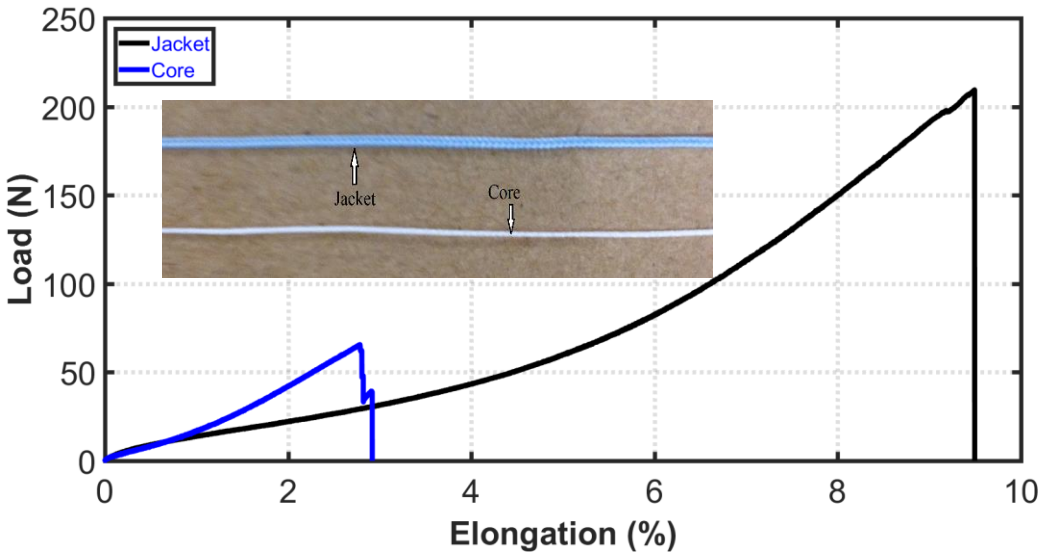

Figure 38: Load-Displacement curves of core and jacket of FiberWire suture

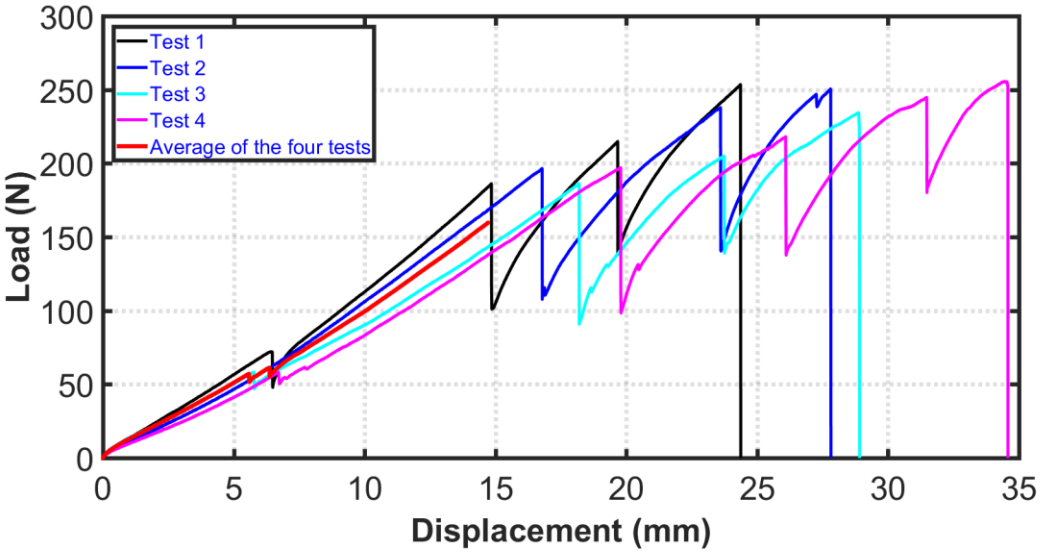

Figure 39: Load-Displacement curves of FiberWire sutures

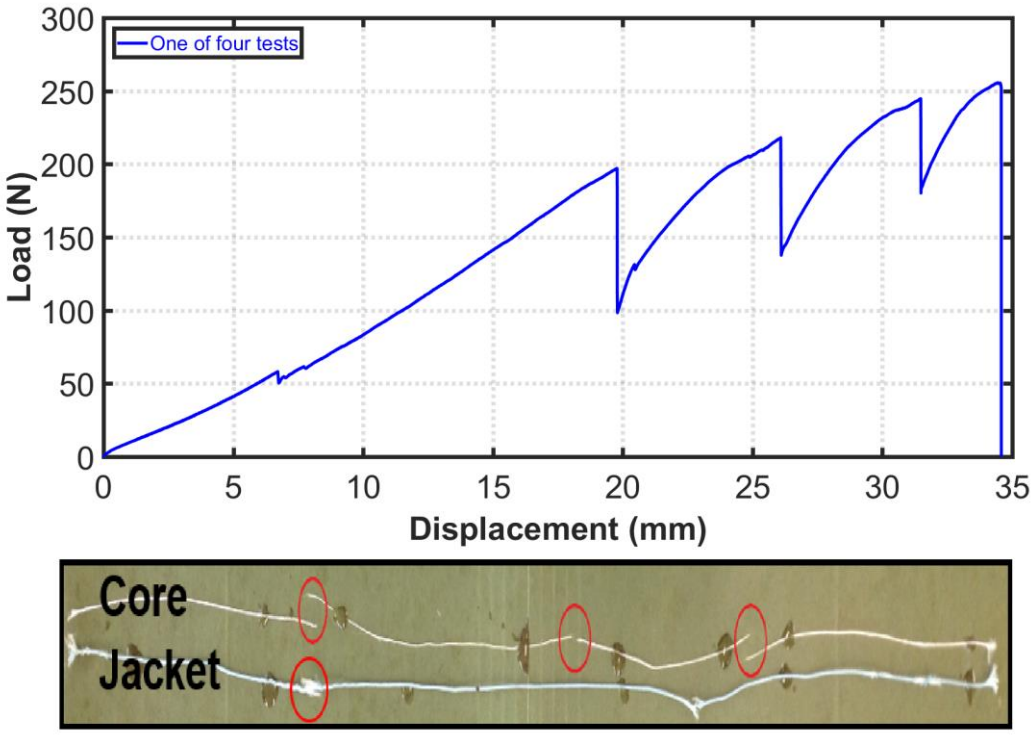

Figure 40: Locations failure of the FiberWire suture

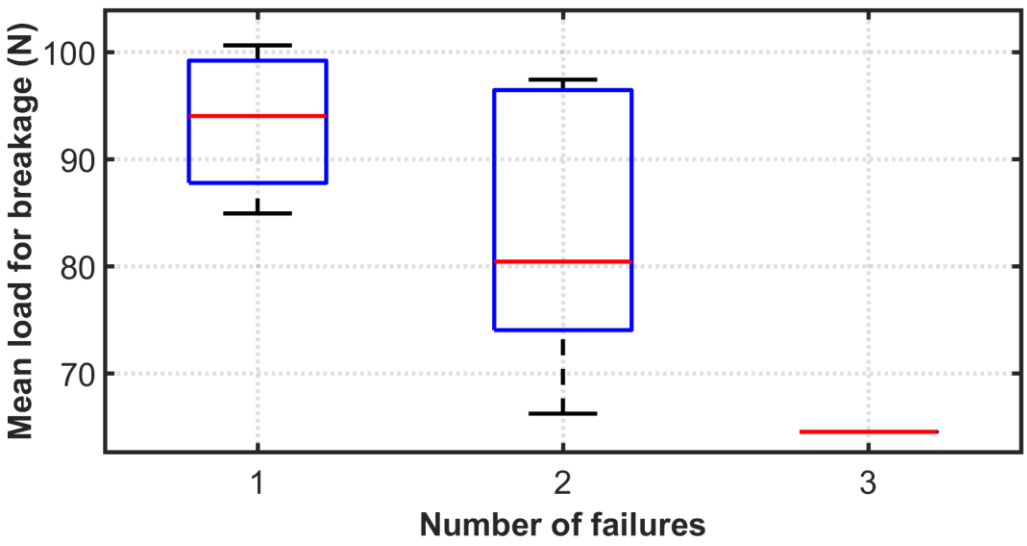

Figure 41: Mean load for breakage versus the number of failures

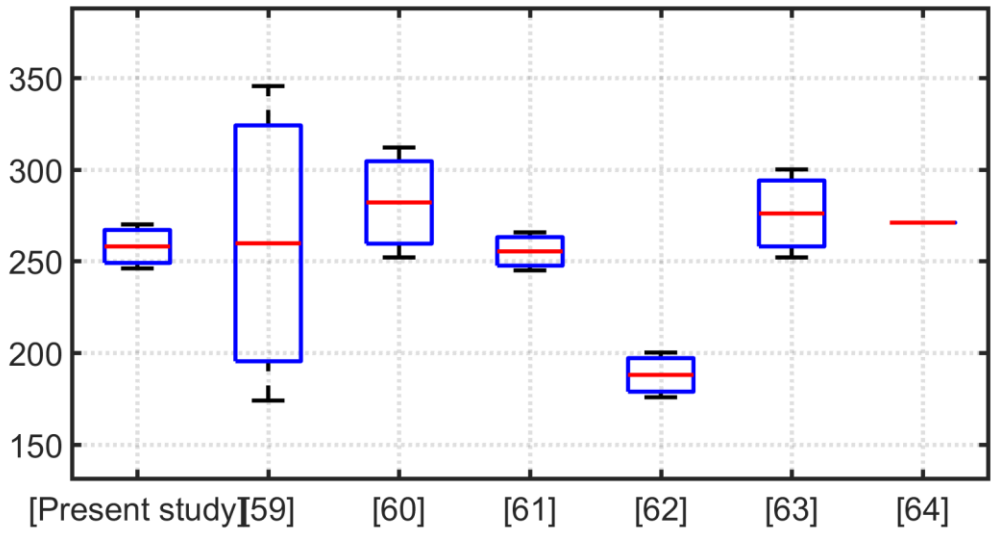

Figure 42: Selected literature for comparison of peak load to failure and loading type of FiberWire suture

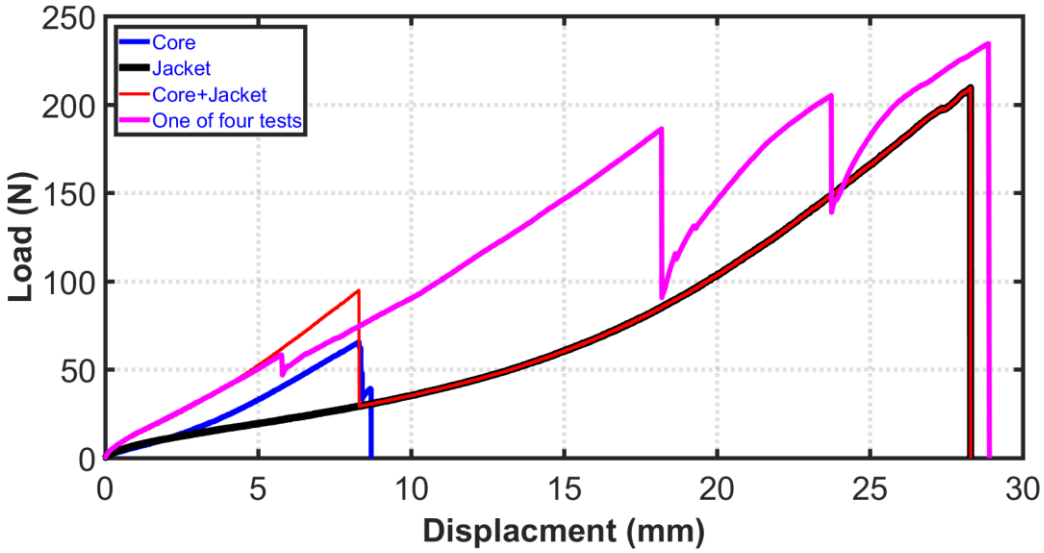

Figure 43: Tensile test results of the FiberWire, core and jacket

4.3.1.1.2.3 Stress and strain

For all specimen's sutures, the homogenized stress-strain curves of the suture (image based and based on displacements) were calculated as shown in Figure 44. The primary strain calculations were based on two procedures; pulley displacement and imaging. In image procedure, load and displacement were measured between two dots that were elected by collecting the data from the images that were captured by the camera. As stress = force/area, and strain = change in length/ original length, the average of the stress-strain curves of the suture for both of the collected data and the MTS machine data were drawn, as shown in Figure 44. Both of the two computed strain outcomes were found to be in agreement. For all sutures, the modulus of elasticity and the maximum stress at failure were calculated and compared to published literature and were found to be correlated, Table 4.

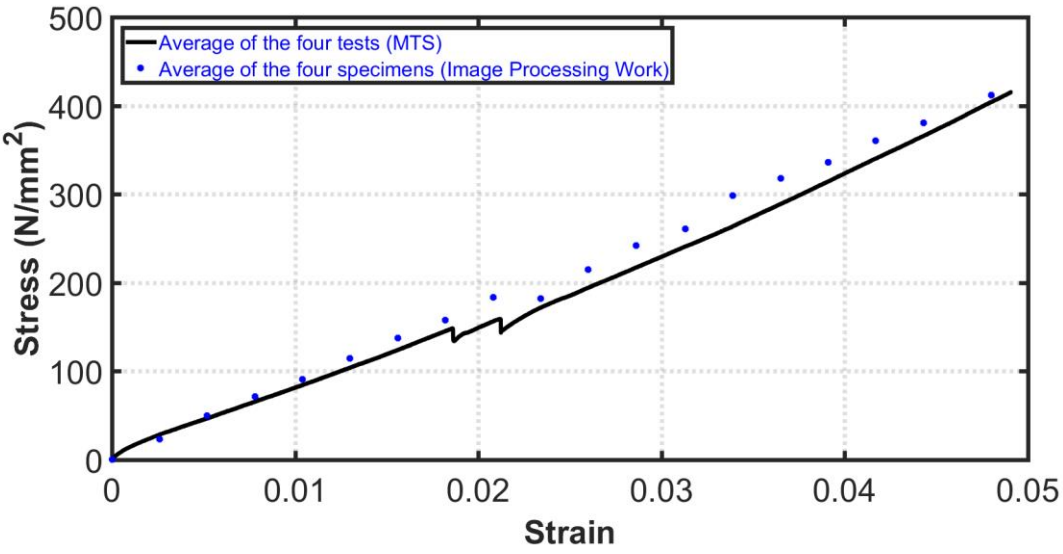

Figure 44: Stress-Strain curve of FiberWire sutures

Table 4: Selected literature for comparison of maximum stress and elastic modulus

Study type	Elastic modulus [Gpa]	Max. Stress [Mpa]
Present study	8.5±0.92	646±29
Najibi et al [60]	4.76±0.5	762±81
Wright et al [61]	7.2±3.52	803±185

4.3.1.1.2.4 Suture behavior under different speed rates

Researchers used different pull rates for destructive testing [129–133]. Therefore, FiberWire sutures with length of (270 mm) were used to determine the effect of the pull rate on the tensile strength. Four different pull rates to failure (0.1, 5, 12.5 and 33 mm/s) were used. Frequency of (0.5 Hz) was utilized. Longer times were related to lower speed rates while shorter times were related to higher speed rates. Therefore, Figure 45 indicates the lower elongation at faster pull rate. The plot showed that the pull rates had no high impact on the maximum load of the first failure and the elastic modulus of the suture, hence, there existed a

little viscoelastic effect. Furthermore, the elastic modulus was within the limits of the previously calculated elastic modulus.

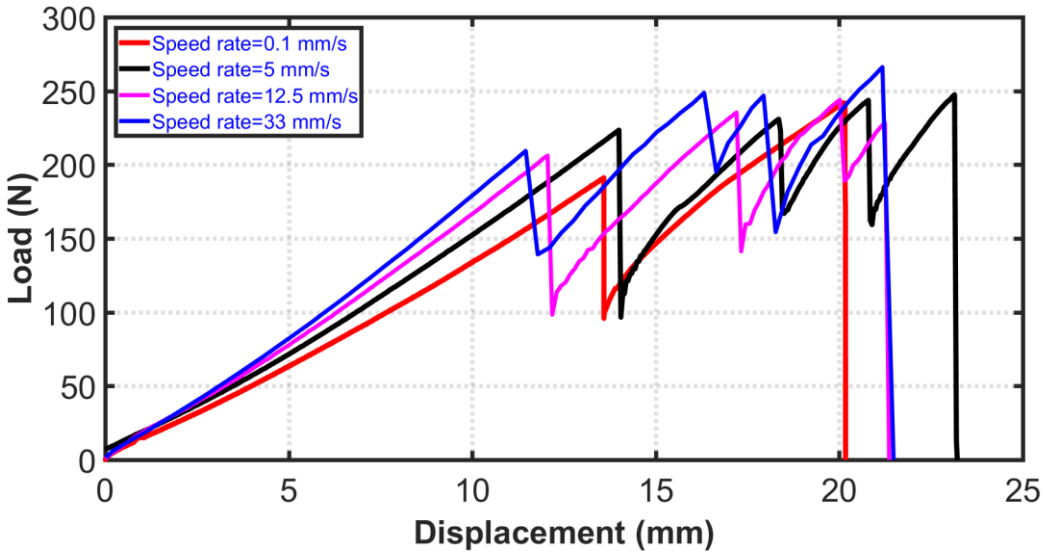

Figure 45: Load versus displacement at pull rates (0.1, 5, 12.5, and 33 mm/sec)

4.3.1.2 Knotted suture

FiberWire suture was used to create a single, two and three throws-knots. Figure 32 depicts the test setup of the knotted suture. Figure 46-Figure 48 show the load-displacement curves of failure region of five tests of each type of knot. Moreover, the figures showed that, for all sutures tests, the sutures had a multi load drops. At all the sutures tests, the failure was occurred adjacent to the knot rather than along the suture. Figure 49 show an example of the picture of failure region. This indicates the influence of the knot and its high stress concentration and friction contact. This result was consistent with published results [144].

Further, the results showed that the required force to break a tied suture was lower than the force required to break an untied suture by 40-50%. This result was consistent with other studies that have reported that the knot was the weakest part of any suture or ligature when

subjected to tension [6], [128], [129]. Further, the average load to failure of the five tests at first failure “drop” was calculated and was approximately (191 N). Also, the mean load at breaking of each types of throws was calculated and compared with non-knotted suture as shown in Figure 50. The failure load and elongation were found to increase with number of throws. For five repetitions of sutures, the average load to failure and standard deviation were calculated as depicted in Table 5. These results were compared with other published results and were found to be correlated [58], [130]–[134].

Subsequently, the mean stiffness of each throw was calculated. Figure 51 depicts the stiffness of the suture at different number of throws. Also, the results shows that the overall stiffness of the suture increased when the number of throws increased as shown in Figure 51. At the knot region, the distribution of strain in the material was non-uniform. This distribution could relate to the breakage point and its impact on the tensile strength of a knotted suture. As the knot become tight, the braided jacket become narrow as fibers coalesced. Further, the braid angle may be changed during loading, which had shown to have a high impact on the strength of the suture [145].

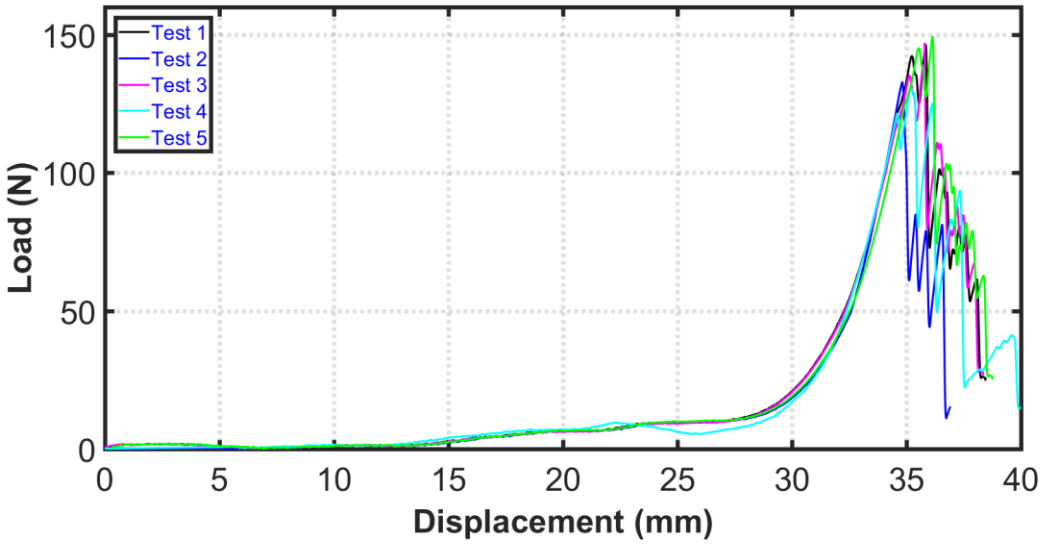

Figure 46: Load-Displacement curve of single throw knot of FiberWire suture

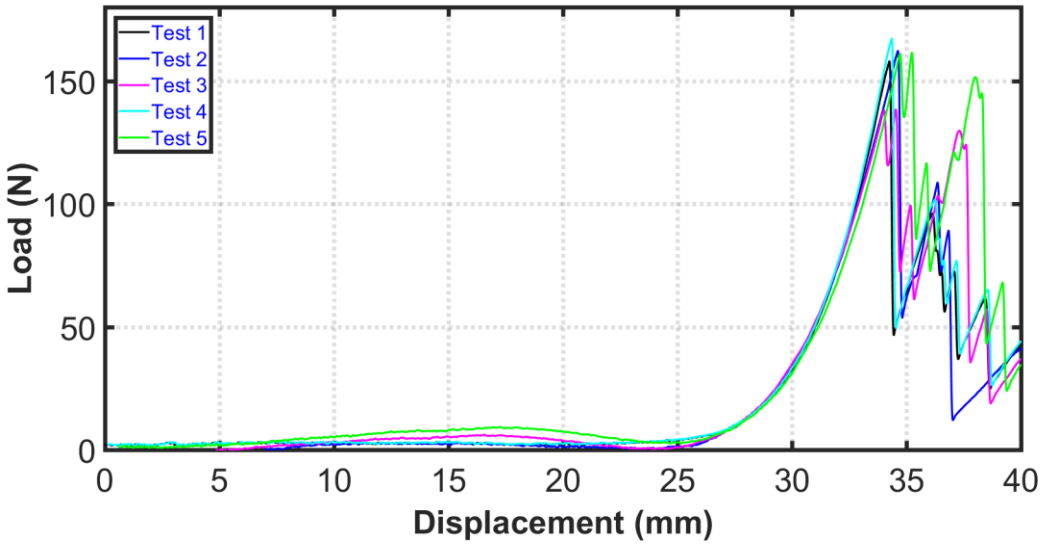

Figure 47: Load-Displacement curve of two throws-knot of FiberWire suture

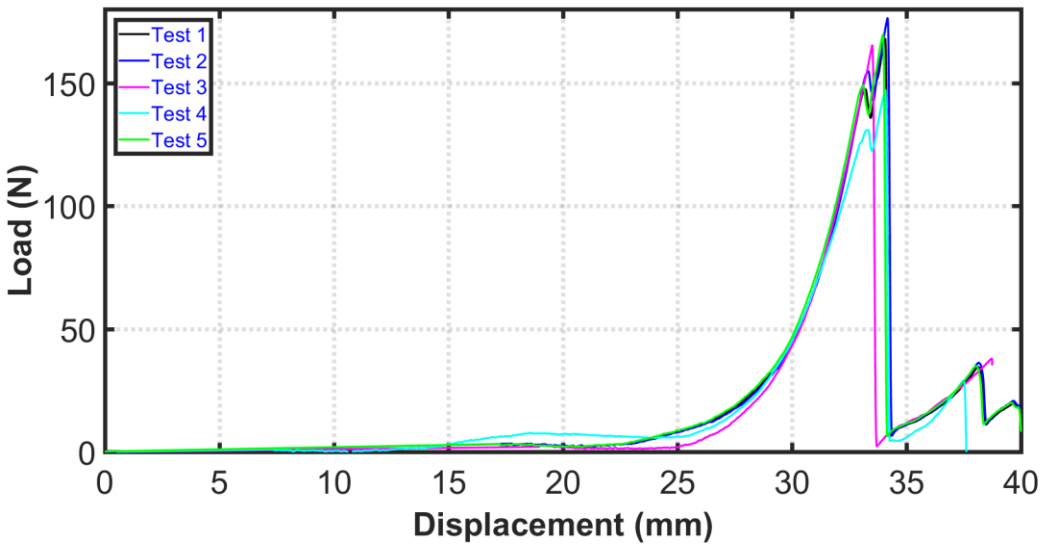

Figure 48: Load-Displacement curve of three throws-knot of FiberWire suture

Figure 49: An example of failure region of FiberWire suture

Table 5: Average load of failure and standard deviation of knotted FiberWire sutures for five samples

Number of Throws		
One	Two	Three
138±12 N	149±15 N	164±12 N

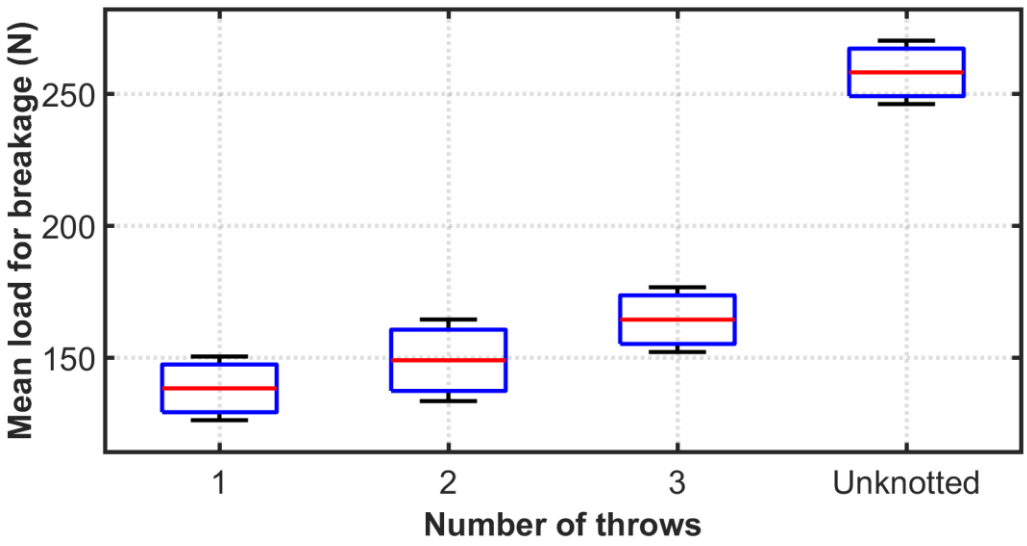

Figure 50: Relationship between the load and number of throws, FiberWire suture

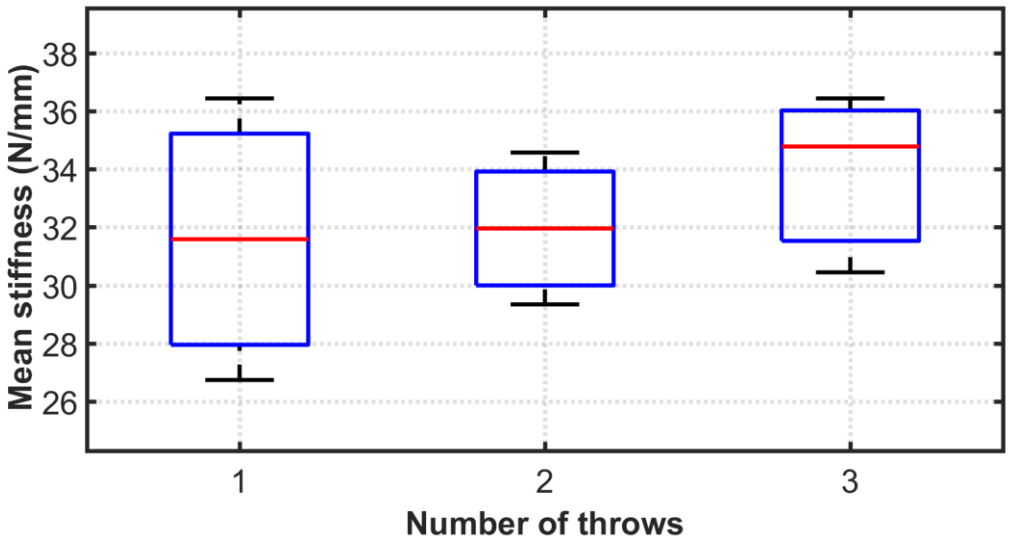

Figure 51: Relationship between the stiffness and number of throws, FiberWire suture

4.3.2 FE results

4.3.2.1 Non-knotted suture

To validate the experimental work, a simple model of the multifilament FiberWire suture without knot was implemented. To improve the results of the model, the mesh convergence was investigated. The mesh convergence parameters included the effect of the friction coefficient, Poisson's ratio, and mesh density on the suture model results.

4.3.2.2.1 Effect of coefficient of friction on the suture model results

The effect of the coefficient of friction assumption between core and jacket for both suture models was quantified over the range of 0.0 to 0.4, as shown in Figure 52. The outcomes refer to the fact that the coefficient of friction had small impact on the failure load. Further, this result overwhelmingly confirmed the view that the coefficient of friction was a function of various variables, including suture structure, suture material, and applied load.

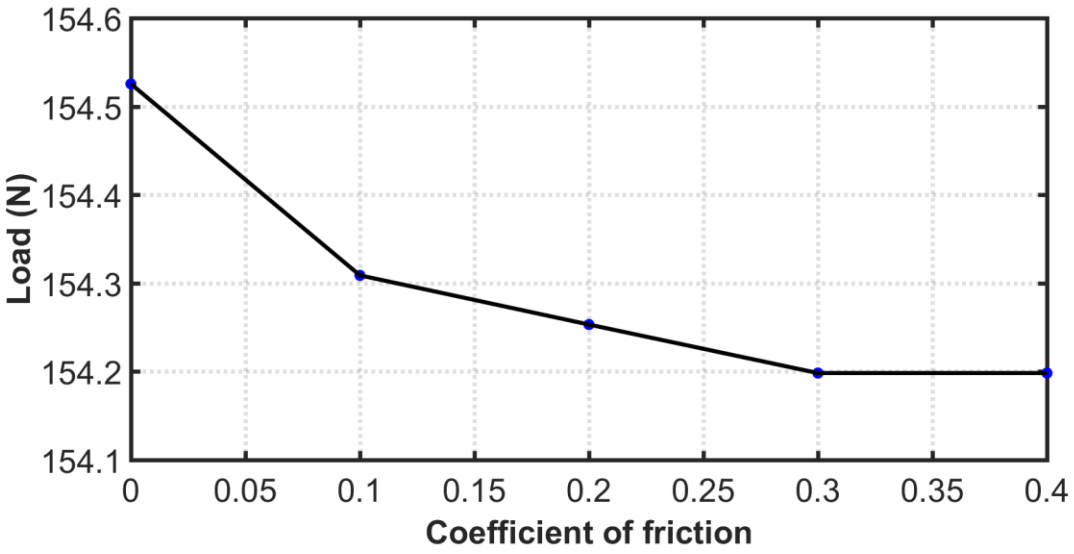

Figure 52: Effect of frictional coefficient on the failure load results of the suture model

4.3.2.2.2 Effect of Poisson’s ratio on the suture model results

As the same Poisson’s ratio was used for both core and jacket, Figure 53 shows the effect of Poisson’s ratio on the results of the suture model. The outcomes showed that the Poisson’s ratio had no significant impact on the maximum load results. This result provided a proof of the Poisson’s ratio definition. For a linear isotropic material subjected only to tension, the material usually tends to contract in the directions transverse to the direction of stretching and this contraction proportional to the Poisson’s value. Moreover, this result overwhelmingly confirmed that the Poisson's ratio is related to elastic moduli, the bulk modulus; the shear modulus; and Young's modulus. The changes in the Poisson’s ratios caused relatively small changes in the cross-section area.

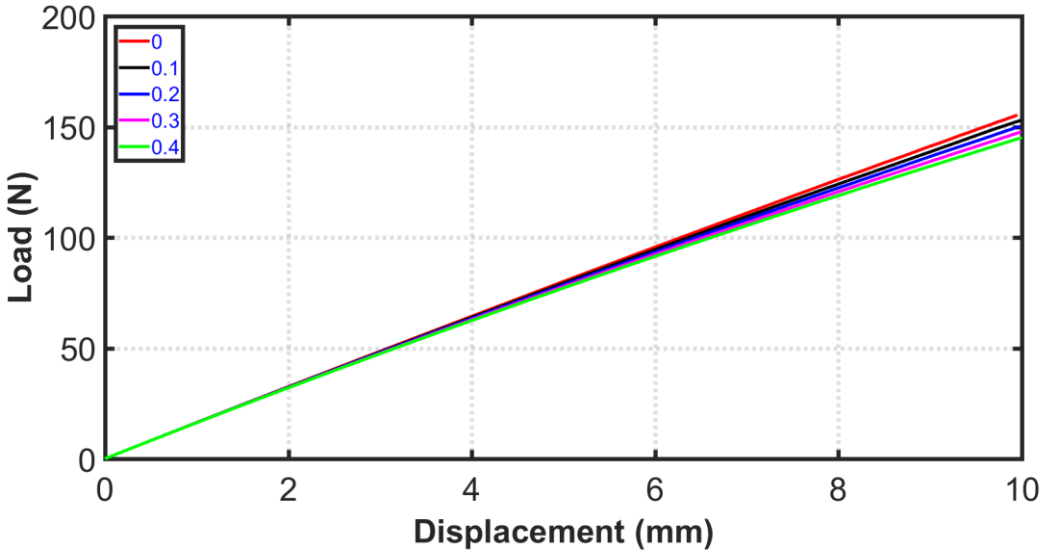

Figure 53: Effect of Poisson’s ratio on the maximum load results of the suture model

4.3.2.2.3 Effect of mesh size on the suture model results

To determine a good enough mesh based on their element density, different convergence runs were implemented to indicate when convergence was achieved. Figure 54

depicts the effect of mesh density on the maximum stress results of the model in the same location. Although, the mesh convergence study showed that a common influence on stress results when using linear elements to represent a surface was that the geometry of the boundary. When the mesh was refined, the geometry was better represented. The refined mesh number of elements was (41790).

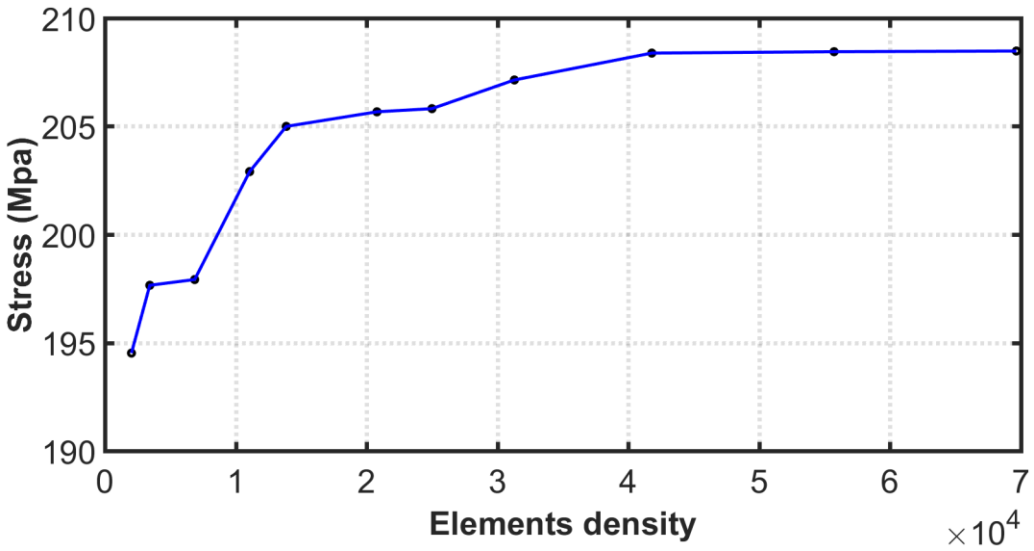

Figure 54: Effect of mesh size on the maximum stress results of the suture model

4.3.2.2.4 Suture model results

The experimental curves were compared with the FE model as indicated in Figure 55. A FE model was approximate and it erred by being stiffer. Mesh refinement was required in order to fulfill the requirement for access to convergent solutions. Mesh refinement was conducted because the model had large-deformation problems and contact problems. Subsequently, the model could suffer from shear and volumetric locking.

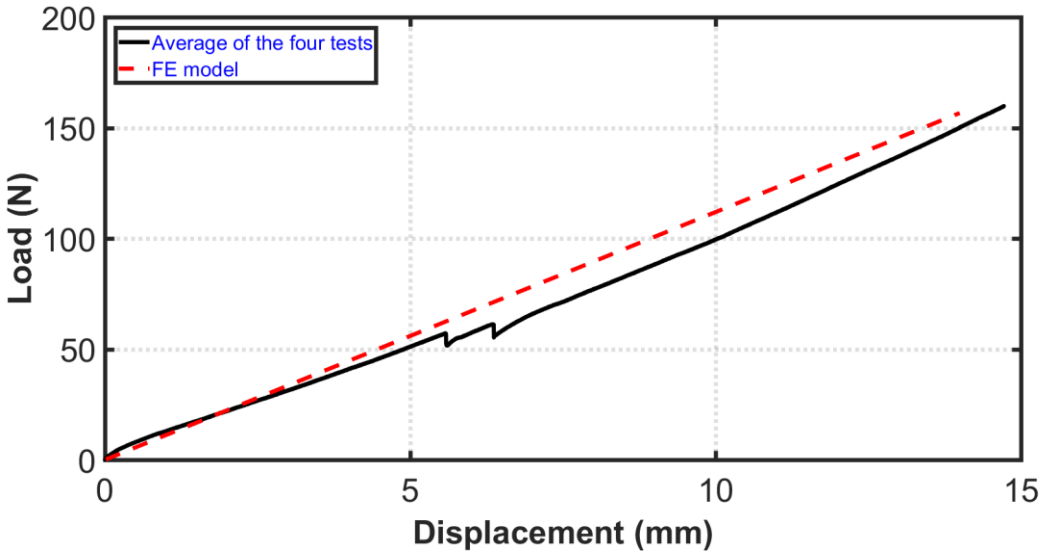

Figure 55: FE versus experimental results of the non-knotted FiberWier suture

4.3.2.2 Knotted suture

The impact of several modeling assumptions was quantified to improve the results of knot model. The effect of the friction assumption over the range of 0.2 to 0.4 and found to be small. The force necessary to cause a knot to slip was approximately proportional to the assumed coefficient of friction. However, the differences in force in this phase were small relative to the forces required to lock the knot. A mesh convergence study showed that a course mesh caused more "noise" (variations in load) than a fine mesh; however, the loads predicted by the dense mesh were similar at the same elongation. For more details, see, 3.3.2.2.

Three models of knot were created: one, two, and three throws as depicted in Figure 56. The FE results of single throw-knot were compared with the experimental results. The consistency of single throw-knot FE results was shown in Figure 57 alongside the experimental results. The FE results were consistent with the non-linear load vs elongation behavior of the experimental sutures. In addition, the FE model results predicted that the

strength of a tied suture was lower than that of untied suture. That could be due to the bending and twisting stresses that were evident as depicted in Figure 39 and Figure 57 respectively.

Figure 58 clarifies the internal energy and kinetic energy in a logarithmic scale. The figure illustrates that the total kinetic energy of the model was found to be small relative to the strain energy over the whole loading cycle, excluding the initialization where strain was very small. The kinetic energy was small and less than 1% of the internal energy in critical phases. Therefore, it was deemed reasonable to treat the results as quasi-static. With a simulation in a quasi-static analysis, the inertial forces were already established and were negligible because the velocity of the material in the model was very small. The results overwhelmingly supported the corollary to both of these conditions was that the kinetic energy might not exceed a small fraction, typically 5% to 10%, of the internal energy throughout most of the process [135], [136].

Figure 59 shows the scenario of tying a single throw-knot of FiberWire suture. Loads were small until the knot tightened, and the subsequently the load increased with additional applied displacement. The predicted stresses and strains were in locations that are qualitatively consistent with expectation. The FE model results predicted strength of a tied suture was lower than an untied suture due to the bending and twisting stresses were evident as depicted in Figure 43 and Figure 59 respectively.

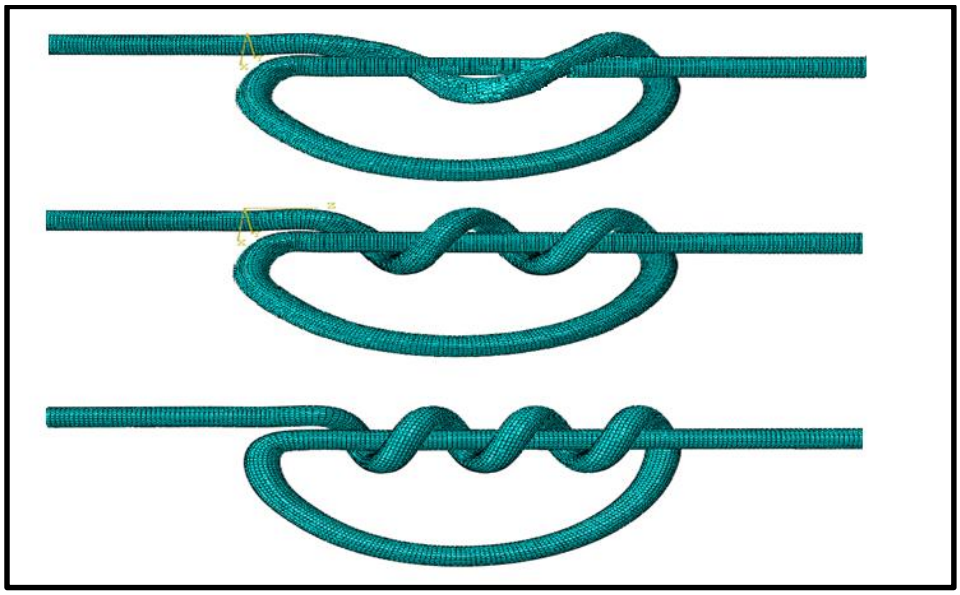

Figure 56: FE models of one, two, and three throws knot

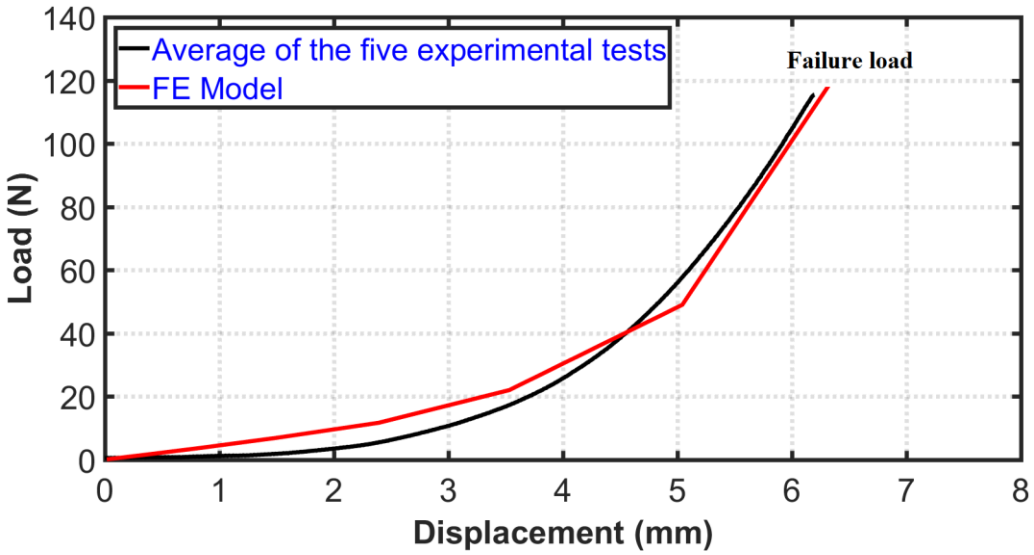

Figure 57: Experimental versus FE model results of single throw model

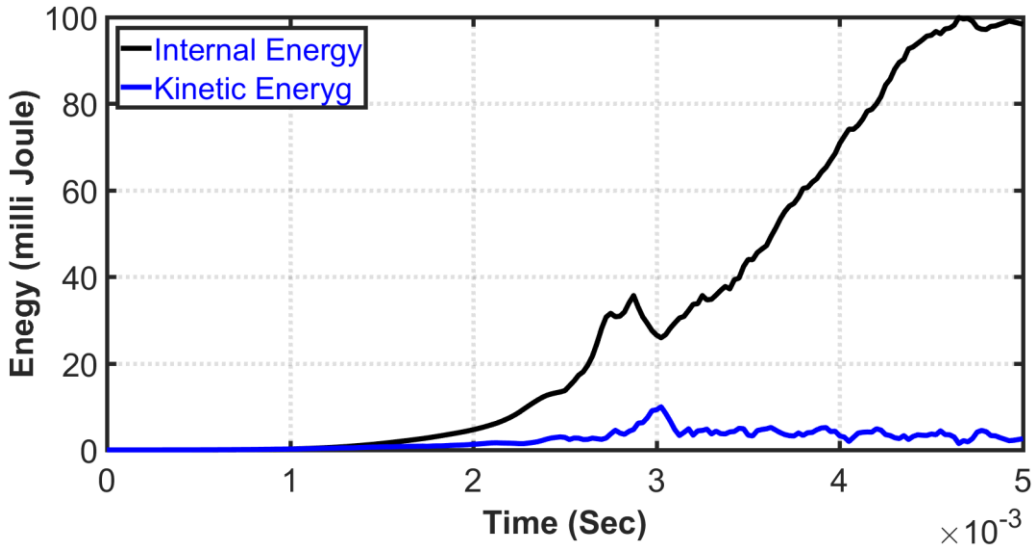

Figure 58: Internal energy and kinetic energy in logarithmic scale of single throw model

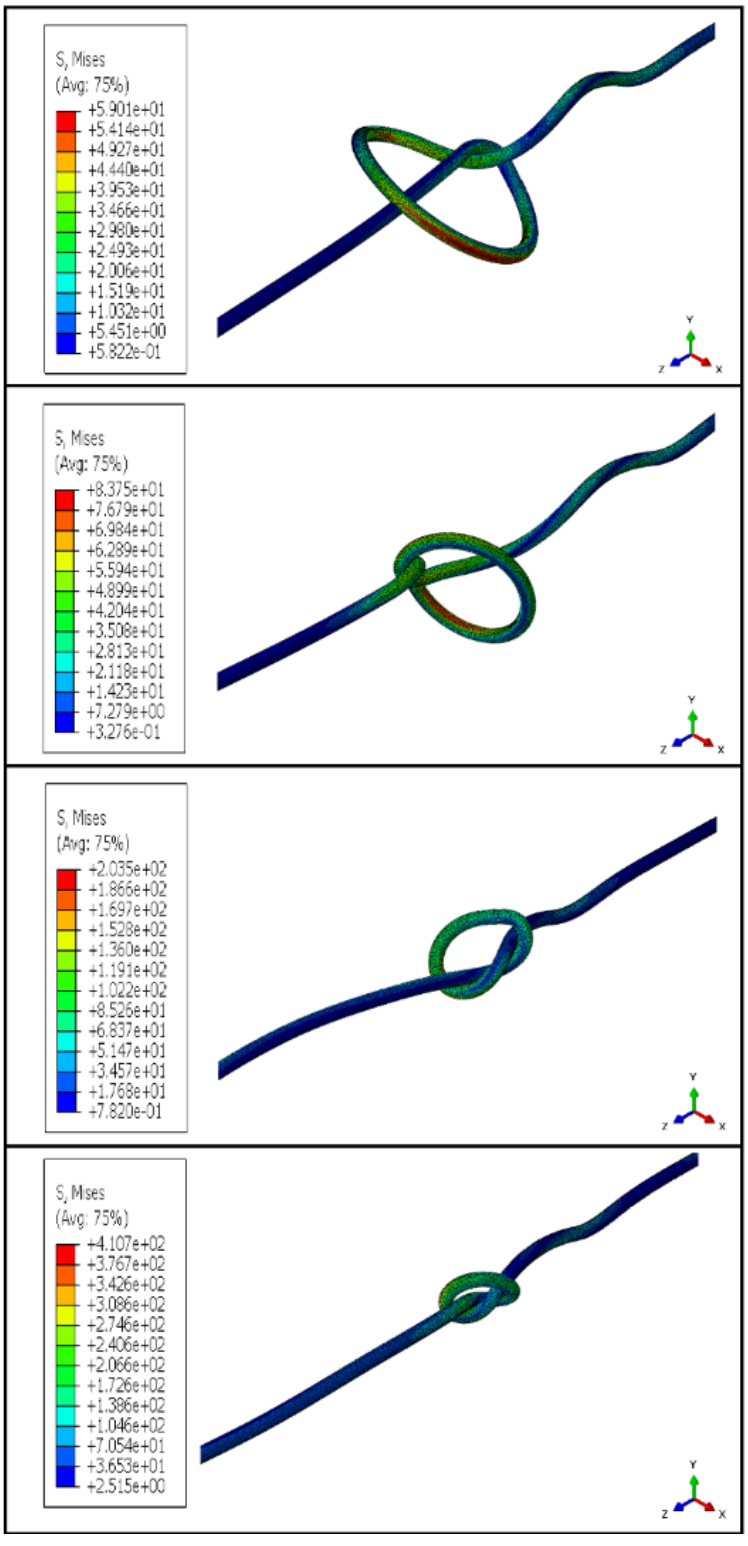

Figure 59: Von Misses stresses of single throw model. Stresses in (MPa)

4.4 Discussion

The pulley fixtures ensured that the suture failure occurred between the two pulleys for all tested suture samples. The diameter and average peak load of the tests to failure were compared to the properties of a manufactured suture and literature data and were found to be well correlated. Furthermore, there was no significant slippage observed in any of the samples. Several prior studies assess the mechanical properties of FiberWire suture. Most of these studies evaluate material properties of specific suture knots [7], [53], [59], or comparison of one type of suture versus another [60], [62], [139]. The current data was found to be consistent with these studies, however, no prior study reported the core and jacket separately. The maximum load of the core and jacket are approximately 65 N and 210 N respectively, and the maximum strain is 2.6% for the core and 9% for the jacket.

The repeated failure of the core prior to complete failure of the suture had not been previously reported. Thus, it merited additional discussion. The jacket was braided and thus undergoes a complex strain behavior. Under tension, the braided jacket lengthened and narrowed while the angle between the warp and weft threads changed. Therefore, the circumference shrinked with increased in tension. Consequently, the jacket compressed the core. In doing so, shear load could be transferred between the core and the jacket. The jacket was observed during experiments to “reload” the core even after core failure. This shear lag phenomenon was familiar from long fiber composite materials. In one example, the core failed 3 times prior to jacket failure. Thus, core failure did not immediately lead to complete load removal. No load reversals were applied in the current experiments, however, load revealed was exhibited a complex behavior that likely decreased the load transferred to the core. The

behavior of the suture was similar and could be understood when compared to the action of a "Chinese finger trap" (a common toy for children).

The results of this study indicated that the suture mechanical behavior was influenced by increasing number of throws; this effect was highly dependent on the suture composition. For all sutures, the failure load of the three throws was the highest. That could be due to the increase of contact density and bending stiffness. In addition, because the composition of FiberWire suture materials was different than monofilament, the failures modes differed.

The difference between load-extension curves of knotted and non-knotted sutures provided useful information to identify the knot stability and strength. The knot resulted in 30~40% strength reduction relative to untied suture and was consistent with published results [6], [128]. This was due the configuration of knot, the tensile forces exerted on a knotted suture are converted into shear forces and eventually suture rupture [6]. Other studies have reported that the knot was the weakest part of any suture or string when subjected to tension [6], [7], [128], [129]. Further, the overall stiffness of FiberWire suture increased when the number of throws decreased whereas monofilament increased. Several parameters may contribute to FiberWire failure that occurred at the knot rather than along the suture. Firstly, forces were being oriented at the knot at an acute angle to the suture fiber. Secondly, the suture fibers in the knot region may be weakened during knot formation and loading. Thirdly. Under tightening the suture, the friction among fibers in the knot region may contribute to failure.

The FE analysis results of the knot were qualitatively correct and were based on the experimental results. Thus, the FE models could be used in additional investigations. The limitations of the current study were the following:

(1) the core and jacket were modeled as a homogeneous linear elastic material.

(2) FE model results were reported only for the single throw knot.

(3) failure of the suture was only one failure mode of a surgical repair.

(4) only the overhand knot with a different number of throws was examined using FE and experiments.

(5) the shape of forming the knot and loading angle might also have an influence on the mechanics of the suture. One shape and one loading angle were used in this study.

4.5 Conclusions

In the present chapter, the mechanical behavior of (non-knotted / knotted) multifilament FiberWire sutures was analyzed. The obtained experimental results help to prove the reliability of the designed fixture to inspect the (non-knotted / knotted) suture. The knot topology and suture material had an important influence on failure load and elongation of the suture. The presence of a knot lowered failure load, and rupture occurred consistently at the knot region. The single throw knots reduced failure strengths relative to non-knotted suture by approximately 40% for FiberWire sutures. The circumference of the jacket shrinks and its length extends under tension “fixed displacement test”; thus the jacket presses on the core. As a result, an additional shear load was transferred between the core and the jacket.

This study presented a validate FE model of a single throw surgical knot. FE models provided qualitatively descriptive and quantitatively accurate results when compared to experiments. Generally, with increasing the knot tightening the deviation between the model and experimental results was decreased from approximately 10% to 1 %. Furthermore, the FE models quantified the stress concentrations at the knot may be due to bending, twisting, and

friction which could not be easily identified experimentally. The FE model was also consistent with published strength reductions.

The FE modeling technique could be applied to discern the governing mechanics of multifilament knot (i.e., surgical technique) as well as the effect of suture performance on soft tissue repairs. Additional experiments with knots, and FE models were being continued to develop. Knot modeling might help engineers and surgeons to understand and better optimize surgical procedures. Numerically, no assessment had been completed of knot security (i.e., how likely the knot is to untie), therefore, clinical recommendations are premature. In the future, the results might provide a framework for clinicians for choosing the suture and knot types for soft tissue repairs.

This study was the first to report the behavior of the core and jacket of No2 FiberWire separately, thereby providing an improved description of the mechanics of this common suture. Also, the repeated failure of the core prior to complete failure of the FiberWire had not been reported yet. Moreover, to the best of my knowledge, nothing had been reported the modeled the (non-knotted/knotted) multifilament FiberWire suture.

CHAPTER V

SHAER-LAG PHENOMENON

5.1 Introduction

The "shear-lag" phenomenon is well-known phenomenon in reinforced structures. It governs the interplay between axial and shear stress around fracture points or geometric discontinuities and provides ongoing load transfer after the initial compromise of a structure. Suture is a generic term for a class of thread-like materials used to bring severed body tissues together in aid of tissue healing. Uniaxial tests to failure of FiberWire surgical suture were conducted to observe the governing mechanics and to obtain data for FE method validation. Chapter four show the experimental results of the sutures and were found to have a fail/reload/fail pattern where load was transferred between suture core and jacket via the shear lag mechanism. Care must be taken to avoid damage to the suture material when handling it. Excessive handling or twisting of the suture within the instrument, such as needle holders and forceps, may also contribute to premature suture failure [146]. Knowledge of the stress distribution at the failure site is essential for predicting the effects of the governing mechanics of load transfer. Traditional tensile testing cannot fully describe the stress distribution and the mechanics of the driving shear lag phenomenon in a failed multifilament surgical suture. Numerical simulation provides a useful tool to examine the governing mechanics of load transfer, but has not previously been applied to multifilament suture such as FiberWire surgical suture.

A core-jacket suture subject to tensile stress can undergo extensive core cracking, while the jacket remains intact. The transfer of load from the surrounding jacket to the core is one of the fundamental micromechanical processes determining the suture failure as a composite material. Furthermore, the core of the suture during the surgery and/or during preparing the suture to the surgery perhaps fails for various reasons, e.g., mechanical trauma [27]. Consequently, this failure in the core probably one of the contributors to the repair failure. This chapter aims are applying the FE method to examine the distribution of normal and shear stresses along a partially failed suture and its clinical implications. Two types of loading are implemented in this investigation: static and cyclic loading.

5.2 Methods

5.2.1 Mechanical testing

An experimental study of suture materials No.2 FiberWire was performed to determine the gross load and strain response in uniaxial tensile load parallel to the fiber direction, and to obtain data for FE model validation. FiberWire suture is composed of a core covered with a jacket; each was tested separately and together as manufactured, see chapter four. The experimental setup was explained in section 3.2.1.1.

5.2.2 FEA models

The material properties of the multifilament FiberWire surgical suture as well as its core and jacket constitutes separately were determined through experimentation, chapter four. A composite cylinder shear lag model is adopted for the analysis of the load transfer between the core and the jacket when the core is broken and intact. ABAQUS was used to create a

validated the FE model to quantify the shear lag effect after FiberWire composite suture core failure. Two FE models of FiberWire suture were created consisting of separate core and jacket. One model included a broken core to investigate its implications. Figure 60 shows the core with a diameter DC is embedded with a length L in a coaxial jacket cylinder with an outer diameter DJ. Suture model, core and jackets, was created by using reduced integration Axisymmetric elements (CAX4R) , as depicted in Figure 61. The suture was modeled assuming a static load in a static model. Large elements are used where stresses are relatively constant, and progressively smaller elements where the stress gradient becomes larger. For this reason, many of the elements in these grids appear in a small area near the end of the broken core where stress concentrations are expected. Also, Figure 61 illustrates the applied boundary conditions. Two boundary conditions were applied to the suture. For both types of loading, load control mode was applied on a reference point that was generated on one side of the suture model.

For cyclic loading, constant amplitude load was applied in a sinusoidal squared waveform. The frequency was chosen to be approximately consistent with the physical time of tying a knot. On the other side of the suture model, displacement/rotation boundary conditions (BC) were constrained in all directions. The FE model of the core and the jacket were assumed homogenous and isotropic elastic material. The cross-section area of the suture, core and jacket, was circular. The models involve contact conditions; therefore, an implicit dynamic quasi-static FE solution was used to overcome this nonlinearity. For static loading, a friction coefficient of 0.3 was assigned between the core and jacket. While for cyclic loading, three types of loadings (10, 30, and 50 N) and coefficients of friction (0.2, 0.3, and 0.4) were

implemented. The ratio of kinetic to internal energy was monitored to ensure that a quasi-static assumption was reasonable.

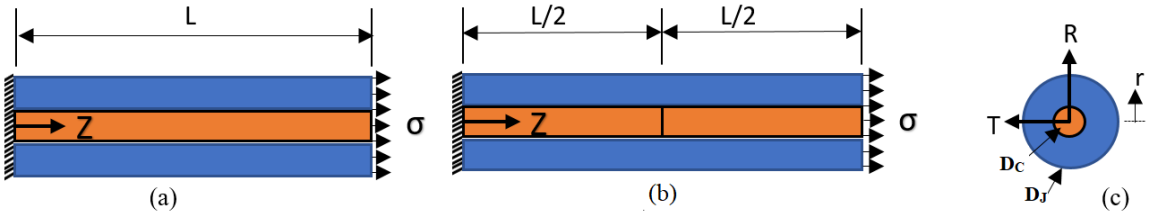

Figure 60: Schematic diagram of the physical model of a core and jacket suture with notation, (a) longitudinal cross section of the jacket with intact core, (b) longitudinal cross section of the jacket with broken core, and (c) transverse cross section of the suture (core and jacket)

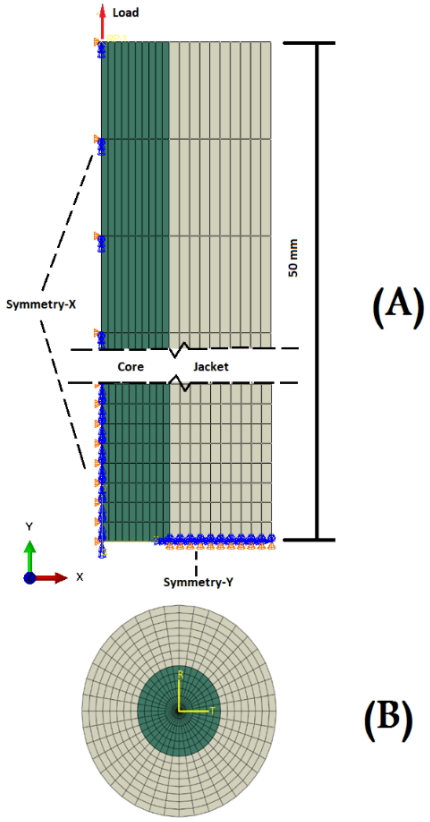

Figure 61: (A) Model mesh and boundary conditions, broken core, (B) Axial cut of the model mesh of the suture (core and jacket)

5.3 Results

Material characterization, mechanical properties, and gross load to failure of the FiberWire suture were determined experimentally and compared to published literature and were found to be consistent, chapter four. In this chapter, a comparison was made to differentiate the impact of a partial failure of core on the mechanical behavior of the FiberWire suture. The comparison was made under static and cyclic loading.

5.3.1 Experimental results

5.3.2 FE results

To make the results easier to understand, cylindrical coordinates were used in reporting model results. A cylindrical coordinate (r, θ, z) is defined and the Z-axis denotes the fiber axial direction. To validate the experimental work, mesh convergence was investigated to improve the results of the model. Moreover, the effect of the friction coefficient, Poisson's ratio, and mesh density on the model results were included.

5.3.2.1 Effect of mesh size on the suture model results

A series of models were run to determine a good enough mesh based on their element density. Figure 62 depicts the effect of mesh density on the maximum stresses results of the suture with the broken and intact core. Also, the findings demonstrate that the stresses were more stability when the element density increases. A mesh of 41790 elements was used in the model. The stresses predicted by (intact/broken) core sutures models were in overall agreement when under the same conditions. In fact, large elements were used where stresses

were relatively constant, and progressively smaller elements where the stress gradient became larger, as shown in Figure 61.

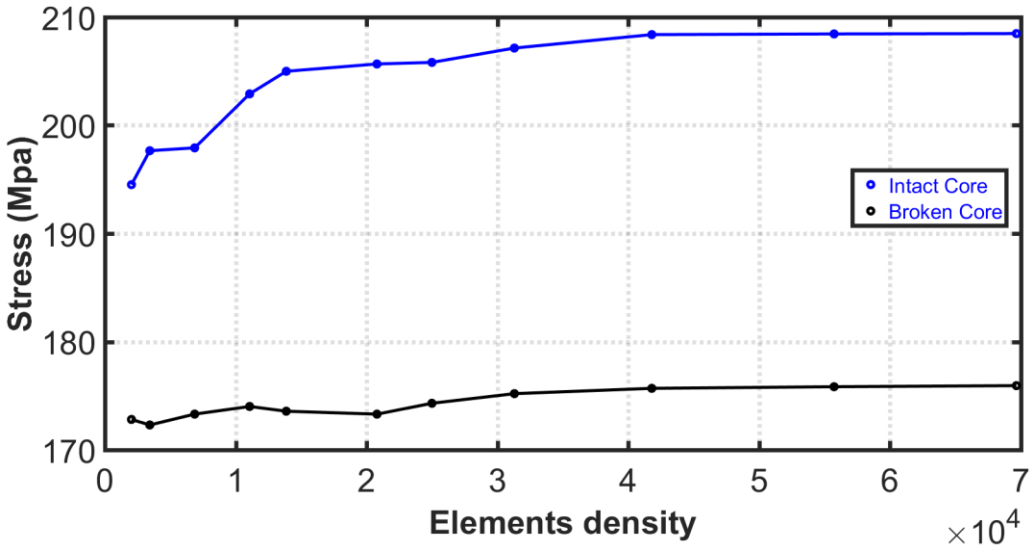

Figure 62: Effect of mesh size on the maximum stresses results of (intact/broken) core sutures models

5.3.2.2 Effect of coefficient of friction on the sutures models results

For (intact/broken) core sutures, the effect of the coefficient of friction assumption between core and jacket was quantified over the range of 0.0 to 0.4, as shown in Figure 63. The outcomes refer to the fact that the coefficient of friction had a negligible effect on the maximum stress of the intact suture. Furthermore, the coefficient of friction had a clear impact on the maximum stress of the broken suture due to the frictional forces, which resist the relative movement of the surfaces. The stresses were calculated at the end of outer core surface.

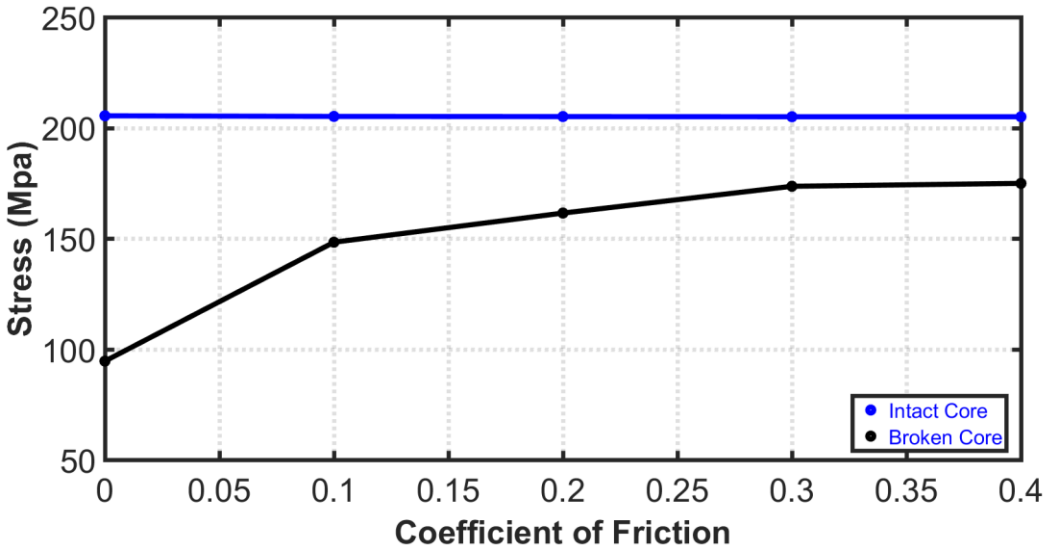

Figure 63: Effect of frictional coefficient on the maximum stresses results of (intact/broken) core sutures models

5.3.2.3 Validation of experimental and FE results

From chapter four, Figure 43 demonstrates the interaction between the core and the jacket during the tensile test. Recall, Figure 55 shows that the FE results were consistent with the experimental results of the suture (core and jacket). As could be observed, the FE result was stiffer than the experimental perhaps due to the model assumptions.

To demonstrate the validity of the quasi-static assumption of the model, the ratio of kinetic to internal energy was calculated. The total kinetic energy of the model was found to be small relative to the strain energy over the whole static loading cycle, excluding the initialization where strain was small. For both (intact/broken) core sutures models, the kinetic energy was less than 1% of the internal energy in critical phases, as depicted in Figure 64 and Figure 65 respectively. Therefore, it was deemed reasonable to treat the results as quasi-static.

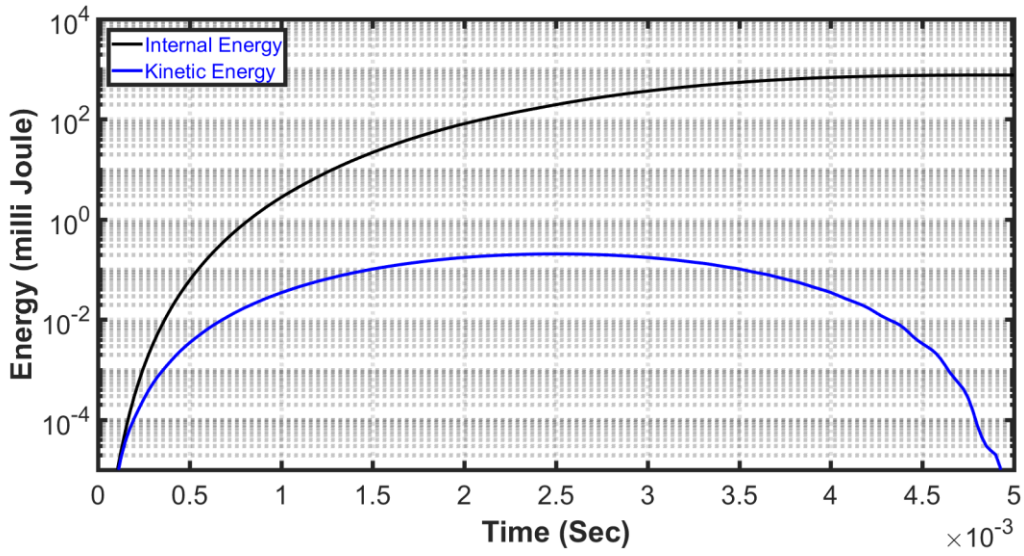

Figure 64: Internal energy and kinetic energy in logarithmic scale, intact core

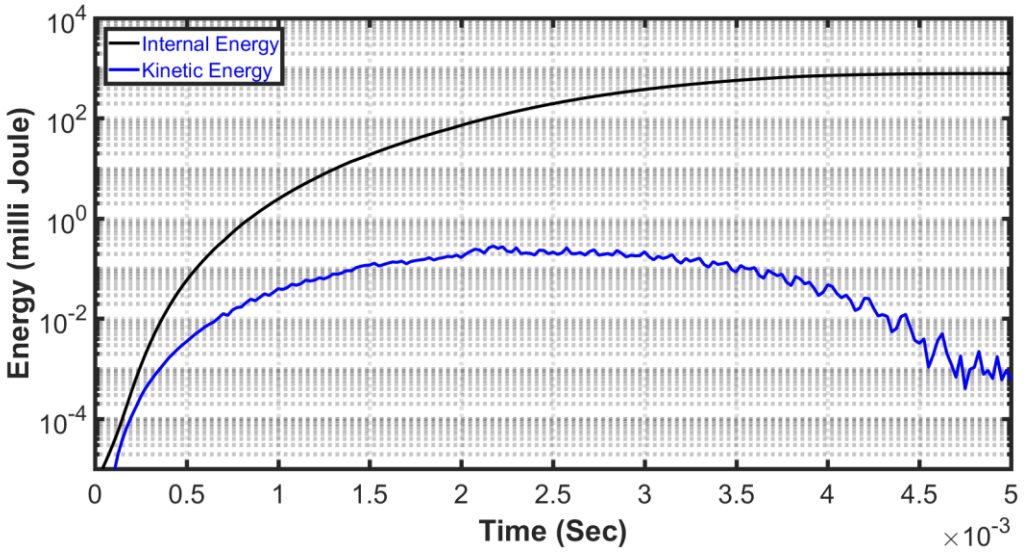

Figure 65: Internal energy and kinetic energy in logarithmic scale, broken core

5.3.2.5 Static loading results

Figure 66 and Figure 67 provide an example of the FE models of (intact/broken) core sutures. The models show detailed stress and strain within the suture: the stresses (in the core and the jacket) varies significantly over their transverse cross-section and longitudinal axis.

The predicted stresses and strains occurred in locations that are qualitatively consistent with expectations based on shear lag theory [39] [147][148]. Figure 68 provides an example of the results of the FE models, a broken core.

Figure 69 and Figure 70 show the normal and shear stresses distribution predicted by FE models of the broken and intact core cores at the interface between the core and the jacket. For intact core, there was no change in the stresses along the suture length and intact fibers equals the nominal level, as shown in Figure 69. While Figure 70 shows that the shear stress at the centers of the broken core region was, of course, zero, due to the symmetry. At the broken core site, the models show that the core filament locally stopped carrying the normal load and shed it to the surrounding jacket via shear lag. Also, the load in the jacket surrounding the broken core built via shear and transferred that load across the broken site as normal stress. Subsequently, the load transferred back to the core again via shear. As shown in the figures, the broken core gradually recovered its stress as a function of the distance to the broken region. The transferred of the load from jacket to core depends upon the core/jacket interface properties, their volume friction, and the core strength. Referring to Figure 69, the normal stresses in the core approached zero (limited by mesh convergence) at the fracture location. The stress distribution asymptotically approached the intact suture stress distribution over a long distance. Normalizing axial position from the point of failure with respect to the total suture diameter (Z/D), the load transfer occurred over approximately Z/D = 35%. The jacket filaments carried the complete load despite complete failure of the core filament.

Figure 71 shows the displacement behavior of the (intact/broken) core sutures along Z/D. At the broken region, the intact core detects continuity of moving at a uniform distance,

while the broken core shows the discontinuity. Also, the figure shows the nonlinearity in the behavior of broken core due to increasing the friction resistance.

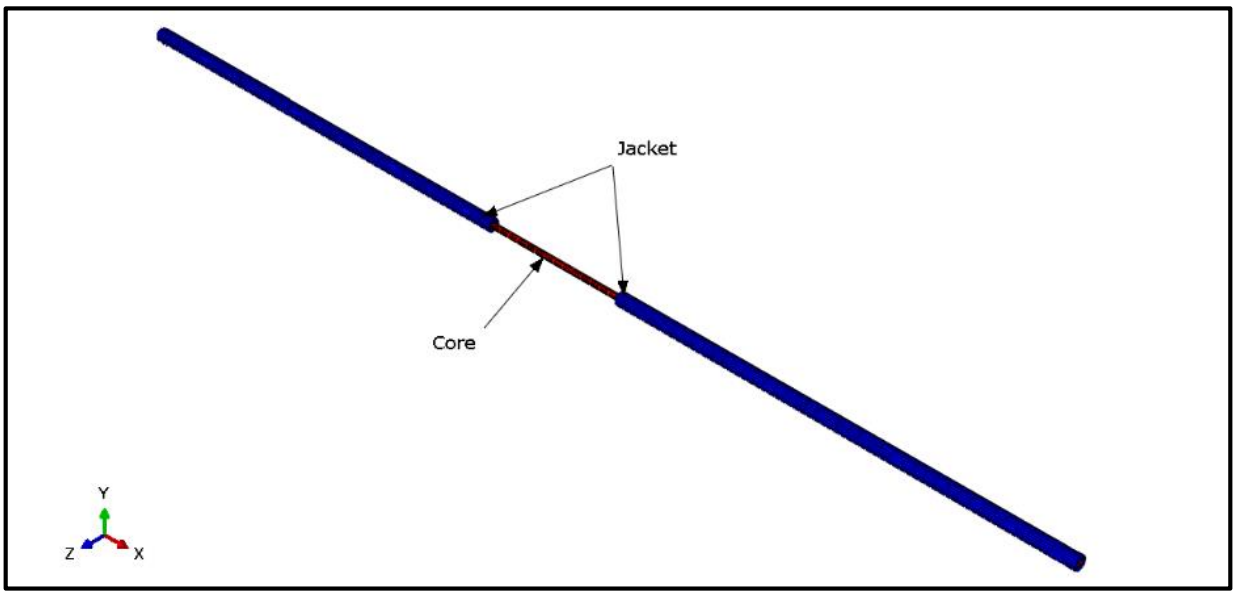

Figure 66: Suture model, intact core

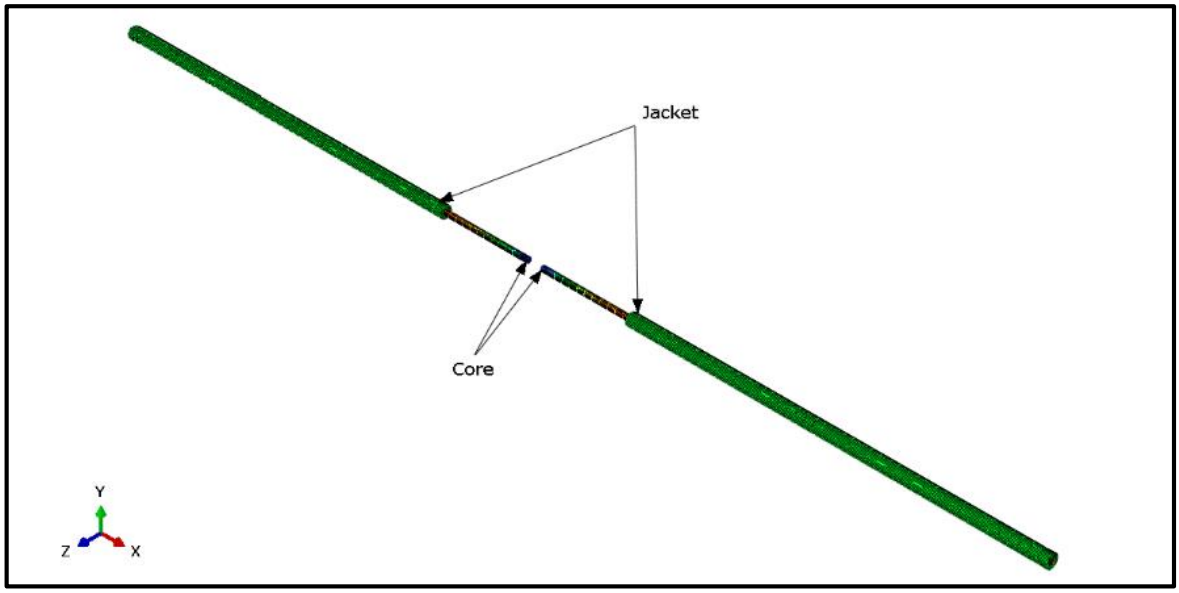

Figure 67: Suture model, broken core

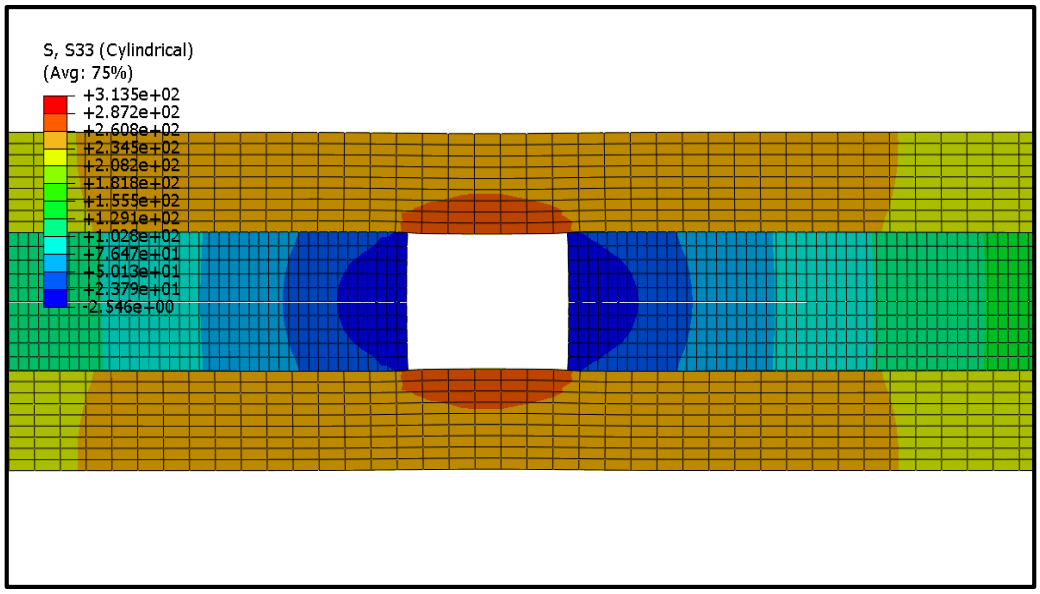

Figure 68: Shear stresses of the suture model, broken core

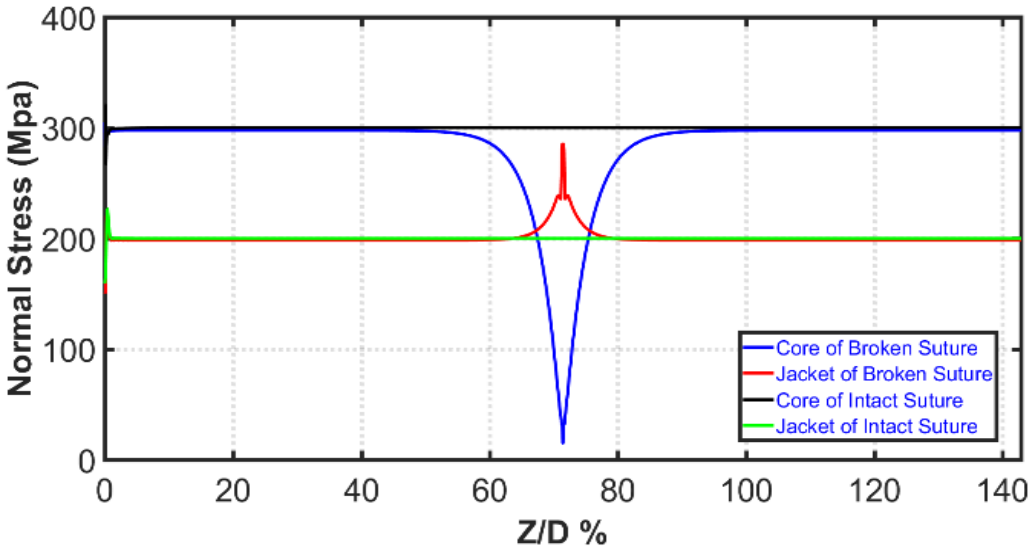

Figure 69: Normal stresses along the suture model

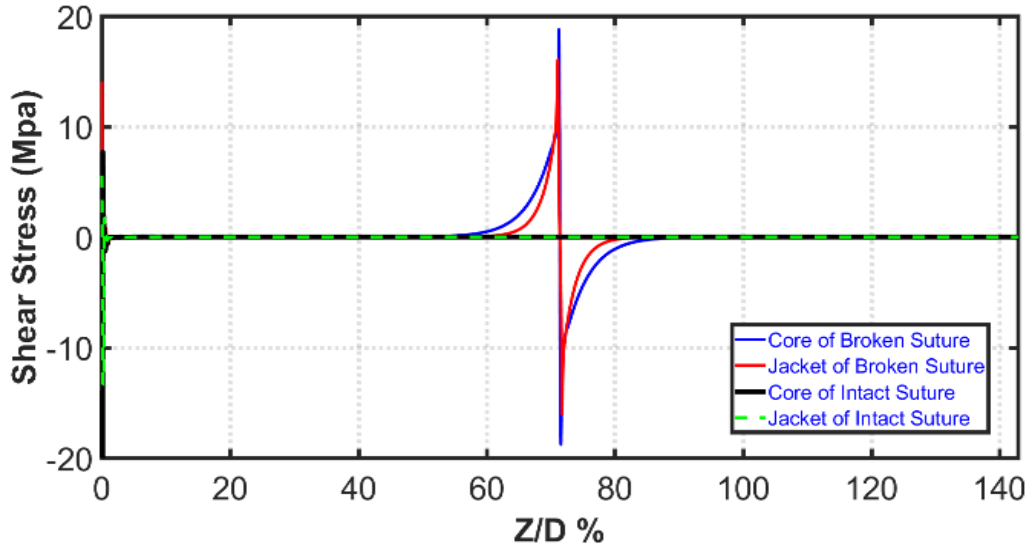

Figure 70: Shear stresses along the suture model

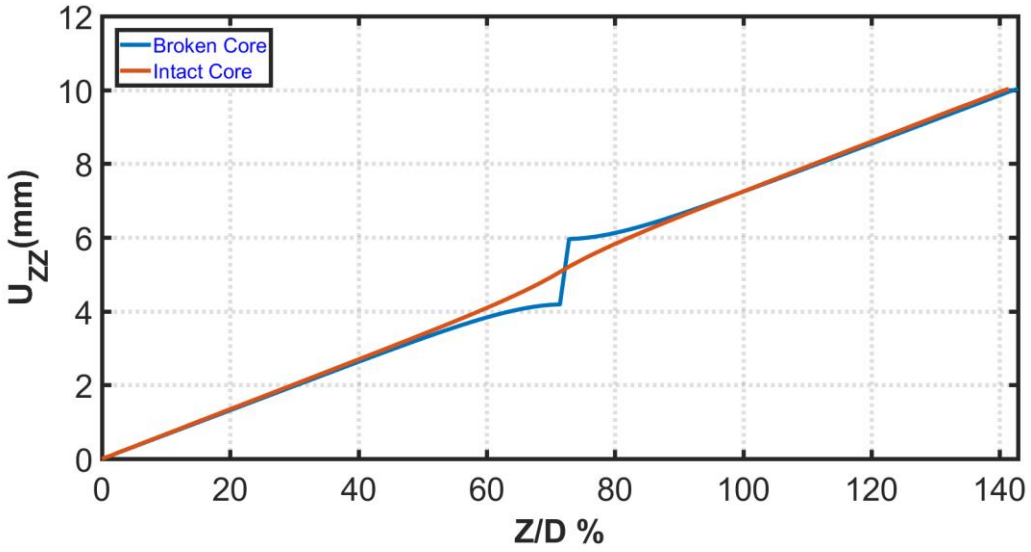

Figure 71: Displacement along the suture length, broken and intact core

5.3.2.5 Cyclic loading results

For both models, the stresses, strains, and displacement along the core interface were calculated and three different locations (nodes 1, node 2, and node 3) that were located on the edge of the broken core. Node 3 location was on the outer interface of the core that in contact

with the jacket. Node 1 was the center of the core while node 2 location was in the middle between nodes 1 and 3, as depicted in Figure 72. Various coefficient of friction (0.2, 0.3, and 0.4) and loads (10N, 30N, and 50N) were implemented in this study. In general, the results of the models were qualitatively correct. This maybe effect suture extension, thus leads to repair failure due to gap formation.

The loading/unloading cyclic tensile of the suture at node 3, load 50N, and coefficient of friction 0.4 were shown in Figure 73. Under the same conditions, the effect of cycle number on the interface slip and hysteresis at 1st, 15th, and 30th cycles was shown in Figure 74. The hysteresis loss energy decreases with increasing applied cycles due to decreasing the interface shear stress.

Effect of cyclic loading on the displacement of (intact/broken) core were shown in Figure 75. The results show that the broken core had more extension than the intact core. Also, the extension of the broken core was increased with increasing applied cycles. With increasing cycle number, the interface shear stress was decreased and the extension increased due to the interface interactions.

The effect of the coefficient of friction (0.2, 0.3, and 0.4) on the stress distribution along the interface of the core were analyzed, as shown in Figure 76. At load (50N,) the results show that the coefficient of friction was an impact on transfer length of the stresses at the end of the broken core. Because increasing coefficient of friction was lead to less sliding, less energy loss, and high shear stresses due to increasing the normal forces.

Moreover, the results show that the ratio of sliding the core was increased with a decreasing coefficient of friction approximately (2%) under the same applied load. Thereby,

the jacket was carried the highest load and the core was carried only a little load. While, with increasing the coefficient of friction the load was shared between core and jacket, and there was a low sliding. Finally, the results show that the broken core was extended approximately 0.1% more than the intact core under the effect of cyclic loading. The increase in the core extension was caused by the lower friction forces at the interface surfaces because increased periodic loading. Thus, the cyclic loading had an effect on the suture and perhaps leads to gap formation during the repair, which maybe extension leads to the repair failure.

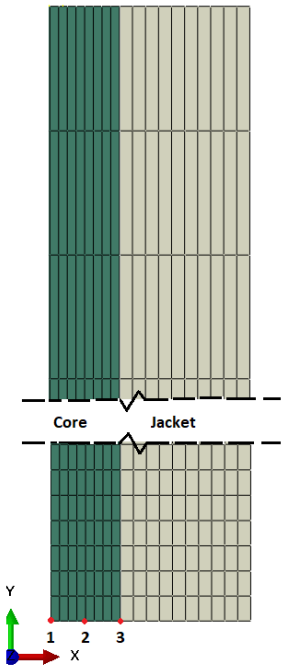

Figure 72: Locations of nodes on the core edge

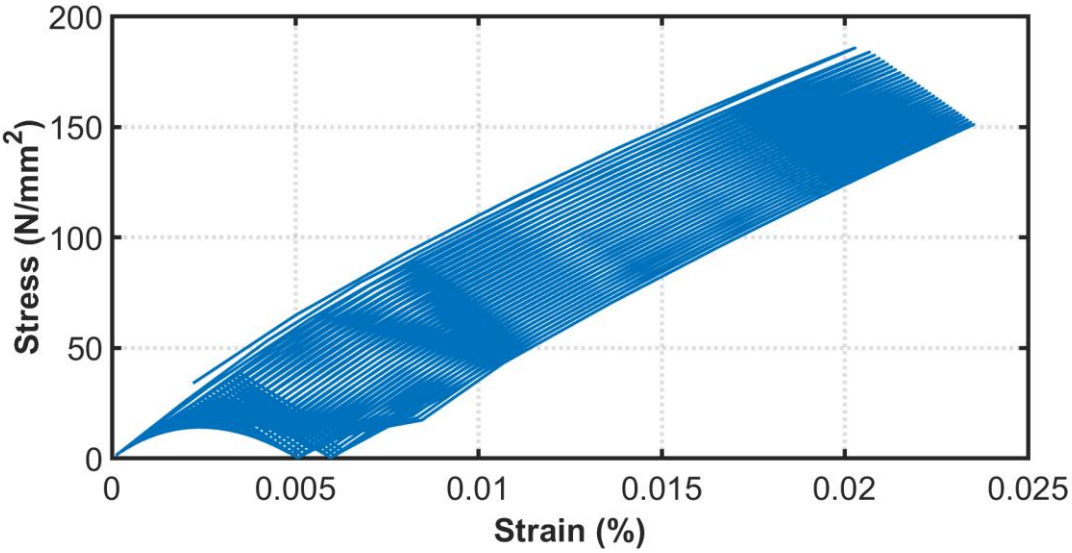

Figure 73: The loading/unloading cyclic tensile stress-strain curve of broken core

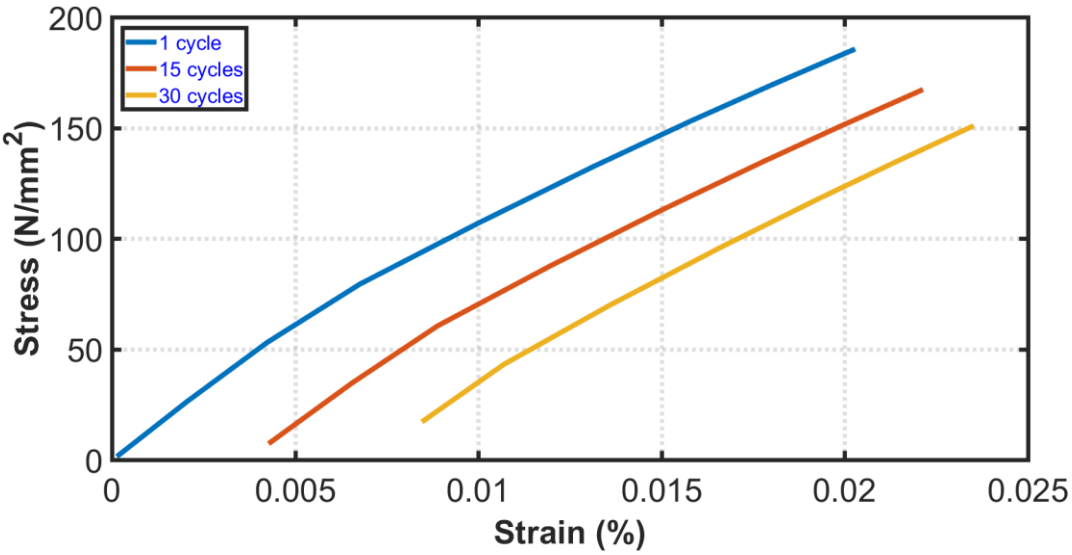

Figure 74: The hysteresis corresponding to different applied cycles

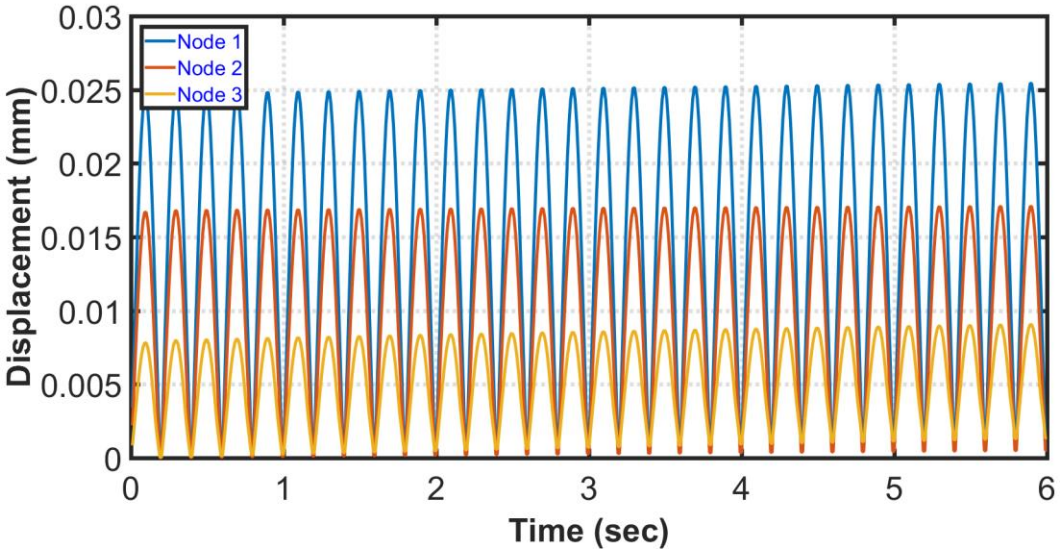

Figure 75: Displacement vs time, broken core

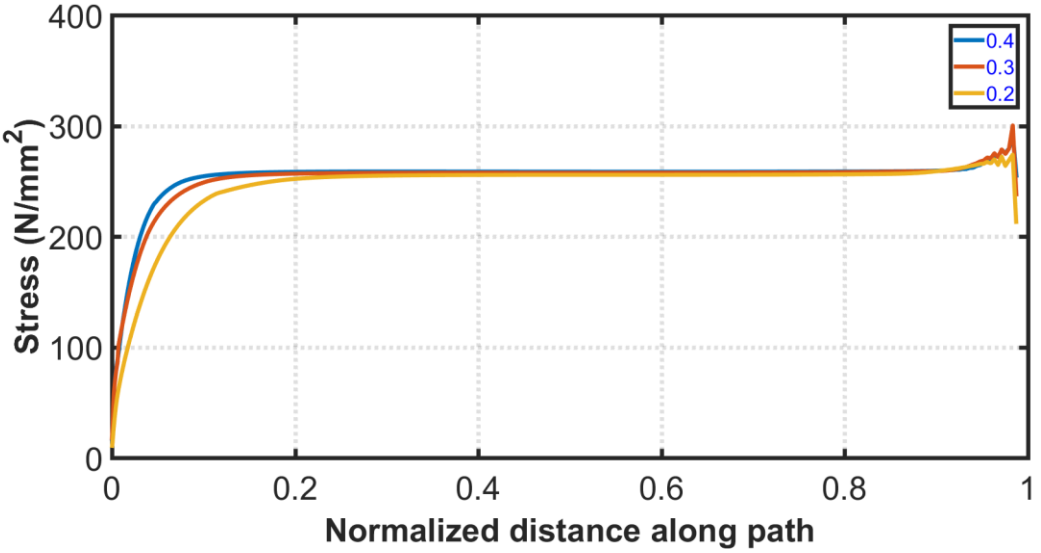

Figure 76: Effect of coefficient of frictions on the stresses along the core interface

5.4 Discussion

The experimental results showed that the suture was undergone a complex strain behavior due to structure complication. Under tension, the braided jacket lengthens and narrows while the angle between the warp and weft threads changes. Therefore, the

circumference shrinks with increases in tension. Consequently, the jacket compresses on the core, and is able to receive load via friction and shear lag when the core fails. This process in suture is similar to what occurs in long fiber reinforced composite materials.

Moreover, the results demonstrated that the shear load could be transferred between the core and the surrounding jacket when the core fails. The stresses are transferred through shear between the interacted fibers as a result of an interaction between neighboring fibers. Each interaction is initially composed of two shear-lag segments, delimited by a specific length. The jacket was observed during experiments to "reload" the core, even after core failure. When the length of the core reached the ineffective length, the jacket no longer shared the load with the core. In this case, the jacket carried the entire load resulting in an unstable failure in the jacket. Thus, this failure led to the rupture of the entire FiberWire suture.

The model results of the suture were consistent with the experimental results. In the region of the broken core, the core locally stopped carrying the axial load and sheds that load to a nearby jacket via shear lag. Also, the jacket surrounding the broken core was loaded in shear, transferred the load across the fractured site, and then transferred stress back onto the core again vis shear. The shear stress transfer in the jacket also caused the nearby core to experience stress concentrations over a certain length. The load transfer occurs over an identifiable characteristic length. The models show detailed stress and strain within the suture: the shear stress (in core and jacket) varied significantly over their cross-section and was highest close to the broken region. The portion (35%) of the Z/D ratio was subjected to both normal and shearing tractions, and the remaining part was to be subjected only to normal tractions. Experimentally, the jacket showed that it could reload the core no more than three times. The jacket filaments were able to carry load despite complete failure of the core

filament, however, the load transfer mechanism was studied over subsequent load cycles. The predicted stresses and strains occurred in locations that are qualitatively consistent with expectations based on shear lag theory. It might also be observed that there was an agreement between the two sets of results: experimental and FE model, and thus served to verify the reliability of the present FE model. Static and cyclic loading were implemented in this study. Under cyclic loading, the results showed that the broken core had more extension, approximately 2%, than the intact core. Thus, the FE model could be used in additional investigations about suture and tissue load transfer. The limitations of the current study were the following:

(1) FE model investigated effect of only one core failure on the stresses distributions.

(2) the effect of the perpendicular jacket cut on the stresses distribution and/or mechanical behavior of the suture has not been studied, while this type of cutting may also be one of the failure patterns of the suture.

5.5 Conclusions

In this chapter, a FE model to describe the shear lag phenomenon in a partially failed surgical suture has been developed. This study presents a validate FE models of (intact/broken) core sutures. It predicts the stress distribution and load transfer around the core fracture site. The FE results are qualitatively consistent with existing shear lag theory and also with experimental results for the subject composite suture. Thus, the FE model describes a biomechanical phenomenon by which failed suture can appear to be competent during a surgical procedure. Hence, a clinician should be aware of the possible failure mode and consider remedial actions when such failures are suspected.

This study is maybe the first to present a developed numerical model for simulating the mechanical behavior of partially failed a multifilament composites surgical suture (such as FiberWire) to identify the shear lag effect after core failure under cyclic loading. The magnitude of expansion of partially failed suture is affected by the number of load cycles. The described method may also provide insights in describing load transfer to soft tissue, and thus provide opportunity for optimization of suture/tissue interfaces. However, clinical recommendations are premature.

CHAPTER VI

FUTURE RESEARCH

This chapter includes three topics:

(1) knotless glenoid suture anchors.

(2) modeling of tendon and suture.

(3) recommendations.

6.1 Knotless glenoid suture anchors

To test the anchors experimentally, a specific fixture design is required to ensure that it is able to carry a high load and no relative movement between the entire system (fixture, bone) during the test. In this chapter, the fixture components and validation steps are illustrated. The knotless suture anchors have not been tested yet.

6.1.1 Background

Arthroscopic reconstructive surgery poses many challenges for the surgeon [109]. One of these is the tying of arthroscopic knots [109], [149]. Arthroscopic knot tying is technically demanding and required extensive practice to master [109], [150]. These facts raise concerns regarding the quality and consistency of arthroscopic knot tying and particularly in the hands of the novice [109]. To resolve the difficulty of tying secure knots with trusted arthroscopic tension, knotless anchors emerged as a viable alternative. Knotless anchors provide also a direct secure low-profile suture anchor repair. Anchors are small devices placed in the bone.

The use of knotless suture anchors for labral repair is first reported by Thal in 2001 [151], [152], and successful use of these anchors has been reported in multiple clinical studies since then [141–147]. New knotless suture anchors continue to be developed [154], [158], [160]. Several biomechanical studies have reported no significant difference in anchor pullout and ultimate load to failure between knotted and knotless anchors [140], [152], [161], [162]. A recent study has shown that there was no significant difference in stiffness between the knotted and knotless anchors [73], [153], [163], [164]. Cyclic loading has also been used to compare the biomechanical performance of suture anchors [165]–[167]. On the other hand, an in vitro comparison study of knot tying versus knotless metal suture anchors demonstrates that after insertion, knotless suture anchors may affect the tension of the repair, leading to gap formation between bone and soft tissue in comparison with knot tying anchors [12].

Suture anchors are widely used as they become the standard of care for stabilization, however, there is no consensus on using a specific anchor [34]. To increase the viability of knotless suture anchors, there are research studies in progress to improve them and to provided added benefit within the surgical area. However, to the best of my knowledge, no one has closely examined knotless anchors and evaluated their long-term performance under cyclic loading with regards to potential loop elongation.

The purpose of this study is to evaluate and compare the biomechanical properties of knotless suture anchors using cyclic displacement by characterizing the loop elongation (length from anchor head to fixation loop) over the load cycles as well as determining the load to failure and mode of failure. Fresh adult porcine femurs were brought from a local abattoir to use in the experimental tests. The test environment is prepared to be consistent with the

previous studies. This study is hypothesized that there will be no difference in these biomechanical parameters among several different knotless anchors.

6.1.2 Anchors

Suture Anchors consist of the following parts:

The Anchor: The Anchor might be made of metal or biodegradable material. It was inserted into the bone by using a screw mechanism or an interference fit.

The Eyelet: The Eyelet was a small hole or a loop in the anchor for passing the suture. This was connected the anchor to the suture.

The Suture: The Suture might be made of a non-absorbable material or absorbable material. It was linked to the anchor through the eyelet of the anchor.

6.1.3 Fixture components

The fixture was manufactured in the college machining workshop at Western Michigan University's Parkview Campus. It was designed for attaching onto the MTS machine in the Laboratory for Advanced Composite at Western Michigan University. Figure 77 depicts the schematic drawing of the fixture.

1. Lower base: A (310 mm*255 mm*10 mm) plate of hot rolled steel was installed in the MTS machine lower wedge grip. It was connected by bolts through this plate to the MTS machine lower wedge grip. On the right and left sides were holes to provide for location in X-direction.

2. Vise: The vise was mounted on the lower base plate and had a capability to be positioned in X-direction to allow for lateral movement. The objective of using it was to provide tilting orientation from (0^0 to 90^0) for the upper base.

3. L-plate: A (95 mm*50 mm*6.2 mm) plate of hot rolled steel had a plate with a slot which allowed for movement along the Z – direction and was clamped in the vise. A metal key was used to avoid the slipping that may occur during loading in the Y – direction.

4. Upper base: A (305 mm*195 mm*4.7 mm) plate of hot rolled steel welded on the L-plate was used to locate the specimen. It contained a longitudinal slot at the upper edge to allow for freedom of movement along the X – direction. Near the middle of this base were multiple holes to allow for more flexibility in mounting the specimen.

5. Screws and muffler clamp: were used to hold the specimen.

6. Plate and screw: A slotted plate was used as an arm to support part number seven below.

7. Beam: A (160 mm* 40 mm* 12.5 mm) beam of hot rolled steel was used to support and hold the specimen. It also had the ability to move along the X - direction.

8. Plate: A (75mm*35mm*6.2mm) plate of hot rolled steel connected parts 6 and 7 and was slotted to provide part 7 movement along the X - direction.

9. C-clamps: C-clamps were used to tie the upper base with the lower base.

10. Plumb-bob: A plumb-bob was placed on the MTS machine top wedge grip to determine the specimen center.

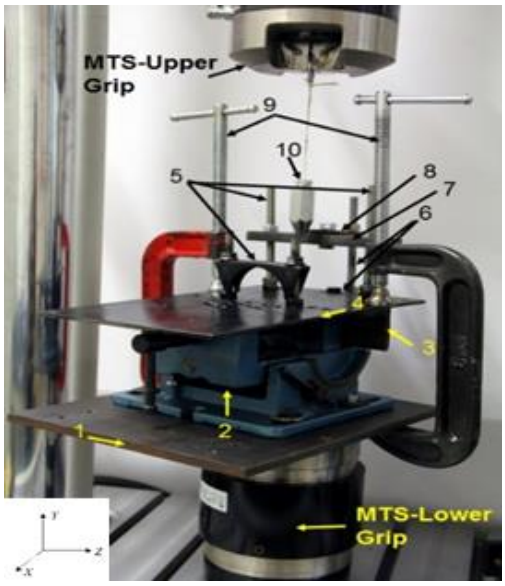

Figure 77: Schematic drawing of the fixture

6.1.3 Validation of experimental setup

A fresh porcine femur model was obtained from a local abattoir for use as specimens. After thawing, the bone was dissected free of all soft tissue, and the spiral screw was placed in the bone. The screw had a maximum external thread of (5.36 mm) and was welded to a steel rod. The screw was inserted, and a pullout test was conducted with the bone at room temperature to avoid any variables in anchor component performance that might be temperature dependent. The prepared specimens (femur holding the screw and rod) were placed in a specially designed fixture that supports the bone. The fixture was attached to the lower wedge grip of the MTS machine. The screw and rod were adjusted manually to become aligned directly under the top wedge grip of the MTS machine. The rod was fixed to the top wedge grip of the MTS machine. Only loads in line with the axis of screw insertion was used to develop data representing the worst case and to avoid angled distortion variations in data.

The criteria that used in this study for determining the failure of the fixture was dependent on the amount of movement of the fixture during pulling the screw. The controller was programmed to produce a displacement rate of 1 mm/sec until screw pullout occurred. The screw failure mode was defined as screw pullout, in which the screw came out of the bone completely or was mostly intact. The system's force and deflection were digitally collected by using a load cell that was linked to the MTS machine. Furthermore, to validate the results, three dial indicators with magnetic bases were used to measure the following:

1. Dial 1: to measure the deflection of the fixture only. The deflection was (0.00 mm).

2. Dial 2: to measure the deflection of the screw only. The deflection was approximately similar to the total deflection that was measured by using a built-in measuring system of the MTS machine.

3. Dial 3: to measure the deflection of the top wedge grip of the MTS machine only. The deflection was approximately similar to the total deflection that was measured by using a built-in measuring system of the MTS machine.

Figure 78 depicts the setup method of fixture, bone, screw and rod, and three dial indicators on the MTS machine. Deflection values of each dial indicator and the MTS machine had been recorded during the test, as depicted in Figure 79. The time lapse of the screw during the tensile portion of the test was depicted in Figure 80.

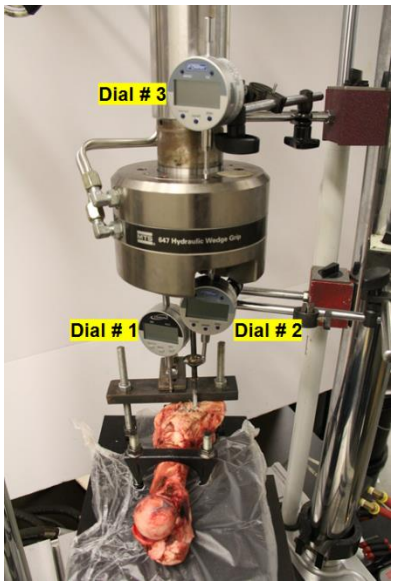

Figure 78: Setup method of fixture, bone, screw and rod, and dial indicators

Figure 79: Values of deflection for dial indicator and MTS machine

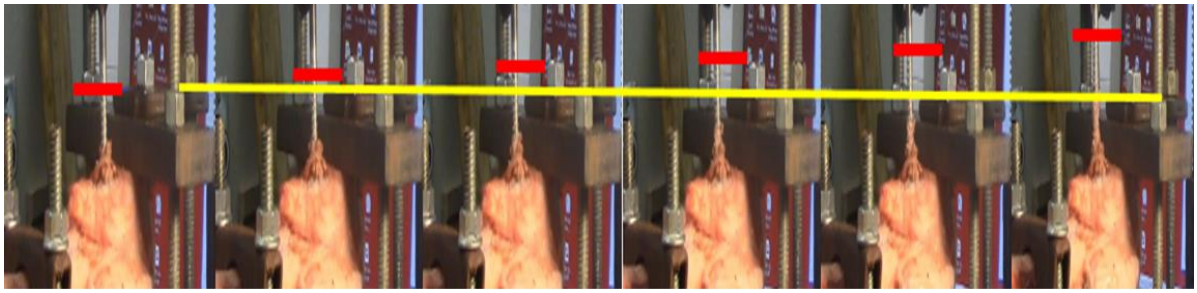

Figure 80: The time lapse of the screw during tensile portion of test

The load-displacement results of the load cell of the MTS machine, dial indicator number 3, and the difference between dial indicator number 2 and dial indicator number 1 were plotted as shown in Figure 81. The results demonstrate that there were no significant differences between the two curves; especially, there was a difference between the precision of dial indicators (1*10-2) and the load cell of MTS machine (1*10-8). Therefore, this outcome and the value of the dial indicator that was placed on the fixture as depicted in Figure 79 certify that there was negligible in the fixture.

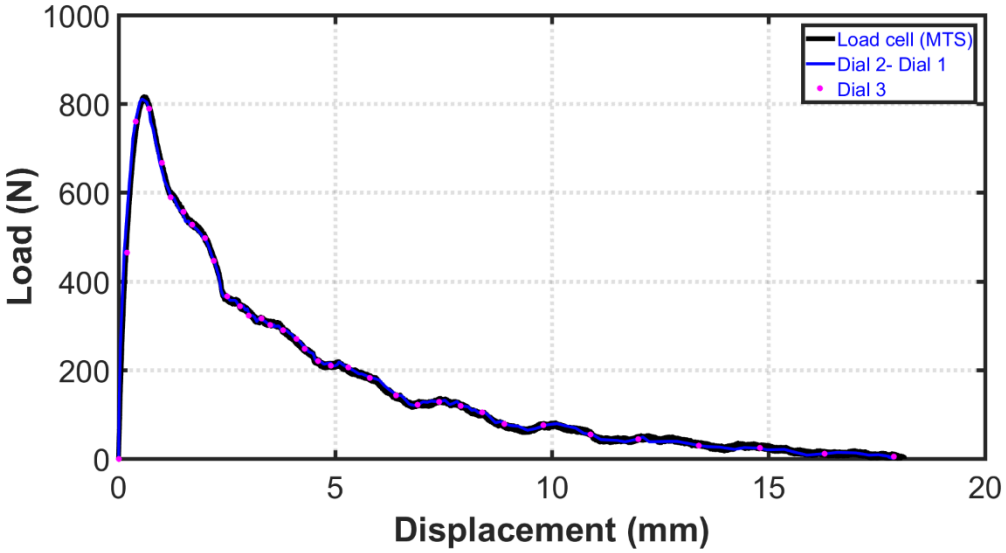

Figure 81: Load-Displacement results of MTS machine versus dial 3 and (dial 2 - dial 1)

The accuracy of the dial indicators that had been used were validated by using two dial indicators that were placed on the upper grip of the MTS machine to compare the MTS machine results with the results of the dial indicators under a tensile test. Appendix-A illustrates the set up for the dial indicators before and during the test, as well as the load-displacement results of the MTS machine and the dial indicator, shown respectively.

6.1.4 Calibration of load transducer

A known measurement from a calibrated device was called the reference. The second device under testing conditions was the unit being calibrated. The axial capacity of the MTS machine was (25 KN). To measure the applied load with a high precision, a load transducer (SM-2224 N) was used. The load transducer was connected to a strain indicator (3800) attached to the MTS machine. The calibration was necessary to ensure that the MTS machine with load transducer signals was precise and accurate. The calibration was split over two aspects: 1. calibration of the load transducer signal, and 2. calibration of the load transducer with known weights, as depicted in Appendix-B.

6.1.5 Proposed biomechanical testing

The anchors will be cyclically loaded and then pulled to failure on an MTS machine. Fresh frozen porcine femurs from a local butcher will be utilized for anchor fixation as has been performed in several similar studies [165], [168]. After thawing for 24 hours at room temperature, the soft tissue will be fully removed from the bone. The anchors' suture loop will be secured around a 2.08-mm diameter dowel, which will mimic the loop used to secure the labral tissue intra-operatively [169]. The anchors will then be inserted into the porcine bone following the manufacturers' specifications. The prepared specimen, with the anchor in place, will be secured to a custom fixture supporting the bone so that the suture is perpendicular to the dowel and directly in-line with the anchor insertion angle, and aligned under the top wedge grip of the load frame so that the applied load is parallel to the axis of anchor insertion, as depicted in Figure 82. A 16mm stainless steel bar was polished and machined to have 3.5 mm ring at the bar's center. The bar is also tapered from each end towards the ring, as shown in

Figure 82. The taper length and diameter reduction are 5mm and 6mm, respectively. The sutures are proximally fixed by winding several times in the tapered region and next to the ring and clamped superiorly by using two screws. The purpose of winding the suture several times is (1) to prevent the suture slippage through increasing friction forces between the suture and the bar gradually, (2) to decrease the stresses concentration along the suture. The purpose of the ring in the bar is to make the process repeatable. Also, this method avoiding the use of knots, which may act as a stress riser as well as introduce an additional variable [170]. The Each anchor will be inserted at least 1 cm from any other anchor to avoid a crack propagation between drill holes during testing [141]. Each insertion site will be unique and will never be used again in a specific bone. In pilot testing, the custom fixture and its restraint are confirmed to have negligible relative movement under loads whose values exceeded those expected during planned anchor testing Figure 81.

At room temperature, anchor insertion and pullout testing will be conducted with the bones to avoid any temperature-dependent variables in anchor component performance and to minimize variations in porcine femur response. A preload of 10 N will be applied to establish a reference state. Subsequently, cyclic loading between 10 and 100 N at 0.5 Hz will be applied for 200 cycles or until failure occurs. We will use a gauge length of suture that as small as allowed or is practical within our setup without compromising the cyclic loading. This gauge length at the base state will be measured and will be used to quantify stretch in the suture or slippage of the suture in the anchor (hereafter, loop elongation) over the duration of load. After completion of 200 cycles, destructive testing will be performed through application of an enforced displacement rate of 12.5 mm per second [165], [171]. The mode of failure will then be recorded. Data sampling of load and loop elongation will be obtained at 100

samples per second. The number of cycles needed to reach 1, 3, and 5 mm of loop elongation will be recorded (if the suture remains intact or lengthens without breaking). The total anchor displacement from its initial position, if any, will also be recorded after 200 cycles and after the suture/anchor has failed [159].

Attempts were made to obtain commercially available knotless anchors from the following companies: Arthrex, DePuy Mitek, Smith & Nephew, Zimmer Biomet, ConMed Linvatec, Stryker, and Parcus Medical. These companies have the largest shares of the knotless glenoid anchor market. Unfortunately, so far only one type has been obtained.

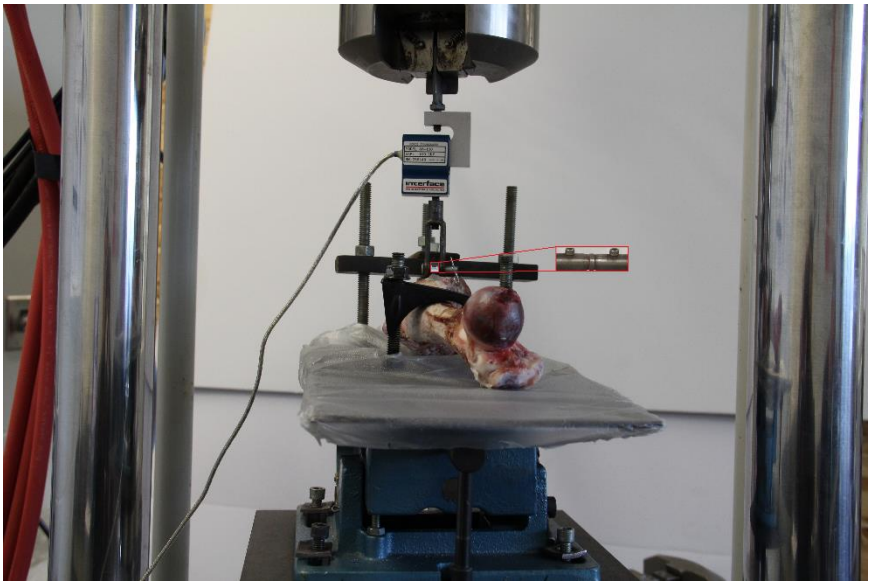

Figure 82: The planned experimental set-up is shown, demonstrating the method for stabilization of the femur

6.2 Modeling of tendon and suture

The goal of this study was to develop a 3D FE model of a sutured tendon repair to observe the stress arising when load was applied to the repair and then to compare the results with Rawson [31]. Abaqus was used as a preprocessor and postprocessor for the FE analysis. Suture and tendon dimensions, properties, and boundary conditions were used by relying on

the research [31]. The components were created using 3D modeling with solid, continuum, and deformable elements. The thickness and width of the modeled tendon were 3.5 and 6.5 mm, respectively, and the suture diameter was 0.2 mm, as depicted in Figure 83. The suture was described as a homogeneous linear elastic material with Poisson's ratio of 0.4 and Young's modulus of 1 GPa. Isotropic linear elastic descriptions were employed to describe tendon tissue with Poisson's ratio of 0.4 and Young's modulus of 2 GPa. The interaction between the tendon and suture was represented by a surface-to-surface interaction. Loads and boundary conditions were defined as depicted in Figure 84. Two types of elements C3D8R hexahedral element and C3D10 tetrahedral element were used to represent the suture and tendon respectively, as depicted in Figure 85. Figure 86 illustrates some preliminary results. Modelling of sutured tendon repair failure has not yet been completed.

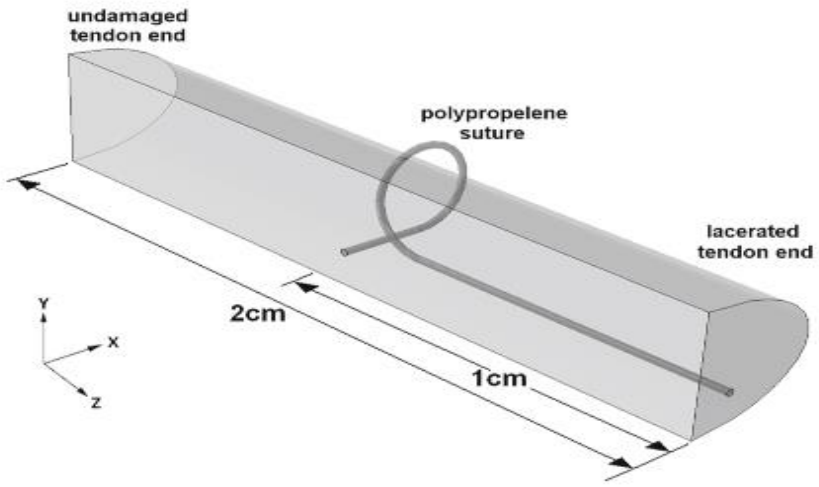

Figure 83: Model dimensions [31]

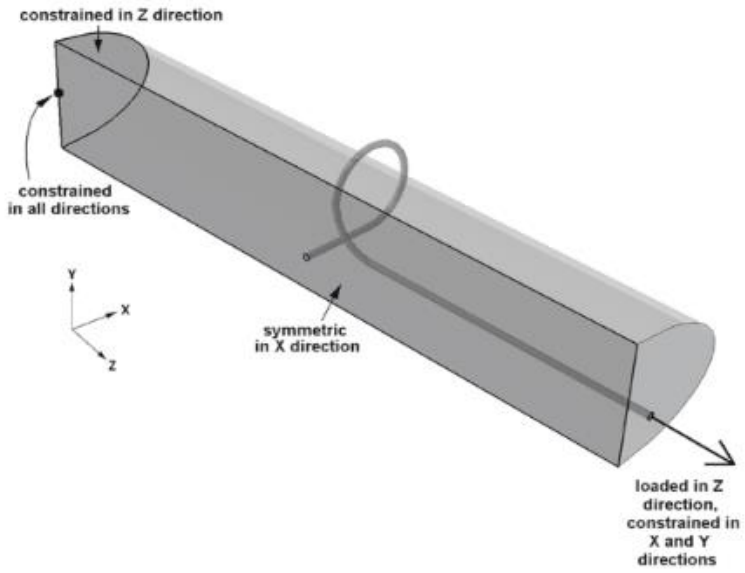

Figure 84: Boundary conditions [31]

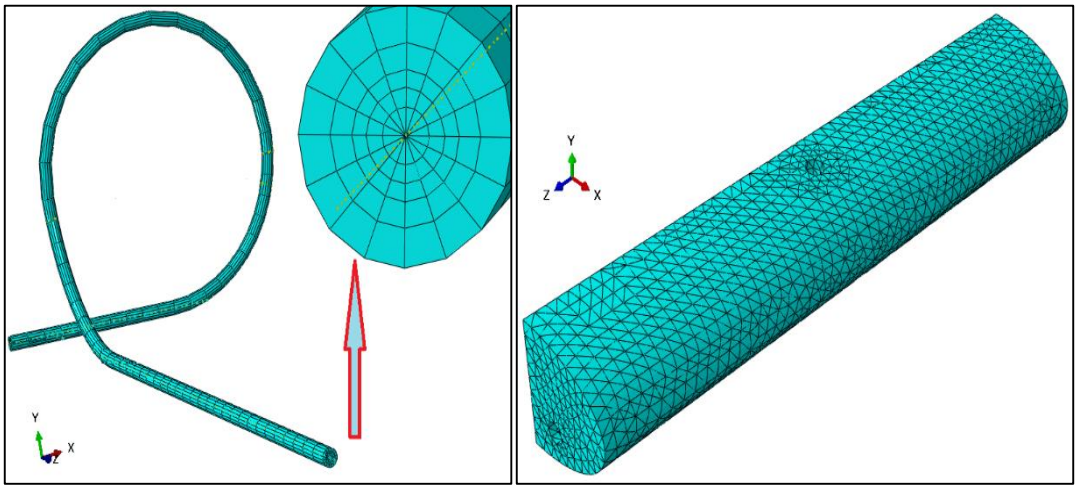

Figure 85: Mesh of parts, left: suture and right: tendon

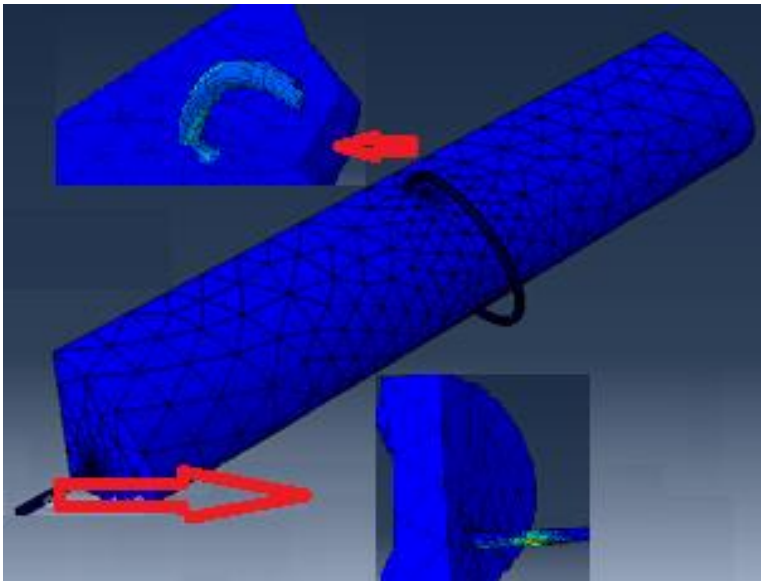

Figure 86: FE results

6.3 Recommendations

It is observed that the suture material and single throw knot have an effect on the failure mechanism and the knot strength. In addition, the absence of proper guidelines to select the optimal suture material and knot technique for a specific clinical situation requires more investigations. However, the area of interest is stress in the suture, knot, and tendon. Therefore, the following is a list of recommended future directions:

1. Pursue an investigation into the possibility of quantifying the impact of multiple knots on the mechanical behavior of the sutures and tendon repair using FE analysis. Experiments also should be conducted to validate the FE results.
2. To extend this work, develop a FE model to investigate the effect of the perpendicular jacket cut on the stresses distribution and/or mechanical behavior of (unknotted/knotted) is recommended. Specifically, the perpendicular jacket cut is one of the failure patterns of the suture and/or repair.

3. A study that demonstrates the effects of the suture cross-section area plus the suture materials, knot configurations and tying technique recommended to determine the mechanical performance of surgical sutures. FiberTape surgical suture has similar structure as FiberWire suture. The tapes provide broad compression and increased tissue cut-through resistance. The tapes can be a good choice for knotless rotator cuff repair, high demand applications, e.g., AC joint reconstruction and other areas where tissue pull-through may be a concern [172].
4. Only the overhand knot was investigated in this study using FE and experiments. The overhand knot is one of the most fundamental knots, and it forms the basis of many others. Therefore, it is critical to studying the influence of other knot types (Weston knot, square knot, granny knot, … etc.) on the mechanical behavior of the sutures and tendon repair using FE analysis and experiments. Study of these additional knot is recommended as an extension of this work.
5. It is recommended to improve the initial FE knot model geometry through finding a mathematical expression that can describe different knot configurations. Particularly, several previous studies have indicated that there is no model yet for the suture knot; despite the fact that failure mostly happens at the knot [31]. This recommendation is an extension of the work done by Rawson et al. The first step to creating equations that described the single throw-knot were done, see the equations below. Further, Figure 87 and Figure 88 show the knot configuration and the primary result of FE model, respectively. $x = \sin(t)+2*\sin(2*t)$

   $y = \cos(t)-2*\cos(2*t)$

   $z = -\sin(3*t)$

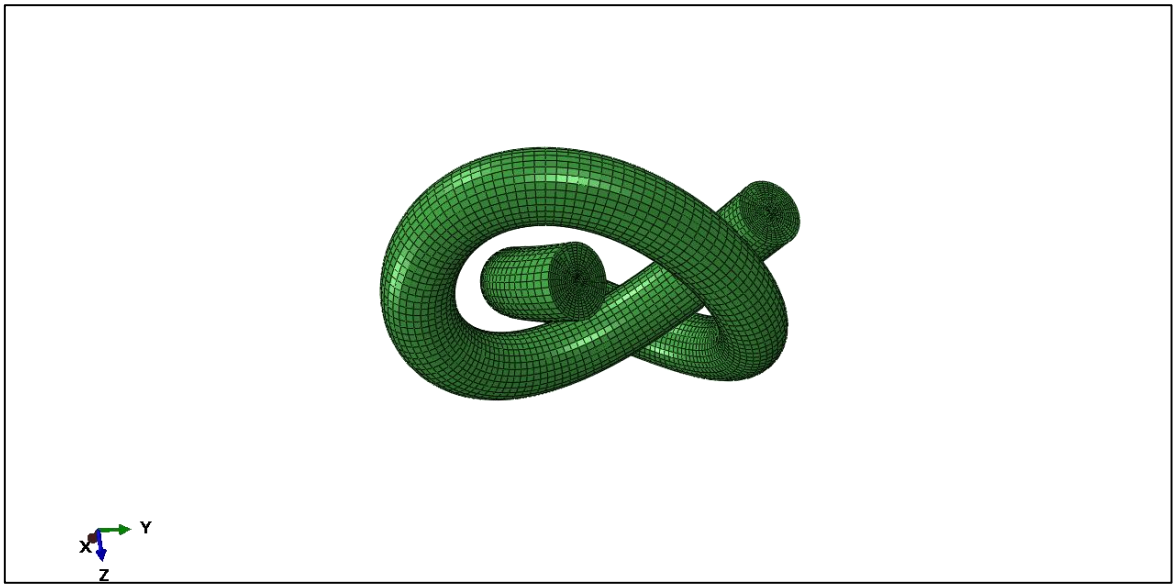

Figure 87: Knot configuration

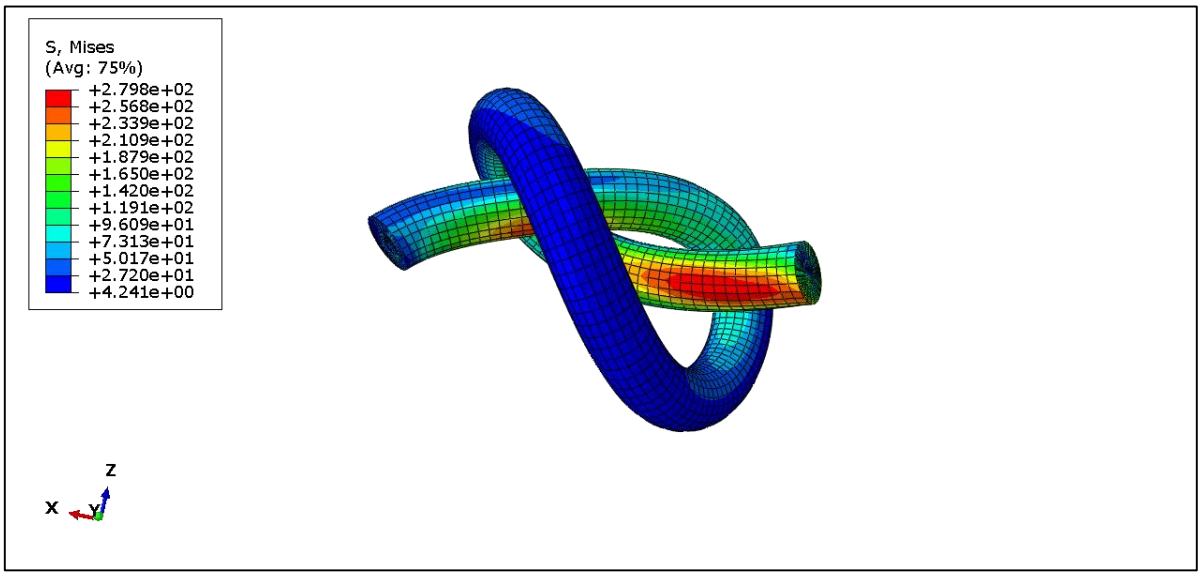

Figure 88: Primary result of FE model

6. It is recommended to proceed with the preliminary work of this study, the failure of the suture, knot and tendon repair can be evaluated under cyclic loading. By employing FE

analysis, this dissertation predicted the location of stresses and strains that were qualitatively consistent with expectations. Therefore, the FE model can also be used in further investigations.

7. Development of an optimal procedure, based on clinical data and/or in-house experimental research of the validated model, and applying it on the suture, knot, and tendon.
8. This study has reported the behavior of the core and the jacket separately. Further investigation to optimize the mechanical properties of the suture can be beneficial. For example, a study can be conducted to investigate the influence of the core diameter on the mechanical properties of the suture, knot, and repair.
9. An important part of the good suturing technique is the correct method in knot tying. Therefore, the effect tightening angle of the suture should be studied.
10. This dissertation presented a valid fixture to test the suture anchors. Therefore, the experimental tests of knotless glenoid suture anchors for labral repair can be accomplished once the other remaining anchors are obtained.
11. Knowing the details effect of cyclic loading on the mechanical behavior of the FiberWire surgical suture is also important in interpreting the results and the modeling. The preliminary investigations of testing the suture under cyclic loading are shown in Appendix-C.

REFERENCES

[1] G. Yang, B. B. Rothrauff, and R. S. Tuan, "Tendon and ligament regeneration and repair: Clinical relevance and developmental paradigm," *Birth Defects Research Part C - Embryo Today: Reviews*, vol. 99, no. 3. pp. 203–222, 2013.

[2] A. J. Lomas *et al.*, "The past, present and future in scaffold-based tendon treatments," *Adv. Drug Deliv. Rev.*, vol. 84, pp. 257–277, 2015.

[3] "Sprains, Strains and Other Soft-Tissue Injuries," *American Academy of Orthopaedic Surgeons*. [Online]. Available: http://orthoinfo.aaos.org/topic.cfm?topic=A00111. [Accessed: 01-Jan-2016].

[4] S. A. Abbah, K. Spanoudes, T. O'Brien, A. Pandit, and D. I. Zeugolis, "Assessment of stem cell carriers for tendon tissue engineering in pre-clinical models.," *Stem Cell Res. Ther.*, vol. 5, no. 2, p. 38, 2014.

[5] J. Maquirriain, "Achilles tendon rupture : Avoiding tendon Lengthening during Surgical repair and," vol. 84, pp. 289–300, 2011.

[6] A. S. Hockenberger and E. Karaca, "Effect of suture structure on knot performance of polyamide sutures," *Indian J. Fibre Text. Res.*, vol. 29, no. 3, pp. 271–277, 2004.

[7] A. G. Heward, R. M. Laing, D. J. Carr, and B. E. Niven, "Tensile Performance of Nonsterile Suture Monofilaments Affected by Test Conditions," *Text. Res. J.*, vol. 74, no. 1, pp. 83–90, Jan. 2004.

[8] P. D. David, *Wound Closure Manual*. The University of Pennsylvania, Philadelphia: ETHICON PRODUCTS, a Johnson & Johnson company.

[9] * Abraham, A. ; * League, N. ; Kulkarni, and F. + Amirouche, “CLOVER HITCH TENDON SUTURE: EXPERIMENTAL TENSILE STRENGTH COMPARISON WITH OTHER TENDON SUTURES.”

[10] X. Avoine, B. Lussier, V. Brailovski, K. Inaekyan, and G. Beauchamp, “Evaluation of the effect of 4 types of knots on the mechanical properties of 4 types of suture material used in small animal practice.,” *Can. J. Vet. Res.*, vol. 80, no. 2, pp. 162–70, Apr. 2016.

[11] Srinivasulu K and N. Dhiraj Kumar, “a Review on Properties of Surgical Sutures and Applications in Medical Field,” *IMPACT Int. J. Res. Eng. Technol. (IMPACT IJRET)*, vol. 2, no. 2, pp. 85–96, 2014.

[12] D. L. Bartel, D. T. Davy, and T. M. Keaveny, *Orthopaedic Biomechanics: Mechanics and Design in Musculoskeletal Systems.* 2006.

[13] C. T. Thorpe, H. L. Birch, P. D. Clegg, and H. R. C. Screen, “Tendon Physiology and Mechanical Behavior: Structure-Function Relationships,” in *Tendon Regeneration: Understanding Tissue Physiology and Development to Engineer Functional Substitutes*, 2015.

[14] D. Docheva, S. A. Müller, M. Majewski, and C. H. Evans, “Biologics for tendon repair,” *Adv. Drug Deliv. Rev.*, vol. 84, pp. 222–239, 2015.

[15] K. M. Heinemeier, “Adaptation of tendon and muscle connective tissue to mechanical loading Involvement of collagen-inducing growth factors,” p. 91, 2007.

[16] S. P. Reese, B. J. Ellis, and J. A. Weiss, “Multiscale Modeling of Ligaments and

Tendons," *Stud. Mechanobiol. Tissue Eng. Biomater.*, vol. 14, pp. 103–147, 2012.

[17] S. W. Linderman *et al.*, "Shear lag sutures: Improved suture repair through the use of adhesives," *Acta Biomater.*, vol. 23, pp. 229–239, 2015.

[18] M. K. Jawed, P. Dieleman, B. Audoly, and P. M. Reis, "Untangling the Mechanics and Topology in the Frictional Response of Long Overhand Elastic Knots," *Phys. Rev. Lett.*, vol. 115, no. 11, 2015.

[19] A. Sood, M. S. Granick, and N. L. Tomaselli, "Wound Dressings and Comparative Effectiveness Data," *Adv. Wound Care,* 2014.

[20] J. G. Thacker *et al.*, "Mechanical performance of surgical sutures.," *Am. J. Surg.*, vol. 130, no. 3, pp. 374–380, Sep. 1975.

[21] E. D. M. Fong, A. S. R. Bartlett, S. Malak, and I. A. Anderson, "Tensile strength of surgical knots in abdominal wound closure," *ANZ J. Surg.*, 2008.

[22] G. D. Monheit, "Wound Closure and Suture Technique," Birmingham, Alabama.

[23] J. E. Tidwell, V. L. Kish, J. B. Samora, and J. Prud'homme, "Knot security: how many throws does it really take?," *Orthopedics*, vol. 35, no. 4, pp. e532-7, 2012.

[24] C. A. Zimmer *et al.*, "Influence of knot configuration and tying technique on the mechanical performance of sutures," *J. Emerg. Med.*, vol. 9, no. 3, pp. 107–113, 1991.

[25] N. Clauvelin, B. Audoly, and S. Neukirch, "Matched asymptotic expansions for twisted elastic knots: A self-contact problem with non-trivial contact topology," *J. Mech. Phys. Solids*, vol. 57, no. 9, pp. 1623–1656, 2009.

[26] B. Audoly, N. Clauvelin, and S. Neukirch, “Elastic knots,” *Phys. Rev. Lett.*, vol. 99, no. 16, pp. 1–5, 2007.

[27] R. F. Edlich, “Surgical Knot Tying Manual.” COVIDIEN.

[28] J. B. Hermman, “Tensile strength and knot security of surgical suture materials,” *Am Surg*, vol. 37, no. 4, pp. 209–17, 1971.

[29] D. J. Carr, A. G. Heward, R. M. Laing, and B. E. Niven, “Measuring the strength of knotted suture materials,” *J. Text. Inst.*, vol. 100, no. 1, pp. 51–56, 2009.

[30] R. C. Dinsmore, “Understanding surgical knot security: a proposal to standardize the literature.,” *J. Am. Coll. Surg.*, vol. 180, no. 6, pp. 689–699, Jun. 1995.

[31] S. D. Rawson, L. Margetts, J. K. F. Wong, and S. H. Cartmell, “Sutured tendon repair; a multi-scale finite element model.,” *Biomech. Model. Mechanobiol.*, vol. 14, no. 1, pp. 123–33, 2015.

[32] “SLiK^{TM} Knotless Screw-In Anchors - PEEK - Parcus Medical.” .

[33] “Suture Anchors.” [Online]. Available: https://www.shoulderdoc.co.uk/article/538. [Accessed: 01-Jan-2016].

[34] T. S. Johnson, C. M. DiPompeo, Z. C. Ismaeli, P. A. Porter, S. L. Nicholson, and D. C. Johnson, “Recycling suture limbs from knotless suture anchors for arthroscopic shoulder stabilization,” *Arthrosc. Tech.*, 2014.

[35] R. Robbe and G. A. Paletta, “Knotless Suture-Based Anchors,” 2004.

[36] “Effect of Heating Method on Microstructure and Mechanical Properties of Zircon Reinforced Aluminum Composites.” .

[37] C. H. Gireesh, “Experimental Investigation on Mechanical Properties of an Al6061 Hybrid Metal Matrix Composite,” pp. 1–10, 2018.

[38] Y. Swolfs, I. Verpoest, and L. Gorbatikh, “A review of input data and modelling assumptions in longitudinal strength models for unidirectional fibre-reinforced composites,” *Composite Structures*. 2016.

[39] Y. Swolfs, I. Verpoest, and L. Gorbatikh, “Issues in strength models for unidirectional fibre-reinforced composites related to Weibull distributions, fibre packings and boundary effects,” *Compos. Sci. Technol.*, 2015.

[40] I. M. Daniel and O. Ishai, *Engineering mechanics of composite materials*. 1994.

[41] C. M. Landis and R. M. McMeeking, “A shear-lag model for a broken fiber embedded in a composite with a ductile matrix,” *Compos. Sci. Technol.*, 1999.

[42] “Finite Element Method – What Is It FEM and FEA Explained.” .

[43] “THE FINITE ELEMENT METHOD.” .

[44] Ö. B. Güntürk, M. Kayalar, İ. Kaplan, A. Uludağ, K. Özaksar, and B. Keleşoğlu, “Results of 4-strand modified Kessler core suture and epitendinous interlocking suture followed by modified Kleinert protocol for flexor tendon repairs in Zone 2,” *Acta Orthop. Traumatol. Turc.*, pp. 3–7, 2018.

[45] T. Pillukat, R. Fuhrmann, J. Windolf, and J. van Schoonhoven, “Nahttechniken und Nahtmaterial in der Beugesehnenchirurgie,” *Chirurg*, vol. 88, no. 3, pp. 259–270, 2017.

[46] T. Moriya, M. C. Larson, C. Zhao, K. N. An, and P. C. Amadio, “The effect of core

suture flexor tendon repair techniques on gliding resistance during static cycle motion and load to failure: A human cadaver study," *J. Hand Surg. Eur. Vol.*, 2012.

[47] S. Wang, H. Wang, and Longwang Yue, "A novel knot-tying approach for minimally invasive surgical robot systems," *Int. J. Med. Robot. Comput. Assist. Surg.*, vol. 4, pp. 268–276, 2008.

[48] B. J. Ollivere, H. A. Bosman, P. W. P. Bearcroft, and A. H. N. Robinson, "Foreign body granulomatous reaction associated with polyethelene 'Fiberwire®' suture material used in Achilles tendon repair," *Foot Ankle Surg.*, 2014.

[49] J. P. Allen and N. Y. . Metropolitan Museum of Art (New York, *The art of medicine in ancient Egypt*. Metropolitan Museum of Art, 2005.

[50] E. Silver, R. Wu, J. Grady, and L. Song, "Knot Security- How is it Affected by Suture Technique , Material , Size , and Number of Throws ?," *J. Oral Maxillofac. Surg.*, vol. 74, no. 7, pp. 1304–1312, 2016.

[51] E. J. van Rijssel, R. Brand, C. Admiraal, I. Smit, and J. B. Trimbos, "Tissue reaction and surgical knots: the effect of suture size, knot configuration, and knot volume.," *Obstet. Gynecol.*, vol. 74, no. 1, pp. 64–68, 1989.

[52] A. Chauhan, B. A. Palmer, and G. A. Merrell, "Flexor tendon repairs: Techniques, eponyms, and evidence," *J. Hand Surg. Am.*, vol. 39, no. 9, pp. 1846–1853, 2014.

[53] O. A. Ilahi, S. A. Younas, D. M. Ho, and P. C. Noble, "Security of knots tied with ethibond, fiberwire, orthocord, or ultrabraid," *Am. J. Sports Med.*, vol. 36, no. 12, pp. 2407–2414, 2008.

[54] J. J. Ivy, J. B. Unger, J. Hurt, and D. Mukherjee, “The effect of number of throws on knot security with nonidentical sliding knots,” *Am. J. Obstet. Gynecol.*, vol. 191, no. 5, pp. 1618–1620, 2004.

[55] I. K. Y. Lo, S. S. Burkhart, K. C. Chan, and K. Athanasiou, “Arthroscopic Knots: Determining the Optimal Balance of Loop Security and Knot Security,” *Arthrosc. - J. Arthrosc. Relat. Surg.*, 2004.

[56] R. K. Lieurance, D. S. Pflaster, D. Abbott, and W. M. Nottage, “Failure characteristics of various arthroscopically tied knots,” *Clin. Orthop. Relat. Res.*, no. 408, pp. 311–318, 2003.

[57] T. Muffly, T. C. McCormick, J. Dean, A. Bonham, and R. F. C. Hill, “An evaluation of knot integrity when tied robotically and conventionally,” *Am. J. Obstet. Gynecol.*, 2009.

[58] D. M. Wüst, D. C. Meyer, P. Favre, and C. Gerber, “Mechanical and Handling Properties of Braided Polyblend Polyethylene Sutures in Comparison to Braided Polyester and Monofilament Polydioxanone Sutures,” *Arthrosc. - J. Arthrosc. Relat. Surg.*, vol. 22, no. 11, pp. 1146–1153, 2006.

[59] F. A. Barber, M. A. Herbert, D. Ph, and R. C. Beavis, “Cyclic Load and Failure Behavior of Arthroscopic Knots and High Strength Sutures,” *YJARS*, vol. 25, no. 2, pp. 192–199, 2016.

[60] S. Najibi, R. Banglmeier, J. Matta, and M. Tannast, “Material properties of common suture materials in orthopaedic surgery,” *Iowa Orthop. J.*, vol. 30, pp. 84–88, 2010.

[61] P. B. Wright *et al.*, “Strength of Damaged Suture: An In Vitro Study,” vol. 22, no. 2, pp. 1270–1275, 2006.

[62] F. A. Barber, M. A. Herbert, D. Ph, D. A. Coons, M. H. Boothby, and F. A. B. E. T. Al, “Sutures and Suture Anchors — Update 2006,” vol. 22, no. 10, pp. 1063–1069, 2006.

[63] G. Abbi, L. Espinoza, T. Odell, A. Mahar, R. Pedowitz, and D. Ph, “Evaluation of 5 Knots and 2 Suture Materials for Arthroscopic Rotator Cuff Repair: Very Strong Sutures Can Still Slip,” vol. 22, no. 1, pp. 38–43, 2006.

[64] “Collective Summary of Strength and Biocompatibility Testing Data Comparisons of Polyester and Polyblend Sutures,” *rthrex FiberWire^{TM}*. [Online]. Available: http://www.arthrexvetsystems.com/en/mediacenter/whitepapers/upload/FiberWire-White-Paper.pdf. [Accessed: 01-Jan-2016].

[65] S. M. Hassinger, M. D. Wongworawat, and J. W. Hechanova, “Biomechanical Characteristics of 10 Arthroscopic Knots,” *Arthrosc. - J. Arthrosc. Relat. Surg.*, 2006.

[66] W. B. J. Rudge and M. James, “Flexor Tendon Injuries in the Hand: A UK Survey of Repair Techniques and Suture Materials—Are We Following the Evidence?,” *ISRN Plast. Surg.*, vol. 2014, pp. 1–4, 2014.

[67] X. Li, M. King, and P. MacDonald, “Comparative study of knot performance and ease of manipulation of monofilament and braided sutures for arthroscopic applications,” *Knee Surgery, Sport. Traumatol. Arthrosc.*, 2004.

[68] J. Tan, B. Wang, Y. Xu, and J. B. Tang, “Effects of direction of tendon lacerations on

strength of tendon repairs," *J. Hand Surg. Am.*, vol. 28, no. 2, pp. 237–242, 2003.

[69] Y. F. Wu and J. B. Tang, "Effects of tension across the tendon repair site on tendon gap and ultimate strength," *J. Hand Surg. Am.*, vol. 37, no. 5, pp. 906–912, 2012.

[70] J. Earp, "The Influence of External Loading and Speed of Movement on Muscle-Tendon Unit Behaviour and its Implications for Training."

[71] T. W. Lin, L. Cardenas, and L. J. Soslowsky, "Biomechanics of tendon injury and repair," *J. Biomech.*, vol. 37, no. 6, pp. 865–877, 2004.

[72] T. Mazurek, M. Strankowski, M. Ceynowa, and M. Roc??awski, "Tensile strength of a weave tendon suture using tendons of different sizes," *Clin. Biomech.*, vol. 26, no. 4, pp. 415–418, 2011.

[73] M. C. Jordan, K. Schmidt, R. H. Meffert, and S. Hoelscher-Doht, "Biomechanical analysis of flexor tendon repair using knotted kessler and bunnell techniques and the knotless bunnell technique," *J. Hand Surg. Am.*, vol. 40, no. 1, pp. 115–120, 2015.

[74] W. Weintraub, *Tendon and Ligament Healing: A New Approach to Sports and Overuse Injury*, 2nd Editio. Berkeley, California: Notrh Atlantic books, 2003.

[75] N. Olsson, "Acute achilles tendon rupture Outcome, Prediction and Optimized Treatment," Gothenburg, Sweden, 2013.

[76] L. A. Dahlgren, "Pathobiology of Tendon and Ligament Injuries," *Clin. Tech. Equine Pract.*, vol. 6, no. 3, pp. 168–173, 2007.

[77] S. Rawson, S. Cartmell, and J. Wong, "Suture techniques for tendon repair; a comparative review.," *Muscles. Ligaments Tendons J.*, vol. 3, no. 3, pp. 220–228,

2013.

[78] M. C. Jordan, S. Ho¨lscher-Doht, M. G. Jakubietz, R. G. Jakubietz, R. H. Meffert, and K. Schmidt, “Suture material for flexor tendon repair: 3-0 V-Loc versus 3-0 Stratafix in a biomechanical comparison ex vivo,” *J. Orthop. Surg. Res.*, 2014.

[79] L. D. Ketchum, “Suture materials and suture techniques used in tendon repair,” *Hand Clin*, vol. 1, no. 1, pp. 43–53, 1985.

[80] J. S. Taras, J. S. Raphael, S. C. Marczyk, and W. B. Bauerle, “Evaluation of suture caliber in flexor tendon repair,” *J. Hand Surg. Am.*, 2001.

[81] A. Viinikainen, H. Göransson, K. Huovinen, M. Kellomäki, and P. Rokkanen, “A comparative analysis of the biomechanical behaviour of five flexor tendon core sutures,” *J. Hand Surg. Am.*, vol. 29, no. 6, pp. 536–543, 2004.

[82] M. H. Kudur, S. B. Pai, H. Sripathi, and S. Prabhu, “Sutures and suturing techniques in skin closure.,” *Indian J. Dermatol. Venereol. Leprol.*, vol. 75, no. 4, pp. 425–434, 2009.

[83] H. Kubota, M. Aoki, D. L. Pruitt, and P. R. Manske, “Mechanical properties of various circumferential tendon suture techniques,” *J. Hand Surg. Eur. Vol.*, vol. 21, no. 4, pp. 474–480, 1996.

[84] T. M. Muffly, N. Kow, I. Iqbal, and M. D. Barber, “Minimum number of throws needed for knot security,” *J. Surg. Educ.*, 2011.

[85] E. N. Kubiak, “The effect of insertion angle on the pullout strength of threaded suture anchors: a validation of the deadman theory,” *Arthroscopy*, vol. 30, no. 8, pp. 900–

905, 2014.

[86] A. S. Ranawat *et al.*, “Modes of failure of knotted and knotless suture anchors in an arthroscopic bankart repair model with the capsulolabral tissues intact.,” *Am. J. Orthop. (Belle Mead. NJ).*, vol. 40, no. 3, pp. 134–138, 2011.

[87] F. M. Pfeiffer, M. J. Smith, J. L. Cook, and K. Kuroki, “The histologic and biomechanical response of two commercially available small glenoid anchors for use in labral repairs,” *J. Shoulder Elb. Surg.*, vol. 23, no. 8, pp. 1156–1161, 2014.

[88] A. García-González *et al.*, “Finite-element simulation of flexor digitorum longus or flexor digitorum brevis tendon transfer for the treatment of claw toe deformity,” *J. Biomech.*, 2009.

[89] I. Wakabayashi *et al.*, “Mechanical environment of the supraspinatus tendon: A two-dimensional finite element model analysis,” *J. Shoulder Elb. Surg.*, 2003.

[90] H. Sano, T. Yamashita, I. Wakabayashi, and E. Itoi, “Stress distribution in the supraspinatus tendon after tendon repair: suture anchors versus transosseous suture fixation.,” *The American journal of sports medicine*, vol. 35, no. 4. pp. 542–6, 2007.

[91] A. Herchenhan, N. S. Kalson, D. F. Holmes, P. Hill, K. E. Kadler, and L. Margetts, “Tenocyte contraction induces crimp formation in tendon-like tissue,” *Biomech. Model. Mechanobiol.*, 2012.

[92] S. P. Reese, S. A. Maas, and J. A. Weiss, “Micromechanical models of helical superstructures in ligament and tendon fibers predict large Poisson’s ratios,” *J. Biomech.*, vol. 43, no. 7, pp. 1394–1400, 2010.

[93] H. Fukuda and T. W. Chou, “An Advanced Shear-Lag Model Applicable to Discontinuous Fiber Composites,” *J. Compos. Mater.*, 1981.

[94] J. M. Hedgepeth, “Stress Concentrations in filamentary structures,” 1961.

[95] A. M. Sastry and S. L. Phoenix, “Load redistribution near non-aligned fibre breaks in a two-dimensional unidirectional composite using break-influence superposition,” *J. Mater. Sci. Lett.*, 1993.

[96] H. D. Wagner and A. Eitan, “Stress concentration factors in two-dimensional composites: effects of material and geometrical parameters,” *Compos. Sci. Technol.*, vol. 46, no. 4, pp. 353–362, Jan. 1993.

[97] J. M. Hedgepeth and P. Van Dyke, “Local Stress Concentrations in Imperfect Filamentary Composite Materials,” *J. Compos. Mater.*, 1967.

[98] J. Goree and R. S. Gross, “Stresses in a three-dimensional undirectional composite containing broken fibers,” no. 1978. pp. 395–405, 1980.

[99] T. Okabe, N. Takeda, Y. Kamoshida, M. Shimizu, and W. A. Curtin, “A 3D shear-lag model considering micro-damage and statistical strength prediction of unidirectional fiber-reinforced composites,” *Compos. Sci. Technol.*, vol. 61, no. 12, pp. 1773–1787, Sep. 2001.

[100] C. M. Landis, M. A. McGlockton, and R. M. McMeeking, “Improved shear lag model for broken fibers in composite materials,” *J. Compos. Mater.*, 1999.

[101] C. M. Landis, I. J. Beyerlein, and R. M. McMeeking, “Micromechanical simulation of the failure of fiber reinforced composites,” *J. Mech. Phys. Solids*, 2000.

[102] S. J. Zhou and W. A. Curtin, “Failure of fiber composites: A lattice green function model,” *Acta Metall. Mater.*, 1995.

[103] M. Ibnabdeljalil and W. A. Curtin, “Strength and reliability of fiber-reinforced composites: Localized load-sharing and associated size effects,” *Int. J. Solids Struct.*, 1997.

[104] A. S. Carrara and F. J. Mcgarry, “Matrix and Interface Stresses in a Discontinuous Fiber Composite Model,” *J. Compos. Mater.*, 1968.

[105] A. Mazzocca, F. Alberta, N. ELATTRACHE, and a ROMEO, “Single incision technique using an interference screw for the repair of distal biceps tendon ruptures,” *Oper. Tech. Sports Med.*, 2003.

[106] R. M. Harrell, J. Tong, P. S. Weinhold, and L. E. Dahners, “Comparison of the mechanical properties of different tension band materials and suture techniques,” *J. Orthop. Trauma*, 2003.

[107] B. C. Carofino, S. A. Santangelo, M. Kabadi, A. D. Mazzocca, and B. D. Browner, “Olecranon Fractures Repaired With FiberWire or Metal Wire Tension Banding: A Biomechanical Comparison,” *Arthrosc. - J. Arthrosc. Relat. Surg.*, 2007.

[108] C. K. Yiannakopoulos, I. Hiotis, and E. Antonogiannakis, “The triad knot: A new sliding self-locking knot,” *Arthrosc. - J. Arthrosc. Relat. Surg.*, 2005.

[109] “Knotless Anchors.” [Online]. Available: https://www.shoulderdoc.co.uk/article/1193. [Accessed: 01-Jan-2016].

[110] Eric K. Everett, “Biomechanical analysis of a novel suture pattern for repair of equine

tendon lacerations," Virginia Polytechnic Institute and State University, 2011.

[111] G. Matheson, S. Nicklin, M. P. Gianoutsous, and W. R. Walsh, "Comparison of zone II flexor tendon repairs using an in vitro linear cyclic testing protocol," *Clin. Biomech.*, 2005.

[112] K. J. EASLEY, T. S. STASHAK, F. W. SMITH, and G. VAN SLYKE, "Mechanical Properties of Four Suture Patterns for Transected Equine Tendon Repair," *Vet. Surg.*, 1990.

[113] A. M. Wilson, M. P. McGuigan, A. Su, and A. J. Van den Bogert, "Horses damp the spring in their step," *Nature*, 2001.

[114] F. Debbabi and S. Ben Abdessalem, "Effect of Manufacturing Conditions on Structural and Handling Properties of Braided Polyamide Suture," *J. Eng. Fiber. Fabr.*, 2015.

[115] "South Bend | Fishing | Everything You Need to Start Fishing Today." [Online]. Available: http://www.south-bend.com/. [Accessed: 13-Sep-2018].

[116] K. Hristov, E. Armstrong-Carroll, M. Dunn, C. Pastore, and Y. Gowayed, "Mechanical Behavior of Circular Hybrid Braids Under Tensile Loads," *Text. Res. J.*, vol. 74, no. 1, pp. 20–26, Jan. 2004.

[117] "Tensile Testing of Surgical Sutures Using Straight-Pull and Knot-Pull Tests - Instron." [Online]. Available: http://www.instron.us/en-us/testing-solutions/by-test-type/tension/surgical-sutures. [Accessed: 13-Sep-2018].

[118] T. Hong *et al.*, "Development of in vitro performance tests and evaluation of

nonabsorbable monofilament sutures for cardiovascular surgery," *ASAIO J.*, vol. 44, no. 6, p. 776—785, 1998.

[119] "MatWeb, Your Source for Materials Information." [Online]. Available: http://www.matweb.com/. [Accessed: 01-Jan-2016].

[120] "Optimum Spring Manufacturing." [Online]. Available: http://optimumspring.com. [Accessed: 01-Jan-2016].

[121] D. J. Carr, A. G. Heward, R. M. Laing, and B. E. Niven, "Measuring the strength of knotted suture materials," *J. Text. Inst.*, vol. 100, no. 1, pp. 51–56, Mar. 2009.

[122] I. K. Y. Lo, S. S. Burkhart, K. C. Chan, and K. Athanasiou, "Arthroscopic Knots: Determining the Optimal Balance of Loop Security and Knot Security," *Arthrosc. - J. Arthrosc. Relat. Surg.*, vol. 20, no. 5, pp. 489–502, 2004.

[123] C. C. Annunziata, D. B. Drake, J. A. Woods, A. J. Gear, G. T. Rodeheaver, and R. F. Edlich, "Technical considerations in knot construction. Part I. Continuous percutaneous and dermal suture closure.," *J. Emerg. Med.*, vol. 15, no. 3, pp. 351–356, 1997.

[124] J. E. Brouwers, H. Oosting, D. de Haas, and P. J. Klopper, "Dynamic loading of surgical knots," *Surg. Gynecol. Obstet.*, vol. 173, no. 6, p. 443—448, Dec. 1991.

[125] S. S. Burkhart, J. L. Diaz Pagàn, M. A. Wirth, and K. A. Athanasiou, "Cyclic loading of anchor-based rotator cuff repairs: Confirmation of the tension overload phenomenon and comparison of suture anchor fixation with transosseous fixation," *Arthroscopy*, vol. 13, no. 6, pp. 720–724, 1997.

[126] V. V Upasani, A. Mahar, and R. A. Pedowitz, “Paper #207 Comparative study of bovine and human rotator cuff anthropometrics,” *Arthrosc. J. Arthrosc. Relat. Surg.*, vol. 19, no. 6, Supplement, p. 105, 2003.

[127] C. J. Petit, R. Boswell, A. Mahar, J. Tasto, and R. A. Pedowitz, “Biomechanical evaluation of a new technique for rotator cuff repair.,” *Am. J. Sports Med.*, vol. 31, no. 6, pp. 849–853, 2003.

[128] S. Baran, E. Johnson, and M. Perret-Gentil, “Understanding and Selecting Surgical Suture and Needle,” *Http://Www.Alnmag.Com/*, pp. 1–9, 2013.

[129] H. Tera and C. Aberg, “Tensile strengths of twelve types of knot employed in surgery, using different suture materials.,” *Acta Chir. Scand.*, vol. 142, no. 1, pp. 1–7, 1976.

[130] D. C. Schubert, J. B. Unger, D. Mukherjee, and J. F. Perrone, “Mechanical performance of knots using braided and monofilament absorbable sutures.,” *Am. J. Obstet. Gynecol.*, vol. 187, no. 6, pp. 1432–1438, Dec. 2002.

[131] R. P. Brown, “Knotting technique and suture materials.,” *Br. J. Surg.*, vol. 79, no. 5, pp. 399–400, May 1992.

[132] E. J. C. van Rijssel, J. Baptist Trimbos, and M. H. Booster, “Mechanical performance of square knots and sliding knots in surgery: A comparative study,” *Am. J. Obstet. Gynecol.*, vol. 162, no. 1, pp. 93–97, Jan. 1990.

[133] J. E. Tidwell, V. L. Kish, J. B. Samora, and J. Prud’homme, “Knot Security: How Many Throws Does It Really Take?,” *Orthopedics*, vol. 35, no. 4, pp. e532–e537,

2012.

[134] J. B. Trimbos, “Security of various knots commonly used in surgical practice.,” *Obstet. Gynecol.*, vol. 64, no. 2, pp. 274–280, Aug. 1984.

[135] Simulia, “Getting Started with Abaqus: Interactive Edition,” *Getting Started with Abaqus: Interactive Edition*, 2012. [Online]. Available: http://www.maths.cam.ac.uk/computing/software/abaqus_docs/docs/v6.12/pdf_books/GET_STARTED.pdf.

[136] A. Sreeranganathan, “Realistic Micromechanical Modeling and Simulation of Two-Phase Heterogeneous Materials Realistic Micromechanical Modeling and Simulation of Two-Phase Heterogeneous Materials,” Georgia Institute of Technology, 2008.

[137] J. Lepetit, R. Favier, A. Grajales, and P. O. Skjervold, “A simple cryogenic holder for tensile testing of soft biological tissues,” *J. Biomech.*, 2004.

[138] A. C. Devkota and P. S. Weinhold, “Mechanical response of tendon subsequent to ramp loading to varying strain limits,” *Clin. Biomech.*, 2003.

[139] F.A.Barber, M.Ruiz-Suarez, and D.A.Coons, “Tensile and cyclic testing of multiple suture anchors for glenoid labral repair: A biomechanical study,” *Arthrex Inc.*, 2006.

[140] C. Uggen *et al.*, “Biomechanical Comparison of Knotless Anchor Repair Versus Simple Suture Repair for Type II SLAP Lesions,” *Arthrosc. - J. Arthrosc. Relat. Surg.*, vol. 25, no. 10, pp. 1085–1092, 2009.

[141] F. Alan Barber, M. A. Herbert, and J. M. Crates, “A comparison of lateral ankle ligament suture anchor strength,” *Foot Ankle Surg.*, vol. 19, no. 2, pp. 108–111, 2013.

[142] F. A. Barber, D. A. Coons, and M. Ruiz-Suarez, “Cyclic Load Testing of Biodegradable Suture Anchors Containing 2 High-Strength Sutures,” *Arthrosc. - J. Arthrosc. Relat. Surg.*, vol. 23, no. 4, pp. 355–360, 2007.

[143] F. Alan Barber *et al.*, “Biomechanical analysis of pullout strengths of rotator cuff and glenoid anchors: 2011 update,” *Arthrosc. - J. Arthrosc. Relat. Surg.*, vol. 27, no. 7, pp. 895–905, 2011.

[144] S. Ben Abdessalem, F. Debbabi, H. Jedda, S. Elmarzougui, and S. Mokhtar, “Tensile and Knot Performance of Polyester Braided Sutures,” *Text. Res. J.*, vol. 79, no. 3, pp. 247–252, Feb. 2009.

[145] and A. P. Anindya Ghosh 1 , S. M. Ishtiaque, R. S. Rengasamy, P. Mal, “Spun Yarn Strength as a Function of Gauge Length and Extension rate: A Critical Review,” *J. Text. apperal, Technol. Manag.*, vol. 4, no. 2, 2004.

[146] M. S. Macsai, Ed., *Ophthalmic Microsurgical Suturing Techniques*. Berlin, Heidelberg: Springer Berlin Heidelberg, 2007.

[147] C. S. Chang and H. D. Conway, “Bond Stresses in Fiber Reinforced Composites Subjected to Uniform Tension,” *J. Compos. Mater.*, vol. 2, no. 2, pp. 168–185, 1968.

[148] Y. Swolfs, R. M. McMeeking, I. Verpoest, and L. Gorbatikh, “Matrix cracks around fibre breaks and their effect on stress redistribution and failure development in unidirectional composites,” *Compos. Sci. Technol.*, vol. 108, pp. 16–22, 2015.

[149] T. D. Loutzenheiser, D. T. Harryman, S. W. Yung, M. P. France, and J. A. Sidles, “Optimizing arthroscopic knots,” *Arthrosc. J. Arthrosc. Relat. Surg.*, 1995.

[150] R. Singh and W. Hawkins, “Sutures, ligatures and knots,” *Surgery (United Kingdom)*. 2017.

[151] R. Thal, “A Knotless Suture Anchor: Technique for use in arthroscopic Bankart repair,” *Arthroscopy - Journal of Arthroscopic and Related Surgery*, vol. 17, no. 2. pp. 189–195, 2001.

[152] R. Thal, “Knotless suture anchor: arthroscopic bankart repair without tying knots,” *Clin Orthop Relat Res*, no. 390. pp. 42–51, 2001.

[153] R. Garofalo *et al.*, “Arthroscopic treatment of anterior shoulder instability using knotless suture anchors.,” *Arthroscopy*, vol. 21, no. 11, pp. 1283–9, 2005.

[154] K. Hayashida, M. Yoneda, N. Mizuno, S. Fukushima, and S. Nakagawa, “Arthroscopic Bankart Repair With Knotless Suture Anchor for Traumatic Anterior Shoulder Instability: Results of Short-Term Follow-Up,” *Arthrosc. - J. Arthrosc. Relat. Surg.*, vol. 22, no. 6, pp. 620–626, 2006.

[155] B. Kocaoglu, O. Guven, U. Nalbantoglu, N. Aydin, and U. Haklar, “No difference between knotless sutures and suture anchors in arthroscopic repair of Bankart lesions in collision athletes,” *Knee Surgery, Sport. Traumatol. Arthrosc.*, vol. 17, no. 7, pp. 844–849, 2009.

[156] M. J. Sileo *et al.*, “Biomechanical Comparison of a Knotless Suture Anchor With Standard Suture Anchor in the Repair of Type II SLAP Tears,” *Arthrosc. - J. Arthrosc. Relat. Surg.*, vol. 25, no. 4, pp. 348–354, 2009.

[157] H. J. Yang, K. Yoon, H. Jin, and H. S. Song, “Clinical outcome of arthroscopic SLAP

repair: conventional vertical knot versus knotless horizontal mattress sutures," *Knee Surgery, Sport. Traumatol. Arthrosc.*, 2016.

[158] R. Thal, M. Nofziger, M. Bridges, and J. J. Kim, "Arthroscopic Bankart Repair Using Knotless or BioKnotless Suture Anchors: 2- to 7-Year Results," *Arthrosc. - J. Arthrosc. Relat. Surg.*, vol. 23, no. 4, pp. 367–375, 2007.

[159] E. Alentorn-Geli *et al.*, "Return to sports after arthroscopic capsulolabral repair using knotless suture anchors for anterior shoulder instability in soccer players: minimum 5-year follow-up study," *Knee Surgery, Sport. Traumatol. Arthrosc.*, 2016.

[160] B. P. Leedle and M. D. Miller, "Pullout strength of knotless suture anchors," *Arthrosc. - J. Arthrosc. Relat. Surg.*, 2005.

[161] R. Thal, "Arthroscopic Bankart Repair Using Knotless Suture Anchors," *Arthrosc. - J. Arthrosc. Relat. Surg.*, vol. 23, no. 5, pp. 566–567, 2007.

[162] E. Yian, C. Wang, P. J. Millett, and J. J. P. Warner, "Arthroscopic Repair of SLAP Lesions with a Bioknotless Suture Anchor," *Arthrosc. - J. Arthrosc. Relat. Surg.*, 2004.

[163] D. Z. Ng and V. P. Kumar, "Arthroscopic bankart repair using knot-tying versus knotless suture anchors: Is there a difference?," *Arthrosc. - J. Arthrosc. Relat. Surg.*, vol. 30, no. 4, pp. 422–427, 2014.

[164] J. T. Cox, P. L. Shorten, G. C. Gould, R. J. Markert, M. D. J. Barnett, and R. T. Laughlin, "Knotted versus knotless suture bridge repair of the achilles tendon insertion: a biomechanical study.," *Am. J. Sports Med.*, vol. 42, no. 11, pp. 2727–

2733, 2014.

[165] F. A. Barber and M. A. Herbert, “Cyclic loading biomechanical analysis of the pullout strengths of rotator cuff and glenoid anchors: 2013 update,” *Arthrosc. - J. Arthrosc. Relat. Surg.*, vol. 29, no. 5, pp. 832–844, 2013.

[166] F. A. Barber, D. A. Coons, and M. Ruiz-Suarez, “Cyclic Load Testing and Ultimate Failure Strength of Biodegradable Glenoid Anchors,” *Arthrosc. - J. Arthrosc. Relat. Surg.*, vol. 24, no. 2, pp. 224–228, 2008.

[167] B. S. Brown, A. D. Cooper, T. E. McIff, V. H. Key, and E. B. Toby, “Initial fixation and cyclic loading stability of knotless suture anchors for rotator cuff repair,” *J. Shoulder Elb. Surg.*, vol. 17, no. 2, pp. 313–318, 2008.

[168] F. A. Barber, M. A. Herbert, R. C. Beavis, and F. Barrera Oro, “Suture Anchor Materials, Eyelets, and Designs: Update 2008,” *Arthrosc. - J. Arthrosc. Relat. Surg.*, 2008.

[169] F.A. Barber, D.A.Coons, and M.Ruiz-Suarez, “Tensile glenoid anchors,” *Arthroscopy*, vol. 24, no. 2, pp. 224–228, 2008.

[170] M. Deakin, D. Stubbs, W. Bruce, J. Goldberg, R. M. Gillies, and W. R. Walsh, “Suture strength and angle of load application in a suture anchor eyelet,” *Arthrosc. - J. Arthrosc. Relat. Surg.*, vol. 21, no. 12, pp. 1447–1451, 2005.

[171] D. Greenwald, S. Shumway, P. Albear, and L. Gottlieb, “Mechanical comparison of 10 suture materials before and after in vivo incubation.,” *J. Surg. Res.*, vol. 56, no. 4, pp. 372–377, 1994.

[172] “Arthrex - FiberTape® and TigerTape™.” [Online]. Available: https://www.arthrex.com/shoulder/fibertape-and-tigertape. [Accessed: 31-Oct-2018].

Appendix A

Dial gauge setup

The accuracy of the dial indicators that have been used were validated by using two dial indicators, placed on the upper grip of the MTS machine to compare the MTS results with the results of the dial indicators under a tensile test. A tensile test was applied to a standard steel specimen. Figure A1 depicts the set up for the dial indicators before and during the test, respectively. The load-displacement results of the MTS machine and the dial indicators that have been used in the tests indicates a good agreement, as shown in Figure A2.

Figure A1: Dial gauge setup on the MTS machine

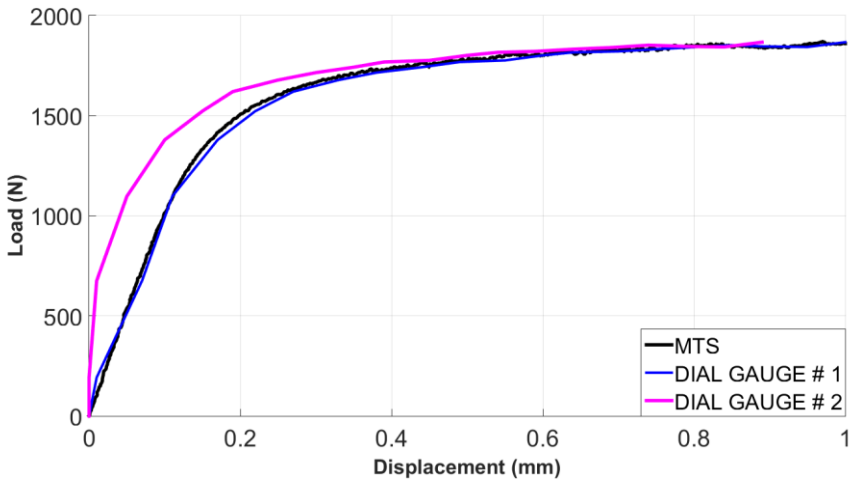

Figure A2: Load-Displacement results of dial gauges versus MTS machine

Appendix B

Calibration

A known measurement from a calibrated device is called the reference. The second device under testing conditions is the unit being calibrated. The axial capacity of the MTS machine is (25 KN). To measure the applied load with a high precision, a load transducer (SM-2224 N) is used. The load transducer connects to a strain indicator (3800) attached to the MTS machine. The calibration is necessary to make sure that the MTS machine with load transducer signals is precise and accurate. The calibration is split over two aspects: one to calibrate the load transducer signal, and the second to calibrate the load transducer with known weights.

B1. Calibration steps of load transducer signal

1. The installation of the load transducer to the MTS machine is shown in the Figure B1.

2. Connect the load transducer wires to the strain indicator as shown in the Figure B2 for reading the tension load. Each color of gage should lead to the identical color of the terminal.

3. Verify full wire bridge wiring.

4. Press Amperage to calibrate and set the amp value to zero as displayed in Figure B2.

5. Record the gage factor (approximately 2).

6. Press Run to calibrate and zero out the balance by rotating the balance knob, as shown in Figure B3.

7. Make certain that the connection between the strain indicator and MTS machine is in place.

8. Adjust the signals on the MTS machine.

9. Rotate the balance knob in the background of the strain indicator to make the signals corresponding, as depicted in Figure B4.

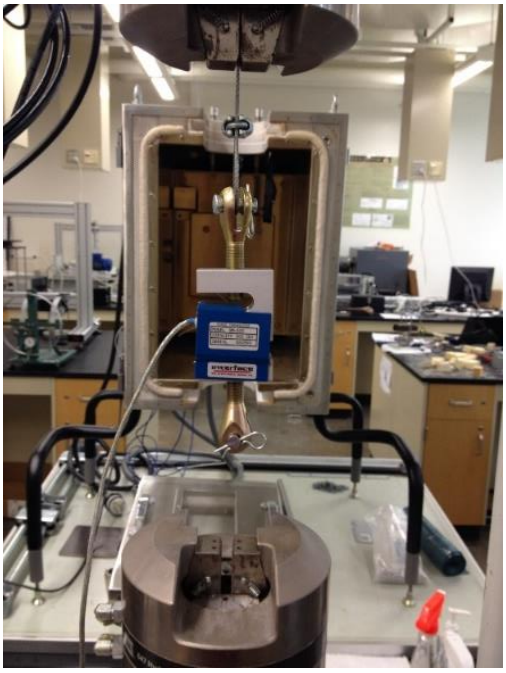

Figure B1: Load transducer installation

Figure B2: Strain indicator (Amperage)

Figure B3: Strain indicator (Run)

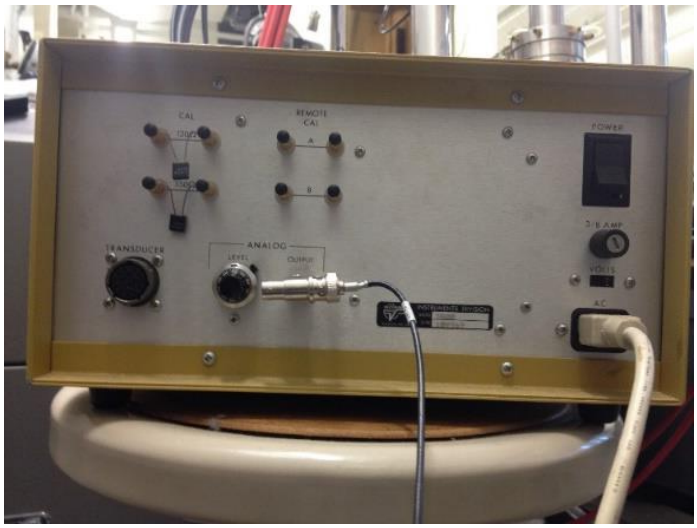

Figure B4: Strain indicator background

B2. Calibration steps of load transducer

To verify that the load transducer data were correct, ten weights were used for calibration: each weight has 10 Ib. To prove that the weights that were used were correct, a digital scale was used to measure the weights, as depicted in Figure B5. The outcome of

checking indicited that one piece had a value (9.99 Ib); three pieces had a value (10.01 Ib); while the others had values of (10.02 Ib) each. The calibration procedures are set out below:

1. Figure B6 illustrates the connecting method of the load transducer and the load hanger with the MTS machine.

2. Repeat the calibration steps (1-8) of 3.1 (Calibration steps of load transducer signal).

3. Set the load and displacement at the MTS machine to zero to account for the weight of the load hanger.

4. Apply weights on the hangers, as shown in Figure B7.

5. Apply loads in increments.

The MTS machine displays the results and a plot graph of apparent load cell can be drawn, Figure B8 and Figure B9 respectively.

Figure B5: Weights measuring

Figure B6: Connecting Load transducer and load hanger with MTS machine

Figure B7: Applying weights

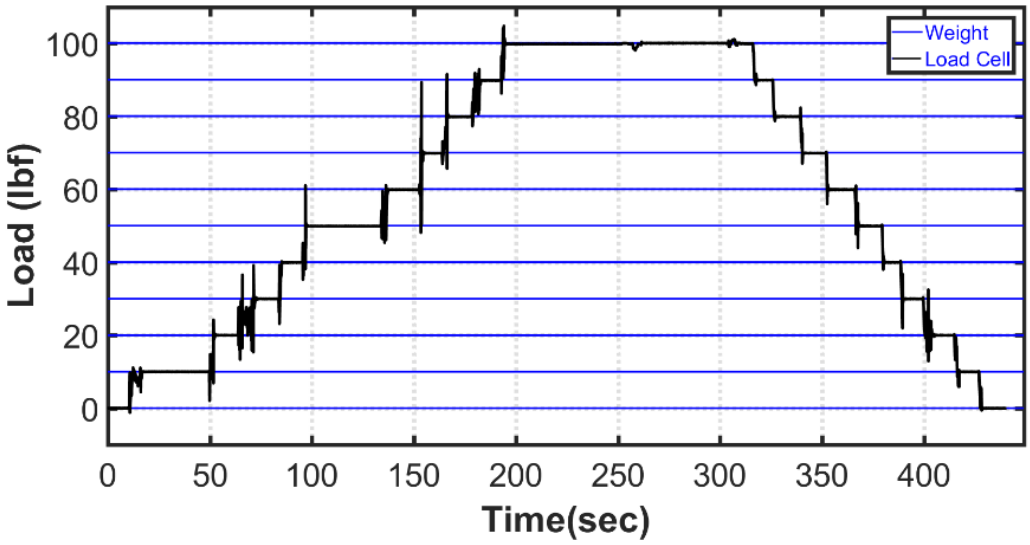

Figure B8: Load-time results

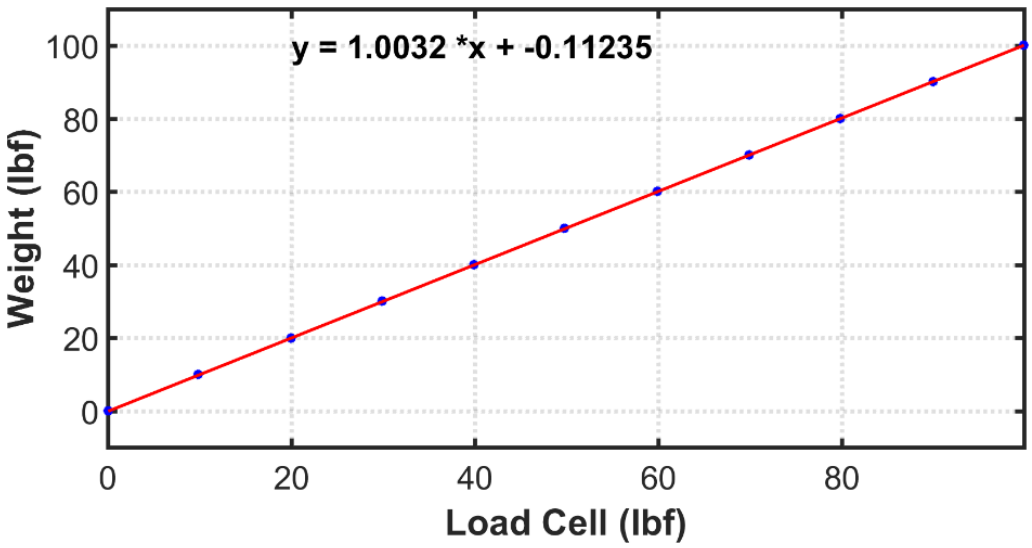

Figure B9: MTS machine load versus weights

Appendix C

Cyclic loading

Two series of cyclic loading experiments with varied loads and displacement were performed on the suture with loading direction parallel to the suture. The first case study consisted of a suture subjected to a force of constantly increasing amplitude on its top. The loading program for the specimen consisted of a load-controlled cyclic loading scheme, where five cycles of displacement were applied at each deformation level, with 10 N/step increments at speed rate 0.5 N/sec, as shown in Figure C1. The results showed the accuracy of load transducer data because they were located in the middle of MTS machine data with slightly different: approximately ±10N. Also, the minimum force applied was not strictly zero may be due to the high capacity of the MTS machine and/or noise effect of the MTS machine. The displacement versus time curve was shown in Figure C2.

Figure Figure C3 shows the load versus the displacement. The shape of load-displacement curves indicated a nonlinear response at the beginning due to friction between the suture and pulleys. In addition, the outcome illustrated that the process was irreversible due to the composition of the suture and the friction between core and suture.

The second case study consists of a suture subjected to a displacement of constantly increasing amplitude on its top. The loading program for the specimen consisted of a displacement-controlled cyclic loading scheme, where four cycles of displacement are applied at each deformation level with 1 mm/step increments at speed rate 0.5 mm/sec, as shown in Figure C4. The minimum force applied is not strictly zero but slightly negative, but this is harmless since negative stresses have no effect on the fatigue behavior, as shown in Figure C5. Load versus displacement is shown in Figure C6.

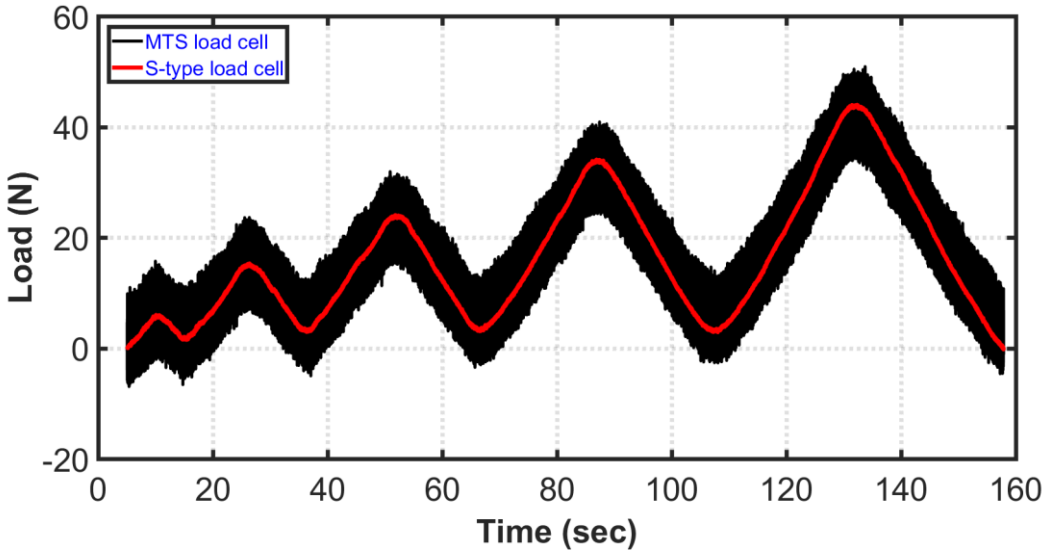

Figure C1: Load versus time

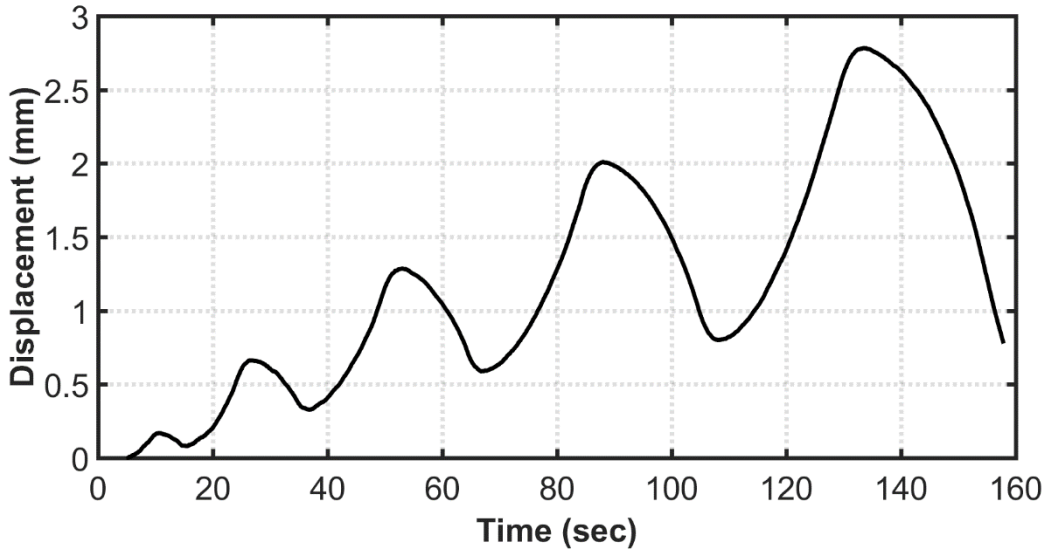

Figure C2: Displacement versus time

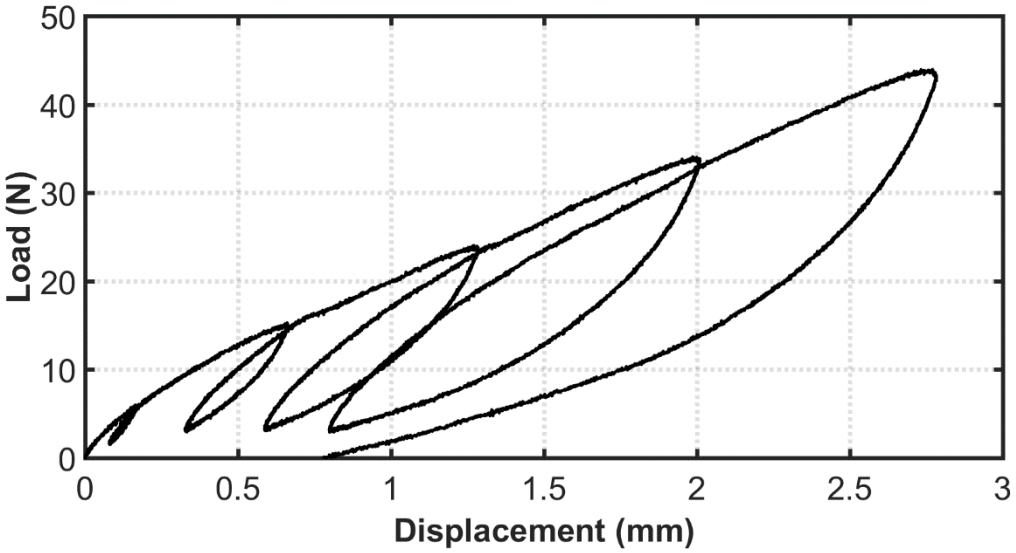

Figure C3: Load versus displacement

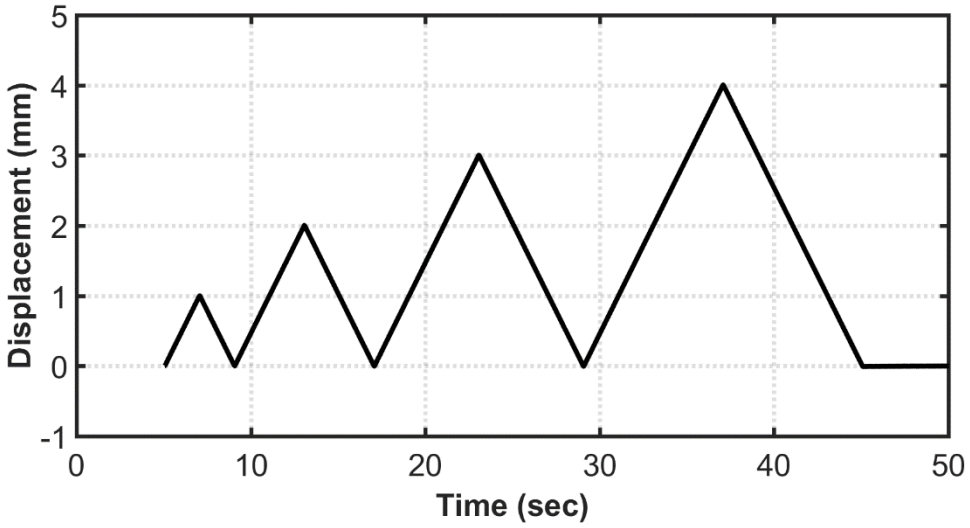

Figure C4: Displacement versus time

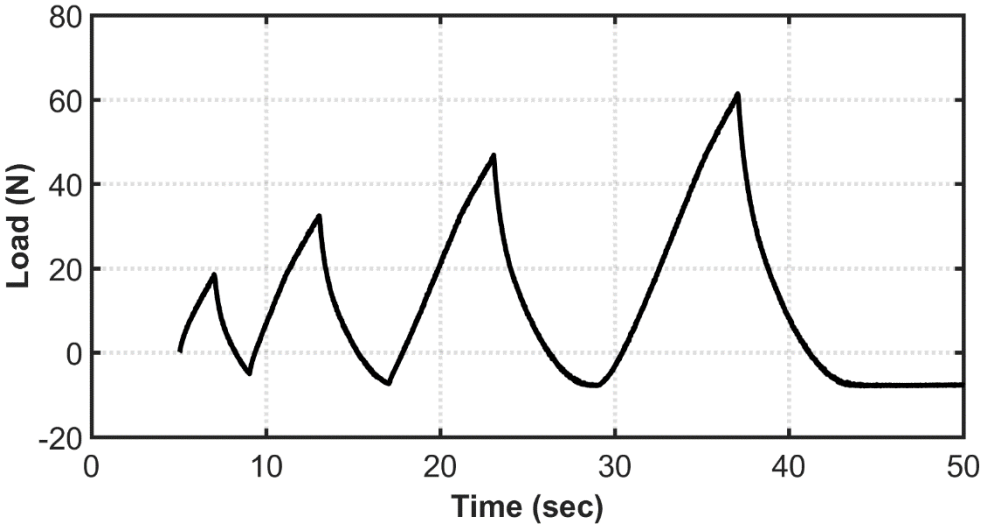

Figure C5: Load versus time

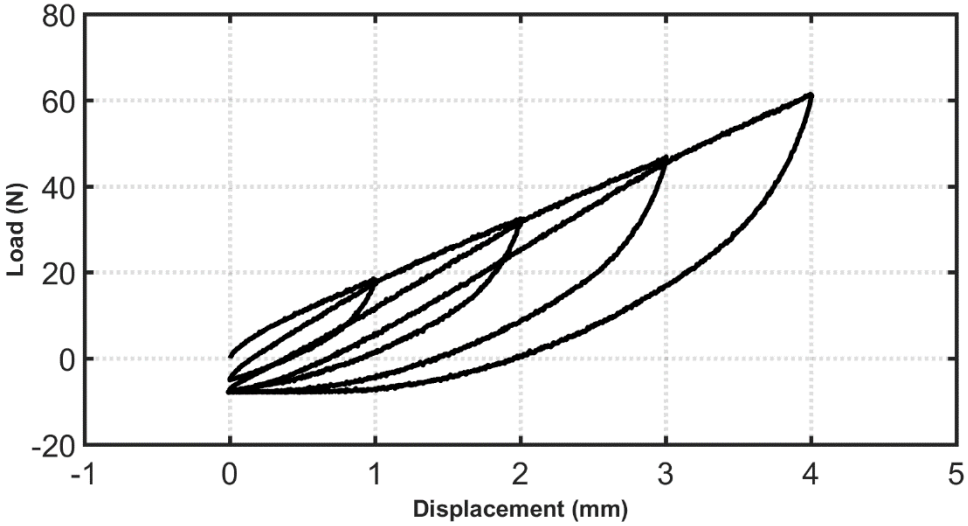

Figure C6: Load versus displacement